Long-term water security in the Aburrá Valley under demographic, land use, and climate change: an RRV framework approach

Nathalia Jastrombek Vieira

Tesis de maestría presentada para optar al título de Magíster en Ingeniería Ambiental

Director

Néstor Jaime Aguirre Ramírez, Doctor (PhD) en Limnología

Asesor

Fabio de Jesús Vélez Macías, Doctor (PhD) en Geografía

Universidad de Antioquia

Facultad de Ingeniería

Maestría en Ingeniería Ambiental

Medellín, Antioquia, Colombia

2025

UNIVERSIDAD DE ANTIOQUIA
1803

Cita	(Jastrombek Vieira, 2025)
Referencia **Estilo APA 7 (2020)**	Jastrombek Vieira, N. (2025). *Long-term water security in the Aburrá Valley under demographic, land use, and climate change: an RRV framework approach* [Tesis de maestría]. Universidad de Antioquia, Medellín, Colombia.

creative commons CC BY NC SA

Maestría en Ingeniería Ambiental , Cohorte XXX.

Grupo de Investigación. GeoLimna

Centro de Documentación de Ingeniería (CENDOI)

Repositorio Institucional: http://bibliotecadigital.udea.edu.co

Universidad de Antioquia - www.udea.edu.co

El contenido de esta obra corresponde al derecho de expresión de los autores y no compromete el pensamiento institucional de la Universidad de Antioquia ni desata su responsabilidad frente a terceros. Los autores asumen la responsabilidad por los derechos de autor y conexos.

Abstract

Water security is increasingly threatened by climate change, land use transformation, and growing urban demand. This research assesses the long-term water security of the Aburrá Valley in Antioquia, Colombia, which depends primarily on the Riogrande II and La Fe reservoirs. The analysis is carried out using the Reliability, Resilience, and Vulnerability (RRV) framework to evaluate system performance under future scenarios. To estimate future demand, a demographic projection was developed over a 50-year horizon using the Logistic Model. On the supply side, climate and land use scenarios were constructed for the source watersheds of both reservoirs, using downscaled outputs from the GFDL-CM4 global climate model and land cover change simulations based on MapBiomas Colombia data and the Dinamica EGO tool. The Soil and Water Assessment Tool (SWAT+) was calibrated and validated to simulate streamflow responses to these changes. Additionally, a custom Reservoir Dynamics module was proposed to address limitations in SWAT+ for simulating reservoir operations. From the resulting unmet demand time series, the RRV indicators were calculated. Results indicate that the Aburrá Valley's water security will become increasingly threatened due to the combined effects of more intense rainfall events and extended dry periods. The Riogrande II and La Fe reservoirs exhibit contrasting responses to projected climate and demand pressures. Riogrande II shows declining reliability and resilience, and increasing vulnerability, particularly under severe climate scenarios. In contrast, La Fe maintains higher performance due to its inter-basin pumping system, which buffers climate variability. However, rising demand leads to consistent declines in reliability and rising vulnerability over time. Its dependence on external watersheds and energy-intensive infrastructure also poses structural risks. These findings highlight that long-term water security in the Aburrá Valley depends not only on climate resilience but also on the sustainability of water transfers and integrated reservoir management. The proposed methodology offers a replicable framework for assessing water security in other urban regions facing similar challenges.

Keywords: Water security, Reservoir modeling, RRV Framework

1 Introduction

The combined effects of demographic growth, land use change, and climate change are increasing pressure on water resources worldwide, with particularly severe consequences in urban areas (Mishra et al., 2021; Rahaman et al., 2022). Urban expansion often leads to a higher concentration of water demand, degradation of natural ecosystems, and disruption of the hydrological cycle (Zhang et al., 2019). As cities grow, the challenge of maintaining reliable, resilient, and sustainable water supply systems becomes more acute. To anticipate and manage such risks, it is crucial to understand the interaction between various drivers of change, particularly population growth, land use dynamics, and climate change.

Population growth is a primary driver of increasing water demand, not only because it leads to a larger number of consumers but also due to changes in spatial distribution and consumption patterns. As urban populations expand, water infrastructure must extend to accommodate denser settlements, often requiring significant investment in supply, treatment, and distribution systems (Flörke et al., 2013). Moreover, rising living standards and economic development typically lead to increases in per capita water consumption, especially in domestic and industrial sectors (Vörösmarty et al., 2000). Migration patterns, such as rural-to-urban shifts, concentrate water demand in cities, intensifying the pressure on already stressed urban water systems. Spatial redistribution of population also alters land use patterns, often reducing permeable surfaces and increasing runoff, which affects local hydrological balances and reservoir recharge rates (Zhang et al., 2019).

Changes in the climate and land use in the catching basin must be deeply integrated with demographic scenarios for long-term water resource planning and management. To estimate future population scenarios based on historical growth trends, is a valuable tool to predict increases in the water demand and inform infrastructure investment decisions (Lomax et al., 2022). Rapid urban growth and overexploitation of water resources have already impacted the spatial and temporal distribution of water in many regions (Rahaman et al., 2022).

Land use dynamics result from complex interactions between natural and socioeconomic factors (Yang et al., 2022; Zhu et al., 2023). Spatiotemporal analysis of these changes is essential for understanding their effects on surface energy flows, ecosystem functioning, and the hydrological cycle. To support this analysis, spatially explicit models, such as cellular automata (CA)-based land use models, have become fundamental tools for simulating driving factors, evolutionary processes, impacts, and future change projections. Since the 1990s, CA models have been widely used to study urban expansion and land use change (Liu et al., 2020; Tong & Feng, 2020; Chakraborty et al., 2022).

In parallel, climate change has altered global hydrological conditions, affecting both the quantity and quality of water resources. Variations in temperature and precipitation patterns, as well as the increased frequency of extreme events, modify key hydrological processes such as infiltration and surface runoff (Ren et al., 2020; Rahaman et al., 2022). Together with land use changes and intensified human activities, climate change negatively impacts watershed performance. Increased frequency, intensity, and duration of drought events are expected under future climate scenarios (Chamani et al., 2022).

Water security refers to the ability of water systems and stakeholders to ensure sustainable, equitable, and affordable access to sufficient and safe water for human well-being, economic development, and ecosystem protection, while also safeguarding against water-related risks such as pollution and disasters (Aboelnga et al., 2019). It is a dynamic concept that emphasizes continuous availability, legal access, and social equity. Moreover, according to UN-Water (2019), water security fits within a broader notion of human security, acting as a central link among political, health, economic, environmental, and other societal concerns, reinforcing its role as a foundation for peace and development.

Assessing water security requires not only an understanding of physical water availability but also an evaluation of how systems perform under stress. The RRV framework, comprising Reliability, which is defined as the frequency of adequate supply, Resilience, which is speed of recovery from failures, and

Vulnerability, that represents the magnitude of failures, has become a widely used approach to quantify system performance in the face of uncertainty (Kjeldsen & Rosbjerg, 2009; Hashimoto et al., 1982). These metrics provide complementary perspectives that support robust water management planning, as demonstrated in case studies from Iran (Biglarbeigi et al., 2020; Moghadam & Malekmohammadi, 2025) and Vietnam (Nguyen et al., 2022).

Colombia is considered a country rich in water resources; however, the quantity and quality of available water are increasingly affected by urban expansion and overexploitation, placing significant pressure on water sources (Vargas-Pineda et al., 2020). The Metropolitan Area of the Aburrá Valley, located in the Department of Antioquia, has undergone an intense process of industrialization in recent decades, accelerating rural-to-urban migration and resulting in a conurbation phenomenon due to the expansion of urban areas around the municipality of Medellín, Antioquia (Área Metropolitana del Valle de Aburrá, n.d.). The Medellín-Aburrá River is the main local river and it is insufficient to meet the current needs, in quality and volume (Osorio Giraldo, 2019). Consequently, the region relies heavily on trans-basin water transfers from the Riogrande II and La Fe reservoirs, which together supply approximately 90% of the domestic water consumed in the metropolitan area (EPM, 2024a).

However, the sustainability of these reservoirs is increasingly challenged by changes in land use and climate in their source watersheds. Conversion of vegetated areas into urban and agricultural land changes infiltration, runoff generation, and sediment dynamics, thereby affecting streamflow and reservoir inflow (Shrestha et al., 2018; Farinosi et al., 2019). In parallel, shifts in precipitation patterns and temperature regimes due to climate change introduce further uncertainty into water availability (Pabón-Caicedo et al., 2020). These changes can compromise the reliability of water systems and make it more difficult to plan and operate reservoirs effectively in the long term (Liu et al., 2020).

To anticipate and manage these risks, integrated modeling approaches are essential. Hydrological models such as SWAT+ (Soil and Water Assessment Tool) allow the simulation of the impacts of climatic and land use changes on streamflow and reservoir inflows (Sánchez-Gómez et al., 2025), while land use change models, like DinamicaEGO, help project future land cover dynamics (Yang et al., 2022). Moreover, water system performance will be assessed using the RRV metrics introduced earlier, offering a structured way to quantify how water supply systems respond to stress and recover from disruptions.

Several studies have investigated the impact of climate change, land use dynamics, and demographic trends on water systems, using a variety of methodologies and focusing on diverse geographic regions. For instance, Vargas-Pineda et al. (2020) studied water balance and water footprint in the Quenano-Quenanito watershed in Colombia. Kumar et al. (2023) modeled land use changes under future climate scenarios in a Hindu basin, while Chamani et al.i (2022) applied RRV analysis to evaluate climate change impacts on a watershed in Iran. Gesualdo et al. (2019) assessed climate change impacts on water security in the Metropolitan Region of São Paulo, Brazil.

While numerous studies have explored the individual impacts of climate and land-use change on hydrological processes such as river flow and sediment yield within watersheds, fewer have investigated their combined effects on reservoir performance, particularly in terms of water supply reliability (Nguyen et al., 2022). This gap is especially critical given the growing importance of reservoirs in securing water supplies for expanding urban areas under future climate scenarios. At the same time, there is a recognized lack of local-level assessments of water security and the application of relevant performance metrics, despite increasing interest in the concept globally (Pabón-Caicedo et al., 2020). As Aboelnga et al. (2019) argue, water security measures must reflect the diverse and dynamic realities of local contexts to effectively address urban water challenges and support the development of robust, adaptive policy instruments.

In response to these challenges, this research aims to evaluate the impact of demographic change, land use, and climate change scenarios on the water security of regions supplied by the Riogrande II and La Fe reservoirs. The evaluation is conducted using the Reliability, Resilience, and Vulnerability framework to answer the central research question: How projected changes in population, land use, and climate will affect the capacity of the Riogrande II and La Fe reservoirs to ensure water security for the Aburrá Valley over the next 50 years? An integrated modeling approach will be implemented,

combining population demand projections, a hydrological simulation tool, and CA-based land use change models, to provide useful insights for water resource planning in the Aburrá Valley. The specific objectives of this research were: (a) to understand changes in water demand in the Aburrá Valley based on demographic trends over the next 50 years; (b) to develop climate and land use scenarios for the source watersheds of the La Fe and Riogrande II reservoirs in Antioquia, with the aim of assessing potential changes in water supply to the Aburrá Valley over the next five decades; and (c) to evaluate the water security of the Aburrá Valley, Antioquia, over time for the different water supply and demand scenarios.

2 Methodology

To assess the long-term water security of the Aburrá Valley, a multi-step methodological framework was developed, integrating demographic, climatic, hydrological, and operational components. The Figure 1 presents a flowchart that summarizes the methodological framework adopted in this study.

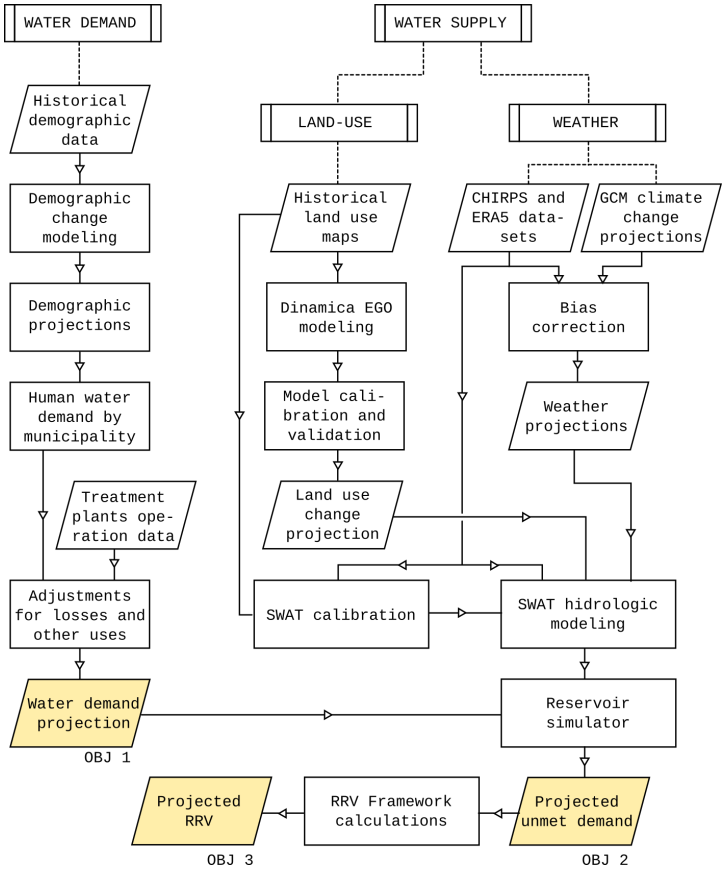

Figure 1. Investigation methodology flowchart. GCM: General Circulation Model; SWAT: Soil and Water Assessment Tool; RRV: Reliability, Resilience and Vulnerability.

The approach begins with the projection of future water demand based on population growth using a logistic model. On the water availability side, climate change scenarios were generated from downscaled GFDL-CM4 global climate model outputs, while land use change was simulated using the Dinamica EGO version 8 model with data from MapBiomas Colombia Collection 1. These inputs were used to drive the SWAT+ hydrological model, which was calibrated and validated to simulate streamflow in the source watersheds (SWAT+ 61.0.1; QSWAT+ 2.5; SWAT+ Editor 3.0.8; SWAT+ Toolbox 3.0.6). To address the limitations of SWAT+ in representing complex reservoir operations, a custom Reservoir Dynamics module was implemented in python. Finally, the Reliability, Resilience, and Vulnerability (RRV) indicators were calculated from simulated unmet water demand time series to evaluate system performance under various future scenarios. All the geoprocessing was conducted on QGIS 3.34.12.

2.1 Study area

The Aburrá Valley is located in the Central Cordillera in the northern part of the Colombian Andes and is divided in ten municipalities: Medellín, Bello, Itagüí, Envigado, Caldas, Copacabana, La Estrella, Girardota, Sabaneta, and Barbosa, covering an area of 1,152 km². The valley has a population of approximately 3.5 million inhabitants, concentrating 59% of the department population in just 1.8% of Antioquia's area (Giraldo, 2017; Ossa et al., 2021).

The Aburrá Valley exhibits a humid tropical climate, characterized by a bimodal precipitation regime with rainfall peaks typically occurring between April–May and October–November. Average annual precipitation ranges from 1400 to 2700 mm, and average temperature of 22ºC (Aristizábal et al., 2022). The climate is strongly influenced by the Intertropical Convergence Zone (ITCZ) and is affected by El Niño and La Niña events, which introduce significant interannual variability. Figure 2 presents the Aburrá Valley region next to its water supply contributing watersheds corresponding to the Riogrande II and La Fe reservoir systems.



Figure 2. Delimitation of study region. Region comprises the basins of Riogrande II and La Fe reservoirs which supply 90% of the Aburrá Valley water demand.

The Riogrande II Reservoir is located in the Department of Antioquia, north of Medellín city. It currently has a capacity of 185 million cubic meters (CNO, 2025), covering an area of 1,169 hectares within the jurisdiction of the municipalities of Santa Rosa de Osos, Belmira, San Pedro, Entrerríos, and Don Matías. Its main tributaries are the Grande River, the Chico River, and the Las Ánimas stream

(Flórez Molina et al., 2017). Figure 3 shows the elevation, soil type and land use chracterization of the Riogrande II reservoir watershed.

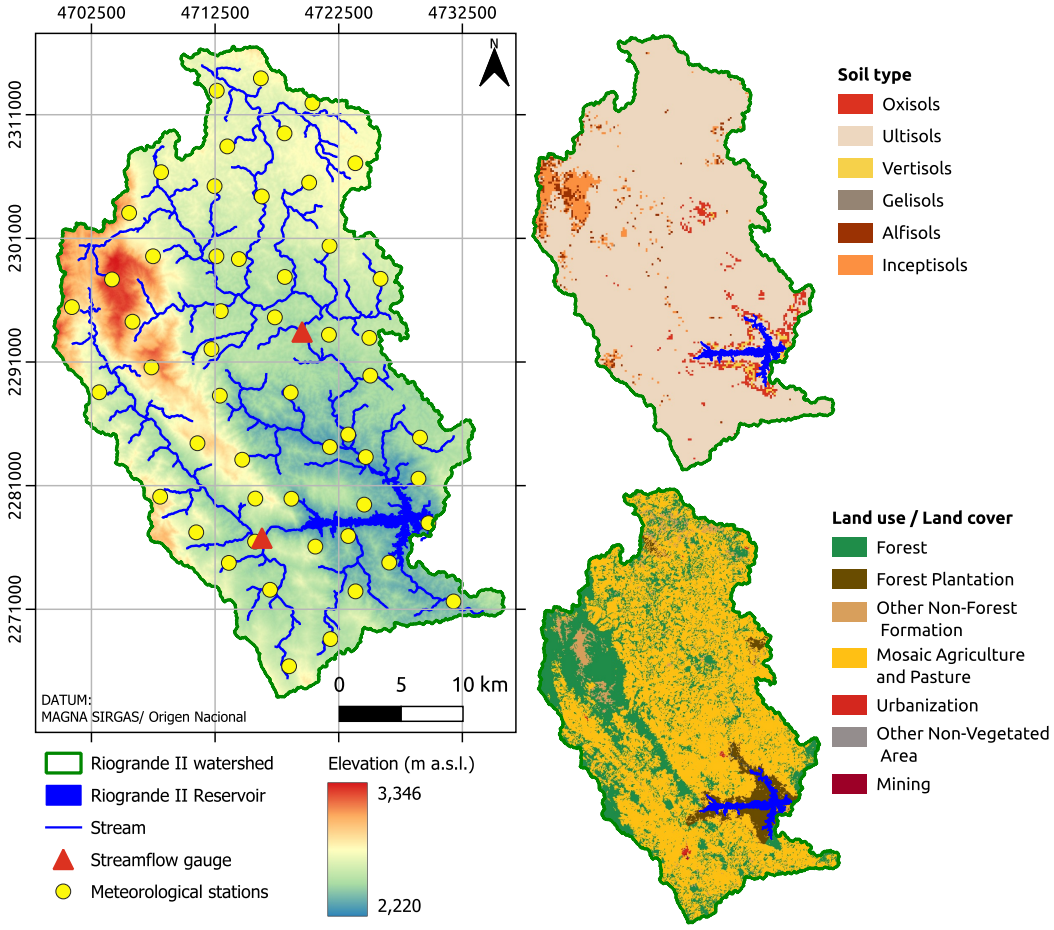

Figure 3. Riogrande II reservoir watershed, with its elevation (m a.s.l), soil type and land use/land cover.

As presented in Figure 3, the catchment area of the Riogrande II reservoir is located in mountainous terrain, with elevation varing between 2,220 and 3,346 meters above sea level. In 2020, land use in this watershed is dominated Mosaic of Agriculture and Pasture (63%), following by Forest (28%) (MapBiomas Colombia, 2024). Soils are primarily composed of Ultisols, following by Inceptisols (López-Ballesteros et al., 2023).

The reservoir has multiple uses, including hydroelectric power generation, potable water supply, and recreation. The Manantiales Water Treatment Plant (WTP Manatiales) has a design flow of 6 m^3/s, with plans to expand to 9 m^3/s; it currently operates at 4.3 m^3/s, supplying approximately 40% of the population of the Aburrá Valley (EPM, 2023; EPM, 2024a, Superintendencia Servicios Públicos Domiciliarios, 2021). The minimum and maximum operating levels are 2,261 and 2,270 meters above sea level, respectively (Flórez Molina et al., 2017; Sepúlveda-Sánchez et al., 2021).

The La Fe Reservoir is located in the municipality of El Retiro, in eastern Antioquia, southwest of the Aburrá Valley. It has a capacity of 12 million cubic meters, covering an area of 1.33 km^2. Its natural tributaries are the Espíritu Santo, Las Palmas, San Luis, Boquerón, Potreros, and La Miel streams, and it also receives water through pumping from the Pantanillo, Buey, and Piedras rivers, the latter contributing 6 m^3/s during dry seasons (Flórez Molina et al., 2018; Amaringo Villa, 2022; Ramírez et al., 2023). Figure 4 shows the chracteristics of La Fe reservoir watershed such as elevation, soil type and landuse/ land cover spatial representation.

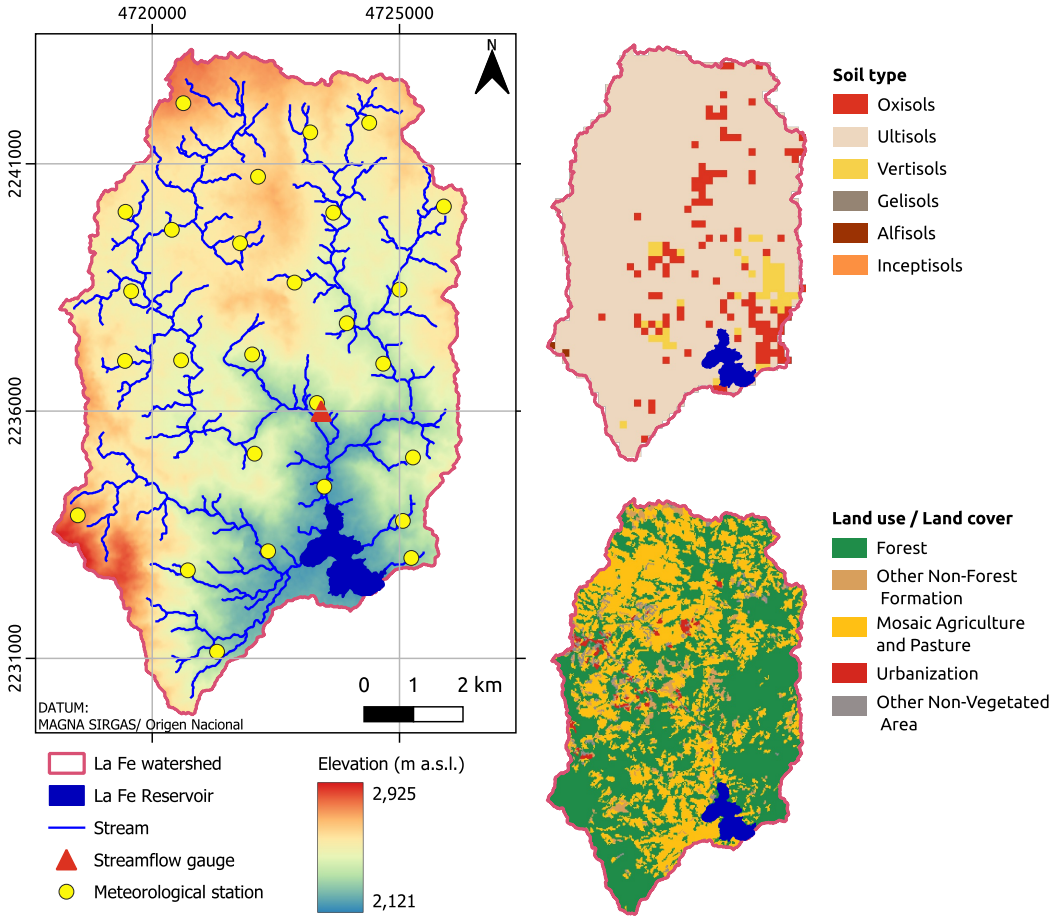

Figure 4. La Fe reservoir watershed chracterization with elevation (m a.s.l.), soil type and land use/ land cover.

As shown in Figure 4, the elevation of La Fe reservoir watershed varies from 2,121 and 2,925 meters above sea level. As in Riogrande II watershed, the most present soil type is the Ultisols (López-Ballesteros et al., 2023). The land use in 2020 in this watershed was mostly Forest (55%), followed by Mosaic of Agriculture and Pasture (37%) (MapBiomas Colombia, 2024). The La Fe reservoir primary purpose is the supply of potable water, followed by energy generation and recreation. The La Ayurá Water Treatment Plant (WTP La Ayurá) has a capacity of 9.2 m^3/s but is currently operating with a flow of 4.6 m^3/s (Superintendencia Servicios Públicos Domiciliarios, 2021), serving 50% of the population of Aburrá Valley (EPM, 2024a). The minimum operating level is 2,146 meters above sea level, while the maximum level is 2,155 meters above sea level. The spillway elevation is 2,257 meters above sea level (EPM, 2019; Flórez Molina et al., 2018).

According to Superintendencia Servicios Públicos Domiciliarios (2021), a series of water transfers are required to supplement the volume of the La Fe Reservoir. A flow of 2 m^3/s is authorized from the Buey River to the Piedras River. From the Piedras River, 2 m^3/s are authorized for transfer to the Pantanillo River, from which 3.10 m^3/s are authorized for pumping to the reservoir. A maximum of four pump units operate simultaneously, with 1.5 m^3/s each. Also based on the report, the pumping system started at the end of the year 2005.

2.2 Water demand

2.2.1 Population Data Collection: Census and Modeled Data

To carry out the demographic projection, information on the urban population was collected from national censuses conducted by the National Administrative Department of Statistics (DANE) between 1938 and 2018, totaling eight censuses (DANE, 1938; DANE, 1951; DANE, 1964; DANE, 1973; DANE, 1985; DANE, 1993; DANE, 2005; DANE, 2018). The Table 1 presents the urban population for the municipalities of the Metropolitan Area of Aburrá Valley for each census.

Year	Medellín	Barbosa	Bello	Caldas	Copaca-bana	Girardota	Itagüí	La Estrella	Envigado Sabaneta
1938	143,952	1,740	8,180	2,847	1,763	2,038	6,659	5,753	4,253
1951	328,294	2,763	28,398	5,846	2,673	2,481	11,027	2,864	13,392
1964	740,311	4,782	87,658	17,704	9,665	4,936	60,318	6,175	47,870
1973	1,122,099	7,830	103,039	28,635	21,231	11,022	90,828	14,533	76,523
1985	1,431,462	11,823	208,439	37,173	29,365	12,729	137,215	17,964	104,579
1993	1,551,160	13,379	257,711	45,251	39,621	17,131	175,626	33,626	130,766
2005	2,183,557	18,721	359,404	52,632	53,033	25,195	213,297	28,538	202,270
2018	2,320,248	21,469	456,897	61,442	62,102	27,896	234,939	57,451	271,842
2020	2,476,569	23,771	529,036	66,917	66,311	30,574	263,685	64,775	306,545
2021	2,506,656	24,868	536,766	68,174	67,553	31,615	267,720	65,928	311,398
2022	2,530,398	25,639	541,917	69,100	68,442	32,324	270,612	66,702	314,539
2023	2,553,621	26,343	546,902	69,957	69,303	32,970	273,385	67,454	317,539
2024	2,574,994	26,808	551,525	70,755	70,051	33,458	275,959	68,149	320,330
2025	2,593,542	27,216	555,509	71,410	70,691	33,900	278,179	68,734	322,772
2026	2,609,841	27,547	559,020	72,014	71,263	34,267	280,103	69,237	324,895
2027	2,624,783	27,825	562,182	72,518	71,790	34,590	281,856	69,695	326,755
2028	2,638,734	28,063	565,149	72,982	72,224	34,836	283,446	70,121	328,519
2029	2,651,875	28,234	567,955	73,385	72,623	35,069	284,915	70,483	330,135
2030	2,664,474	28,379	570,593	73,737	72,976	35,227	286,,266	70,829	331,665
2031	2,676,581	28,499	573,087	74,055	73,321	35,378	287,538	71,159	333,084
2032	2,688,112	28,599	575,484	74,363	73,620	35,515	288,736	71,424	334,432
2033	2,698,987	28,699	577,760	74,647	73,896	35,623	289,866	71,715	335,705
2034	2,709,188	28,774	579,881	74,920	74,157	35,737	290,897	71,990	336,927
2035	2,718,758	28,865	581,834	75,152	74,407	35,835	291,878	72,228	338,018

Table 1. Urban population of the municipalities in the Metropolitan Area of the Aburrá Valley reported in each national census and the DANE projections for the period 2020-2035.

About the numbers shown in Table 1, it is important to consider that the municipality of Sabaneta was a district of Envigado and was officially established as a municipality in 1967 (Municipio de Sabaneta, n.d.). Therefore, in this study, the two municipalities were considered as one to maintain consistency in the sampled area. In 1938, there was no recorded urban population for the municipalities of Itagüí and La Estrella. For adjustment purposes, the rural population was considered as the urban population. In the 1993 national census, the urban population data for Medellín was adjusted population, while for the other municipalities, the data corresponded to the actual census counts. As there were only a few observation points (eigth censuses), municipal demographic projection values produced by DANE for the period from 2020 to 2035 were included in the analysis (DANE, 2023), totaling 24 years of "observation".

The choice of the demographic projection model was based on the analysis of the relative annual population growth rate of the municipalities between 1951 and 2018. Figure 5 presents the relative annual population growth rate for the Aburrá Valley municipalities.

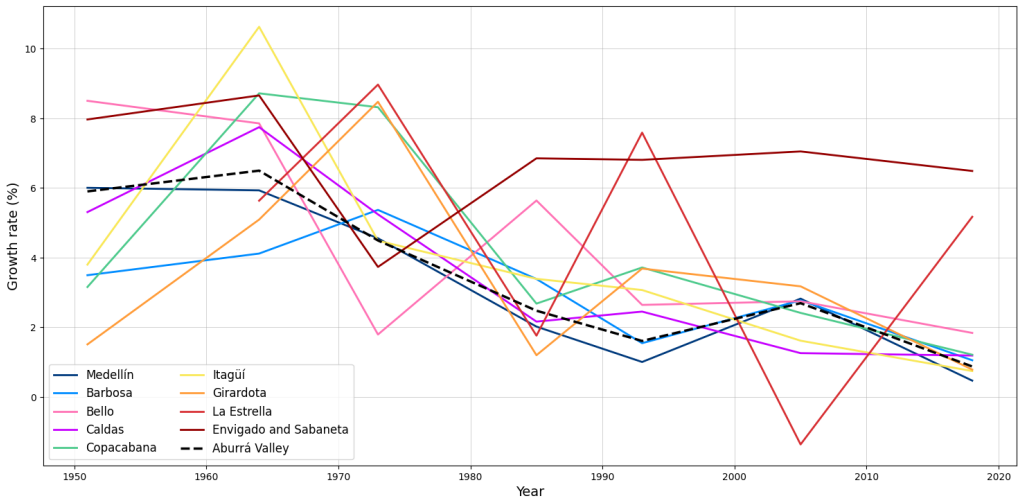

Figure 5. Relative annual population growth rate of the municipalities in the Metropolitan Area of the Aburrá Valley from 1951 to 2018. While most municipalities show a decreasing growth trend over time, Envigado and Sabaneta maintained a nearly constant growth rate from 1985 onward.

According to Figure 5, in general, the annual growth rate of the municipalities decreased over the sampled period, with the exception of Envigado/Sabaneta, which maintained a nearly constant growth rate from 1985 onward. La Estrella, on the other hand, does not exhibit a clearly defined pattern. Therefore, the demographic model used was the Logistic Growth Model.

2.2.2 Logistic Curve Model

The Logistic Model, was proposed by the mathematician Verhulst as a modification of the Malthusian exponential growth law, which assumes unrestricted population growth (Equation 1). Verhulst's modification considers that growth depends on the distance between the current population and some saturation population (Adhikari and Raya, 2018).

$$P_t = \frac{P_s}{1+e^{-kt_m}} \tag{1}$$

where P_s is the saturation population, k is the growth rate, and t_m is the year in which half of the saturation population is reached (inflection point of the curve).

To find the best-fitting curve, the least squares method was used, in which the variables Ps , k, and tm are defined by minimizing the sum of the squared residuals between the observed values and those predicted by the model for each population data point (Miller, n.d.). The population data used in the fitting have irregular temporal variation and are composed of both observed (census) and modeled (DANE projections) data. Therefore, in the least squares fitting, a weighted adjustment was applied, where the weight equation p is given by:

$$p = r \times w \tag{2}$$

where r is the observational importance and w is the temporal importance for each value. The observational importance is an arbitrary value defined by the user. In this research, census data were assigned r=1 and DANE projections r=0.5. Temporal importance reflects the time interval that each data point represents and is given by the following equations:

$$w_0 = \frac{(t_1 - t_0)}{2\triangle t} \tag{3}$$

$$w_f = \frac{(t_f - t_{(f-1)})}{2\triangle t} \tag{4}$$

$$w_i = \frac{(t_{(i+1)} - t_{(i-1)})}{2\triangle t} \tag{5}$$

where w_0 is the temporal importance for the first observation, the w_f is the temporal importance for the last observation and the w_i is the temporal importance for the intermediate observations.

2.2.3 Calculation of Domestic Water Demand

The calculation of domestic water demand was based on the Water and Sanitation Regulation 330 of 2017 (Minvivienda, 2017), which stipulates a maximum net allocation of 130 liters per person per day (L/person**.**day) for elevations between 1200 and 2000 meters above sea level. The maximum gross allocation (Db) is given by the equation:

$$D_b = \frac{D_{\text{net}}}{(1-p)} \tag{6}$$

where D_{net} is the maximum net allocation, and represents the percentage of system losses, which must not exceed 25%.

According to EPM (2024a), the Loss Index, which includes both technical and commercial losses, was 35.18% for the 2023–2024 period. This actual value was used in the calculation of gross water demand. In the press briefing EPM (2024a), it was reported that the Riogrande II and La Fe reservoir are interconnected and supplie approximately 90% of the water demand in the Aburrá Valley, therefore the total domestic water demand (TDWD) is given by:

$$\text{TDWD} = 0.90 \times D_b \tag{7}$$

2.3 Water availability

2.3.1 Soil and Water Assessment Tool - SWAT+

SWAT (Soil and Water Assessment Tool Plus) is a widely used catchment-scale hydrological model designed to simulate long-term, continuous hydrological and land management processes (Arnold et al., 2012; Gassman et al., 2014). It is physically based and computationally efficient, simulating components such as surface runoff, infiltration, evapotranspiration, lateral and base flow, soil moisture dynamics, and groundwater recharge. Additionally, it models plant growth, nutrient and pesticide transport, pathogen movement, and land use practices (Arnold et al., 2012).

The model divides the landscape into Landscape Units (LSUs) based on topographic characteristics, which are further subdivided into Hydrologic Response Units (HRUs)—unique combinations of land use, soil, and slope used to simulate localized hydrological behavior. HRU outputs are aggregated at the LSU level, which facilitates more accurate representation of spatial heterogeneity and supports routing and concentration time estimation (Bieger et al., 2017).

While the original SWAT model allowed for some management actions such as reservoir operation and irrigation, it had limited flexibility (Neitsch et al., 2009), often requiring external coupling for complex scenarios. SWAT+, a restructured version, overcomes these limitations with a more flexible spatial framework and improved representation of management operations (Sánchez-Gómez et al., 2025).

A key innovation in SWAT+ is the decision table framework (Arnold et al., 2018), which triggers management actions based on specific simulation conditions. It also introduces a dedicated water allocation module, allowing detailed control of water transfers between model elements, critical for simulating irrigation, inter-basin transfers, and other interventions (Sánchez-Gómez et al., 2025).

Reservoir behavior is also more accurately modeled in SWAT+. Reservoirs are no longer confined to main channels or subbasin outlets; they can interact directly with various landscape elements and aquifers. This flexibility allows water to enter reservoirs from upstream reaches, lateral flows, or groundwater, improving the realism of water balance simulations (Bieger et al., 2017).

These advancements make SWAT+ a powerful and versatile tool for simulating both natural hydrological processes and human interventions. It addresses key limitations of earlier model versions and enhances decision-making in complex and evolving environmental and climatic contexts.

Model calibration and validation

Calibration was performed by selecting parameters related to runoff generation, soil properties, and aquifer processes, based on the SWAT+ documentation. Monthly streamflow calibration was carried out using the Dynamically Dimensioned Search (DDS) algorithm with 500 iterations (Tolson and Shoemaker, 2007), constrained within defined parameter ranges.

For the Riogrande II watershed, streamflow data from the two most important rivers in terms of flow contribution Río Chico and Puente Belmira gauging stations were used (Uribe et al., 2020; Valencia et al., 2024). Calibration was performed for the period 1997–2008, and validation for 2009–2015. For the La Fe watershed, Las Palmas station, which is the main natural contributor to the reservoir, was used, with calibration spanning 1993–1995 and validation in 1996 (Área Metropolitana del Valle de Aburrá, 2008).

All calibration procedures were conducted using the SWAT+ Toolbox v3.0.6. The streamflow curves were extracted from the figures of the mentioned studies using the tool automeris.io.

To evaluate the performance of the SWAT+ model in simulating streamflow, five statistical indicators were used: the coefficient of determination (R^2), the Nash–Sutcliffe Efficiency (NSE), the Root Mean Square Error (RMSE), the Percent Bias (PBIAS), and the Kling–Gupta Efficiency (KGE). These metrics provide complementary insights into the correlation, accuracy, and reliability of model outputs.

- Coefficient of Determination (R^2): R^2 assesses the strength of the linear relationship between observed and simulated values, ranging from 0 (no correlation) to 1 (perfect correlation). It is commonly used in hydrological modeling for assessing temporal correspondence between datasets (Krause et al., 2005) and it is given by:

$$R^2 = \left(\frac{\sum_{i=1}^{n} (Q_i^{\text{obs}} - \bar{Q}^{\text{obs}})(Q_i^{\text{sim}} - \bar{Q}^{\text{sim}})}{\sqrt{\sum_{i=1}^{n} (Q_i^{\text{obs}} - \bar{Q}^{\text{obs}})^2} \sqrt{\sum_{i=1}^{n} (Q_i^{\text{sim}} - \bar{Q}^{\text{sim}})^2}} \right) \tag{8}$$

  where Q is the streamflow, obs is the observation, sim is the simulated and the bar indicates de mean.

- Nash–Sutcliffe Efficiency (NSE): NSE measures how well the predicted time series matches the observed data. A value of 1 indicates a perfect fit, while values less than 0 suggest that the model performs worse than the mean of the observations (Nash & Sutcliffe, 1970):

$$\text{NSE} = 1 - \frac{\sum_{i=1}^{n} (Q_i^{\text{obs}} - Q_i^{\text{sim}})^2}{\sum_{i=1}^{n} (Q_i^{\text{obs}} - \bar{Q}^{\text{obs}})^2} \tag{9}$$

- Root Mean Square Error (RMSE): RMSE evaluates the average magnitude of model prediction errors. It is sensitive to outliers and is expressed in the same units as the variable being modeled (Willmott, 1981).

$$\text{RMSE} = \sqrt{\frac{1}{n} \sum_{i=1}^{n} (Q_i^{\text{obs}} - Q_i^{\text{sim}})^2} \tag{10}$$

- Percent Bias (PBIAS): PBIAS measures the average tendency of the simulated values to be larger or smaller than their observed counterparts. A value of 0 indicates a perfect match, while positive or negative values indicate systematic underestimation or overestimation, respectively (Moriasi et al, 2007).

$$\text{PBIAS} = 100 \frac{\sum_{i=1}^{n} (Q_i^{\text{obs}} - Q_i^{\text{sim}})}{\sum_{i=1}^{n} Q_i^{\text{obs}}} \tag{11}$$

- Modified Kling–Gupta Efficiency (KGE'): It was developed to overcome limitations of NSE by combining correlation, bias, and variability into a single metric (Gupta et al., 2009). Varying between -0.41 and 1, where the value of 1 indicates perfect agreement between simulated and observed data.

$$\text{KGE}' = 1 - \sqrt{(r-1)^2 + (\beta-1)^2 + (\gamma-1)^2} \tag{12}$$

  where r is the Pearson correlation coefficient, the β is the bias ratio and γ is the variability ratio.

Following the guidelines by Moriasi et al. (2007, 2015) (Table 2), NSE values above 0.50 are generally considered satisfactory, above 0.65 good, and above 0.75 very good for monthly streamflow. For PBIAS, values within ±25% are satisfactory, ±15% good, and ±10% very good. Similarly, RMSE is interpreted relative to the standard deviation of observed data, while R^2 values above 0.60 typically indicate acceptable correlation. For KGE, values greater than 0.75 are considered very good (Gupta et al., 2019; Kling et al., 2012), making it a robust alternative for integrated model evaluation.

Metric	Very good	Good	Satisfactory	Unsatisfactory
NSE	> 0.85	$0.70 < \text{NSE} \leq 0.80$	$0.50 < \text{NSE} \leq 0.70$	≤ 0.50
R^2	> 0.85	$0.75 \leq R^2 < 0.85$	$0.60 < R^2 \leq 0.75$	≤ 0.60
PBIAS	$\leq \pm 3.00$	$\pm 3.00 < \text{PBIAS} < \pm 10.00$	$\pm 10.00 \leq \text{PBIAS} \leq \pm 15.00$	$> \pm 15.00$
KGE'	> 0.80	$0.60 < \text{KGE'} \leq 0.80$	$0.40 < \text{KGE'} \leq 0.60$	< 0.40

Table 2. Performance rating criteria for model evaluation statistics used in hydrological modeling. Thresholds for NSE, PBIAS, RMSE, R^2, and KGE are based on the guidelines from Moriasi et al. (2007, 2015) and Knoben et al. (2019), with classifications of model performance ranging from unsatisfactory to very good.

Input data and parameters

The input data for topography, soil type, land use and land cover, and climate were obtained from various sources (Table 3). Slope classes were derived from a 12.5 m resolution Digital Elevation Model (DEM) from ALOS PALSAR (ASF DAAC, 2014) and categorized into five ranges: 0–5%, 5–15%, 15–40%, 40–60%, and >60%.

The soil map and its parametrization were based on the Digital Soil Open Land Map (DSOLMap), a global dataset with a 250 m resolution designed for compatibility with the SWAT+ model (López-Ballesteros et al., 2023). Although DSOLMap includes a six-horizon profile, the data were simplified to three horizons with a total depth of two meters to reduce model complexity and facilitate groundwater representation.

The land use and land cover map was sourced from MapBiomas Colombia Collection 1, with 30 m resolution data available annually from 2000 to 2020 (MapBiomas Colombia, 2024). Its parametrization was made using the default *plant* and *urban* database from SWAT+ (Appendix A). Climate data inputs included daily precipitation from CHIRPSv2, 0.05º resolution (Funk et al., 2015) and hourly temperature and solar radiation from ERA5, 0.25º resolution (Hersbach et al., 2023).

Climate data were interpolated to generate station-based time series. The number of virtual climate stations was defined relative to watershed area: one station per 20 km² for Riogrande II (53 stations total) and one per 3 km² for La Fe (27 stations). These were distributed to capture topographic and land-use variability across the watersheds (Figures 3 and 4).

Data	Description	Source
Digital Elevation Model	Elevation data at a resolution of 12.5 m	ALOS PALSAR
Soil type	Soil map of the Riogrande II and La Fe watersheds, 250 m resolution	DSOLMap
Land use/ Land cover	Annual land-use/land-cover maps (2000–2020), 30 m resolution	MapBiomas Colombia
Precipitation	Daily gridded data, 0.05º resolution	CHIRPSv2
Temperature and solar radiation	Hourly gridded data, 0.25º resolution	ECMWF (ERA5)

Table 3. SWAT+ input data

CHIRPSv2 was selected based on its acceptable performance in representing Colombian precipitation patterns compared to other products (Valencia et al., 2023). Hourly ERA5 temperature data were aggregated to derive daily minimum and maximum values. A lapse rate correction of -6.5 °C/km was applied to adjust temperature according to elevation. Solar radiation data were also converted to daily values based on hourly ERA5 input. Potential evapotranspiration (PET) was estimated using the Priestley–Taylor equation (Priestley & Taylor, 1972), and streamflow routing within the channel network was modeled using the Muskingum method (Chow et al., 1988).

2.3.2 Reservoir modeling

SWAT+ Limitations for Reservoir Management

SWAT+ includes enhanced capabilities for water resources management through features such as decision tables and a water allocation module. However, several limitations persist, particularly in the current implementation of the user interface and its ability to represent complex reservoir operations:

- Land-use dynamics: SWAT+ does not support the inclusion of one land use map per simulation year. Instead, land use changes must be modeled using decision tables, which only allow rule-based transitions of land use–soil combinations at the HRU level. This approach prevents the spatially explicit integration of land use changes generated by external models such as Dinamica EGO. As a result, the detailed spatial and temporal patterns produced by these models are lost, making it difficult to represent realistic land use dynamics and their hydrological impacts.
- Inflow representation constraints: SWAT+ does not allow for direct external inflows to reservoirs beyond what is routed from upstream subbasins. For instance, in the La Fe reservoir, additional water is pumped into the reservoir during dry months from neighboring catchments. Such engineered transfers cannot be modeled directly in the standard reservoir setup, limiting the model's ability to replicate operational realities.
- Temporal Resolution of Reservoir Operations: In SWAT+, reservoir outputs can be analyzed at daily, monthly, or yearly time steps. However, it was observed that daily release values sometimes exceeded flow rates that could be safely handled by the reservoir structure or the receiving river channel. In contrast, the corresponding monthly values were within expected operational limits. This suggests that while SWAT+ respects management constraints at the monthly scale, the daily outputs may not adequately reflect physical or operational limitations, indicating a limitation in the temporal disaggregation of reservoir releases.

Implemented Algorithm for Reservoir Simulation

Instead of dealing with the available reservoir management methods available in SWAT+, a customized reservoir program (`resv_dyn.py`) was written in python to perform a more precise calculation that includes: continuous changes in the water demand, continuous changes in the land use and realistic reservoir releases. The reservoir volume evolution is calculated daily from the water balance equation:

$$V_{n+1}=V_n+V_{\text{inflow},n}+V_{\text{pcp},n}-V_{\text{evap},n}-V_{\text{outflow},n}-V_{\text{withdraw},n}, \tag{13}$$

where V_n is the reservoir volume on the beginning of the n'th day and the remaining components correspond to sources and sinks of water during the n'th day. The resulting relation between one day and the next is a discrete dynamical system, or map, that allows to determine the daily evolution of the reservoir volume based on the conditions of each day. In the equation (13) V_{inflow} is the water inflow from the reservoir basin, V_{pcp} is the precipitation water directly over the reservoir, V_{evap} is the evaporated volume during the day, V_{outflow} is the released water if the reservoir level goes above some safety level and, finally, V_{withdraw} is the volume used to satisfy the total demand, which includes the ecologic demand, energy production and human consumption. The introduced map is then iterated from a known initial reservoir volume V_0 up to the desired number of projection days (N). Figure 6 presents the general overview of the resv_dyn module.

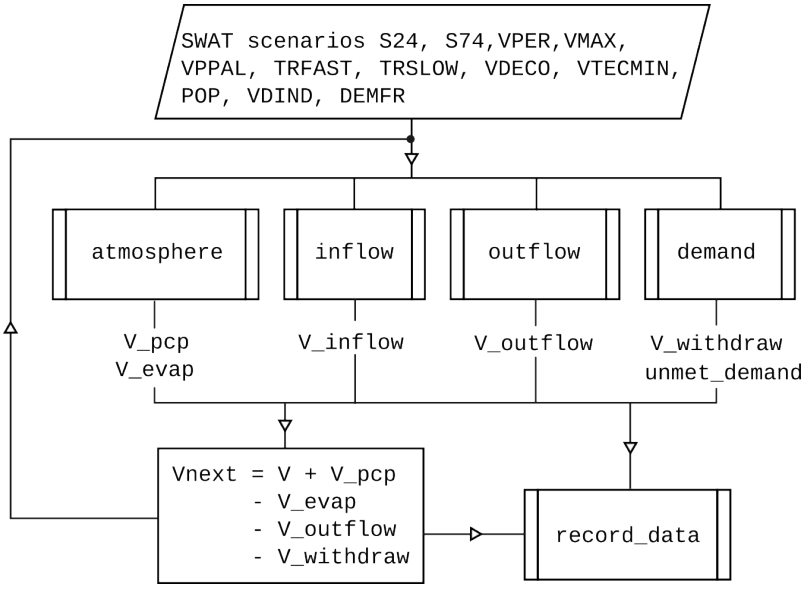

Figure 6. General overview of the `resv_dyn.py` module.

Water Inflow

The amount of water that arrives at the reservoir during the day can be calculated using SWAT+ for a given configuration of the land use, but it is difficult to consider changes in the land management in the simulation, as it requires a new setup for each configuration. Instead, we can calculate the inflow for every day in two fixed land-use scenarios S24 and S74, where S24 is the land use in 2024 and S74 is the projected land use in 2074, then we can average the n'th day water inflow as

$$V_{\text{inflow},n} = \left(\frac{N-n}{N}\right) V_{\text{inflow},n}(S24) + \left(\frac{n}{N}\right) V_{\text{inflow},n}(S74) + V_{\text{extra_inflow},n}, \tag{14}$$

where N is the total number of days to be projected in the simulation. This equation smoothly transitions between the current and final inflows without abrupt changes in the land use configuration emulating a smooth transition in the land use management without the need to discretize the evolution in shorter periods.

The additional term $V_{\text{extra_inflow}}$ accounts for additional artificial inflows like pumped water from a lower basin or channel. In the case of a pump system, the number of pumping units depends on the current level of the reservoir and availability of the lower source. Two stages operation scenario were considered: (I) The reservoir volume is below VTECMIN and a strong pumping is used, and (II) the reservoir is below VPPAL and a slow pumping is used

$$V_{\text{extra_inflow}}(\text{I}) = \text{VPIN_FAST}, \tag{15}$$
$$V_{\text{extra_inflow}}(\text{II}) = \text{VPIN_SLOW}. \tag{16}$$

When the reservoir level is below the technical minimum, the natural basin inflow is not being able to sustain the reservoir level against the water demand and the system is likely to enter in a failure mode. The pumping system is dimensioned so that the combined action of the pumping and the natural inflow enhance the capacity of the reservoir to supply the demand. Figure 7 presents the overview of the inflow algorithm.

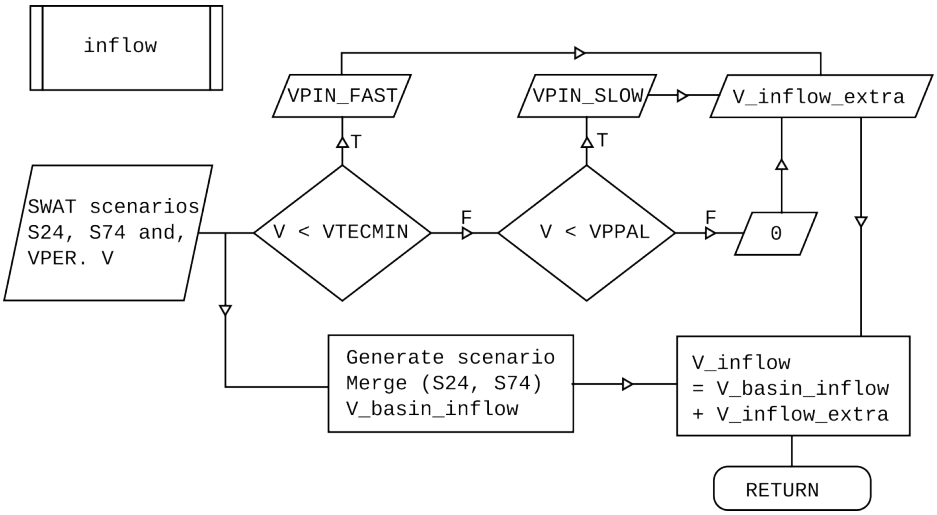

Figure 7. Overview of the Inflow subroutine, part of `resv_dyn.py` module.

Precipitation and Evaporation

Are simply obtained by multiplying the accumulated precipitation/evaporation during the day (m) by the current reservoir area (m^2).

Since the total evaporated and precipitated volumes must be obtained from the climatic data, then, a simple reservoir simulation is performed with SWAT+. Since the reservoir module only returns total volumes (m^3), the accumulated values (in m) are obtained by dividing the total volumes by the total simulation reservoir area, then the resulting values are used to calculate the precipitation/evaporation total volume for the corresponding area in resv_dyn.py on each simulation day.

Outflow

For the outflow calculation three scenarios are considered (see Table 5 for volume definitions): (I) The reservoir volume is below the principal volume, (II) The reservoir volume is above the principal volume and below 95% of the maximum volume and (III) The reservoir volume is above 95% of the maximum volume. In scenario (I) there is no outflow, as the reservoir volume must increase to achieve its principal value (VPPAL). In the scenarios (II) and (III) the outflow is calculated by setting a corresponding recovery time (in days) for the reservoir to reach the principal value

$$V_{\text{outflow}}(\text{II}) = \frac{V_n - \text{VPPAL}}{\text{TRSLOW}}, \tag{17}$$

$$V_{\text{outflow}}(\text{III}) = \frac{V_n - \text{VPPAL}}{\text{TRFAST}}, \tag{18}$$

where TRSLOW was set to 2 days of recovery and TRFAST to 1 day. Notice that in scenario (III) the time is shorter to prevent reservoir overflow in the case of strong precipitations as the volume is close to the reservoir maximum. Since the other components of the water balance are not included in this calculation it is not expected that the system will return to the principal volume in the defined number of days, it can take more or less time depending on the current watershed inflow and precipitation. Figure 8 shows a overview of the algotrithm of outflow/releases from the Reservoir Module.

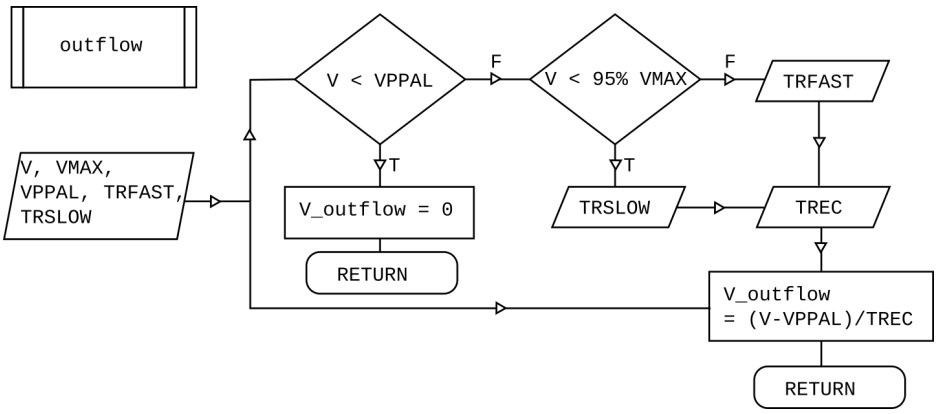

Figure 8. Overview of the Outflow subroutine, part of `resv_dyn`.py module.

Withdrawal

The withdrawal calculation is a little more involved, as it must take into account the water demand and the reservoir status. There are three scenarios of interest: (I) The reservoir is above the technical minimum (VTECMIN), (II) The reservoir is below the technical minimum and above the permanent volume, and (III) The reservoir is below the permanent volume (VPER). The base demand from the reservoir has the form

$$\text{base_demand}=\text{VDECO}+\text{DEMFR}\times\text{POP}\times\text{VDIND}+\text{EXTRA_OUT}, \tag{19}$$

where VDECO is the daily ecological volume, DEMFR is the fraction of the city demand satisfied by the reservoir, POP is the total population and VDIND is the individual daily demand. The extra outflow EXTRA_OUT includes known demands for other uses or unspecified populations connected to the reservoir. There are tabulated values for the individual daily demand that take into account human needs and network losses, however they do not consider other uses that take place from economic activities or city maintenance. These activities are nonetheless related to the current population levels, as more population directly affects the level of economic and maintenance activities. To determine a realistic value of VDIND, reference values obtained from the operation of the potabilization plant are used with the known value of DEMFR. For instance, consider that the population and operation of the plant are known at some point in time (POP_REF, DEMAND_REF), then, VDIND can be obtained from the previous equation at that moment in time

$$\text{VDIND}=\frac{\text{OPER_REF}}{\text{POP_REF}\times\text{DEMFR}}. \tag{20}$$

Depending on the reservoir level there are two different levels of energy production so as to prioritize human consumption over energy production.

$$\begin{aligned}
\text{demand(I)} &= \text{base_demand}+\text{reg_erg_demand_day}, &(21)\\
\text{demand(II)} &= \text{base_demand}+\text{min_erg_demand_day}, &(22)\\
\text{demand(III)} &= \text{base_demand}+\text{min_erg_demand_day}, &(23)
\end{aligned}$$

where reg_erg_demand_day is the volume of water to satisfy the regular energy demand and min_erg_demand_day is some volume of water to satisfy a lower energy demand when the energy production can compromise the water treatment. When the reservoir falls below the permanent level the withdrawal can not occur, in that case the required volume becomes an unmet demand

$$\begin{aligned}
V_{\text{widthdraw}}(\text{I}) &= \text{demand(I)}, &(24)\\
V_{\text{widthdraw}}(\text{II}) &= \text{demand(II)}, &(25)\\
V_{\text{widthdraw}}(\text{III}) &= 0, &(26)\\
V_{\text{unmet}} &= \text{demand(III)}, &(27)
\end{aligned}$$

Although the evolution is calculated daily, the results are later added to express them on a monthly basis that is more useful in an engineering setting. Figure 9 shows a overview of the algotrithm of outflow/releases from the Reservoir Module.

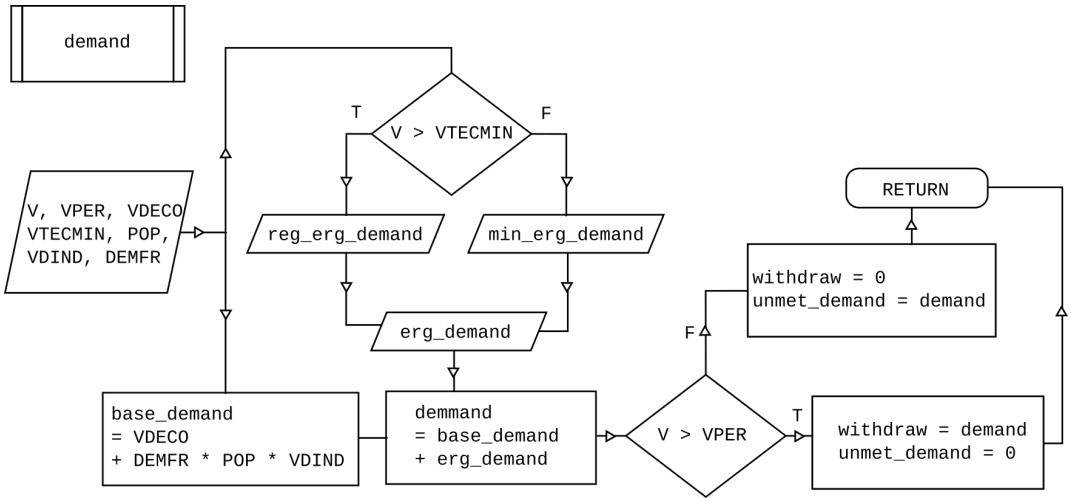

Figure 9. Overview of the Demand subroutine, part of `resv_dyn.py` module.

The implementation in python of the Reservoir Dynamics module are provided in Appendix B.

Reservoir configuration

The Riogrande II and La Fe reservoir systems are interconnected through the supply network. Each reservoir supplies a different water treatment plant (WTP), but the treated water is distributed via an integrated urban supply system that serves the Aburrá Valley. Figure 10 illustrates the operational structure of the system.

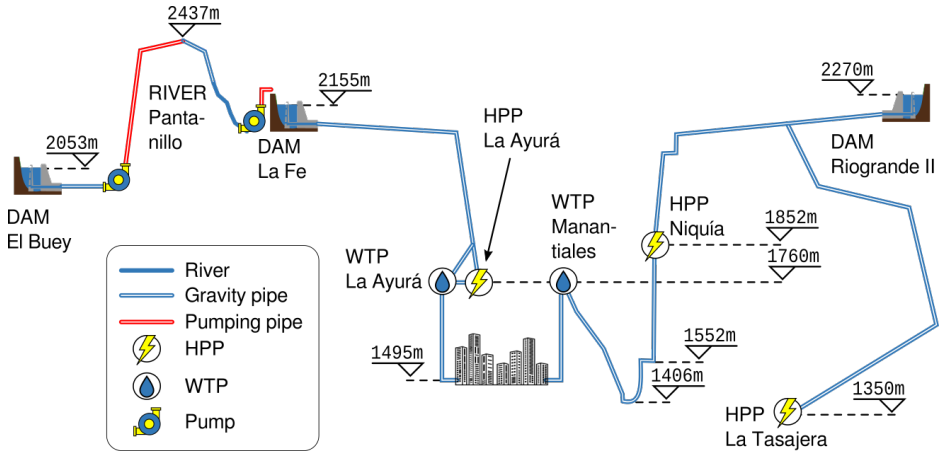

Figure 10. Diagram of Riogrande II and La Fe reservoir systems. Adapted from Superintendencia de Servicios Domiciliarios (2021).

As shown in Figure 10, water from the Riogrande II reservoir is withdrawn through two main outlets. One flow is directed to the La Tasajera hydropower plant (HPP) and then discharged into the Medellín-Aburrá River. Another withdrawal supplies the Niquía HPP and subsequently flows to the Manantiales WTP, which distributes treated water to the Aburrá Valley (Superintendencia de Servicios Públicos Domiciliarios, 2021).

The Riogrande II reservoir relies entirely on natural inflows from its own watershed. In contrast, the La Fe reservoir depends on a more complex system involving inter-basin water transfers based on pumping infrastructure. Water is first diverted from the El Buey reservoir through a tunnel into the Piedras River. From there, it is pumped into the Pantanillo River, where up to 6 m^3/s can be further pumped directly into the La Fe reservoir (Superintendencia de Servicios Públicos Domiciliarios, 2021).

Water withdrawn from the La Fe reservoir passes through the La Ayurá HPP before reaching the La Ayurá WTP, which supplies treated water to the regional distribution network.

Water withdrawal from each reservoir was governed by operational rules reflecting storage-dependent management. Withdrawals are computed at the end of each daily time step. Water uses for both reservoirs include energy generation, human consumption, and environmental flow, summarized in Table 4.

Reservoir	Use	Normal operation (m^3/s)	Exceptional operation (m^3/s)
Riogrande II	Energy generation	26.50	13.25
	Human consumption	4.30	4.30
	Environmental flow	13.27	13.27
	Total	**44.07**	**30.82**
La Fe	Energy generation	5.20	5.20
	Human consumption	5.20	5.20
	Environmental flow	4.35	4.35
	Total*	**9.55**	**9.55**

Table 4. Summary of water uses and allocation thresholds for the Riogrande II and La Fe reservoirs, including withdrawals for energy generation, human consumption, and environmental flow (CORANTIOQUIA, 2015; CORNARE, 2023; EPM, 2023; Superintendencia Servicios Públicos Domiciliarios, 2021). *The non-environmental flow for La Fe Reservoir goes through the energy generation stage and later enters the treatment facility (so it only is counted once), while in the Riogrande II reservoir the flow is split for these usages.

In Table 4 are presented two scenarios of operation for Riogrande II, varying in the water flow used to generate energy generation. The information required to configure volumes and areas of the Riogrande II and La Fe reservoirs is summarized in Table 5. These data was derived from bathymetric studies conducted by Empresas Públicas de Medellín (CNO, 2025; EPM, 2015; EPM, 2019). Since no information was available on the initial reservoir volumes at the simulation start date, it was assumed that the reservoirs began at 80% of principal storage capacity.

Parameters	Description	Riogrande II reservoir	La Fe reservoir
Principal Volume (Mm^3)	Volume of water needed to fill the reservoir toprincipal spillway	185.26	11.33
Principal area (ha)	Reservoir surface area when reservoir is filled to principal spillway	980.00	126.00
Emergency volume (Mm^3)	Volume of water needed to fill the reservoir to emergency spillway	235.99	13.53
Emergency area (ha)	Reservoir surface area when reservoir is filled to emergency spillway	1152.00	138.00
Initial volume (Mm^3)	Reservoir volume at the beginning of simulation	148.21	9.06

Table 5. Summary of configuration parameters for the Riogrande II and La Fe reservoirs. The data were obtained from bathymetric studies conducted by Empresas Públicas de Medellín (CNO, 2025; EPM, 2015; EPM, 2019).

2.3.3 Land use and land cover scenarios

DinamicaEGO

The land use and land cover (LUCC) data used in this study were generated by modeling LUCC dynamics for the Riogrande II and La Fe watersheds using Dinamica EGO (Environment for Geoprocessing Objects). This free, user-friendly platform allows the construction of spatially explicit environmental models—ranging from simple to highly complex—through a graphical interface. It

integrates standard GIS functions with specialized land change simulation tools, such as cellular automata and calibration algorithms. While Dinamica EGO offers high flexibility and performance, it may simplify underlying processes (Almeida et al., 2008, Soares-Filho et al., 2013, Soares-Filho et al., 2013, Rodrigues & Soares-Filho, 2018). To model the land use and land cover of the Riogrande II and La Fe watersheds it was used the land use change algorithm as described in the documentation, MODULE VIII (Leite-Filho et al., 2020).

Input Data

The MapBiomas Colombia Collection 1, released in November 2023, provides annual LUCC maps from 1985 to 2022 at 30-meter resolution. These maps were created using pixel-by-pixel Landsat classification and machine learning in Google Earth Engine (MapBiomas Colombia, n.d.). The dataset includes two hierarchical levels: Level 1 with five general LUCC classes and Level 2 with 18 detailed classes. For Level 2, the overall classification accuracy is 91.2%, with 6.3% assignment disagreement and 2.5% area disagreement (MapBiomas Colombia, n.d.).

For this study, the period 2000–2020 was selected for calibration and validation to reflect recent land change dynamics. Eight Level 2 classes were present in at least one study area: Forest, Pinus, Other Non-Forest Formation, Mosaic of Agriculture and Pasture, Urbanization, Other Non-Vegetated Cover, Mining, and Water Bodies.

Calibration and Validation

Calibration begins with defining a transition matrix (TM), which quantifies how LUCC classes change over time. Each column represents the current class and each row the probability of changing to another class. The matrix can represent single or multiple time steps. In this study, a yearly multi-step TM with 20 steps was generated to translate the observed changes of the period 2000-2020.

The next step involves computing Weights of Evidence (WoE), a Bayesian approach adapted to LUCC modeling to assess the influence of spatial variables on specific transitions (e.g., deforestation from forest to agriculture). Variables such as slope, elevation, and distance to roads are categorized, and weights are assigned based on their association with change. Positive weights suggest increased likelihood; negative, reduced likelihood; and values near zero, no effect (Leite-Filho et al., 2020). For the present study, it was considered the effect of slope, soil, and municipality limits.

WoE relies on spatial independence between variables. To verify this, tests such as Chi-square, Cramer's V, and Joint Uncertainty Information were used. If correlated, variables were either excluded or combined. Transition probability maps were generated from the weights and used to calibrate the model.

For validation, cross-tabulation was used to compare observed and simulated maps to assess classification accuracy. This method provides overall, user's, and producer's accuracy (García-Álvarez et al., 2022):

- Overall Accuracy: proportion of correctly classified pixels.
- User's Accuracy: likelihood that a pixel labeled as a class on the map truly belongs to it (commission error).
- Producer's Accuracy: probability that a reference pixel was correctly classified (omission error).

For change detection, the Figure of Merit (FoM) quantifies spatial agreement between observed and simulated LUCC maps, ranging from 0% (no agreement) to 100% (perfect match):

$$\text{FOM}=\frac{B}{A+B+C+D} \tag{28}$$

where A are the observed change not simulated (misses), B are the correctly simulated change (hits), C are the wrong change category (wrong hits) and D are the simulated change not observed (false alarms).

Cross-tabulation and accuracy metrics were computed using the Semi-Automatic Classification Plugin in QGIS, following procedures described in Land Use Cover Datasets and Validation Tools, Chapter III (García-Álvarez et al., 2022).

To complement the validation process, a multiple-window similarity analysis was applied. This method uses a decay function (e.g., exponential or constant) across varying spatial windows to evaluate the similarity between simulated and observed changes. Unlike pixel-to-pixel comparisons, it assesses agreement based on the number of changed cells within a window, regardless of their exact location. This approach allows for the evaluation of model performance at different spatial resolutions, making it particularly valuable when analyzing high-resolution maps, as is the case in this study (Leite-Filho et al., 2020).

In Dinamica EGO, this analysis is implemented using a fuzzy similarity algorithm based on the method proposed by Hagen, 2002. In this study, a constant decay function was selected, meaning that any correspondence between observed and simulated changes within the analysis window is considered an agreement, regardless of the specific location of the changes within that window.

2.3.4 Climate change scenarios

The GFDL-CM4 model was selected for this study due to its demonstrated ability to reasonably simulate both seasonal precipitation and near-surface air temperature patterns in Colombia (Arias et al., 2021; Ortega et al., 2021). GFDL-CM4 is one of the few models consistently identified as providing realistic simulations of the seasonal behavior of both variables, which is particularly relevant for hydrological studies. These findings align with broader assessments of CMIP6 models in Central and South America, where GFDL-CM4 has been highlighted for its improved representation of seasonal climate dynamics compared to CMIP5.

Daily near-surface temperature (maximum and minimum), precipitation and solar radiation outputs from GFDL-CM4 were obtained at a spatial resolution of $1° \times 1°$ from the Earth System Grid Federation (ESGF) (Adcroft et al., 2019). These data were extracted for nine grid cells covering the study watershed, and used for further processing and bias correction.

The SSP-RCP framework combines Shared Socioeconomic Pathways (SSPs), which describe plausible future socio-economic developments, with Representative Concentration Pathways (RCPs), which represent distinct levels of radiative forcing by 2100. These scenarios provide a coherent framework for projecting future climate conditions, integrating assumptions about population growth, technological change, land use, and climate policy (IPCC, 2024).

While widely adopted, the SSP-RCP framework also has limitations, including simplified assumptions about global cooperation, uniform reductions in ozone-depleting substances, and limited representation of non-CO_2 greenhouse gases, aerosols, and ocean-atmosphere interactions. These factors can influence the precision of long-term projections (IPCC, 2024).

This research used two climate change scenarios from the CMIP6 framework: SSP2-4.5 and SSP5-8.5. The SSP2-4.5 scenario represents a stabilization pathway, with greenhouse gas (GHG) emissions peaking around mid-century and a radiative forcing of 4.5 W/m^2 by 2100. It reflects a future of moderate societal vulnerability and mitigation. In contrast, SSP5-8.5 represents a high-emissions trajectory with continued fossil-fuel-driven economic growth and minimal climate policy implementation, resulting in 8.5 W/m^2 of radiative forcing by 2100. These scenarios were selected to capture a plausible range of future climate conditions, from intermediate to extreme warming, and are widely used in CMIP6-Endorsed Model Intercomparison Projects (MIPs) (O'Neill et al., 2017; IPCC, 2023).

These two climate change scenarios were compared to a Reference scenario, that is simply the 'paste and copy' of the historical records of precipitation, temperatures and solar radiation.

Bias correction

Statistical bias correction aims to adjust systematic deviations in climate model outputs using empirical relationships derived from historical observations and simulations. The correction model was trained using a historical reference period of 1994–2023, during which both observed and simulated data were available. Since future observations do not exist, the method assumes stationarity—that the statistical relationship between observed and modeled series remains constant over time (Lehner et al., 2021). This assumption should be considered when interpreting future projections. For this study, bias correction was applied to daily precipitation, maximum temperature, minimum temperature and solar radiation over the grid cells covering the study watershed.

Several techniques exist for statistical bias correction, from simple mean adjustments to more complex methods like quantile mapping. For this study, the Quantile Delta Mapping (QDM) method was selected (Cannon et al., 2015), as it corrects the full distribution while preserving the climate change signal across quantiles, including extremes. This is particularly important for hydrological applications sensitive to changes in precipitation variability and temperature extremes.

The correction was implemented using the QuantileDeltaMapping function from the *xclim* python library (Bourgault et al, 2023). This function adjusts each quantile based on empirical cumulative distribution functions (CDFs) of historical observations and model outputs, ensuring consistency in corrected future time series. The bias-corrected daily series were subsequently used as inputs for hydrological simulations to evaluate the performance of the regional reservoir system under projected climate change scenarios.

2.3.5 Modeling scenarios

Given the ability of the *resv_ dyn.py* program to generate a curve that transitions between the land use scenarios of 2024 and 2074, it is possible to produce a curve for each climate scenario. Therefore, the simulation scenarios (Table 6) combine two land use scenarios: 2024 and 2074, with three climate scenarios: a reference scenario (R), SSP2-4.5 (M, for Moderate), and SSP5-8.5 (E, for Extreme), which the last two are based on the GFDL-CM4 climate model. The reference climate scenario consists of repeating the observed period (1994–2023) up to the year 2074.

Climate \ Land use	**2024**	**2074**
Reference	R24	R74
Moderate (SSP2-4.5)	M24	M74
Extreme (SSP5-8.5)	E24	E74

Table 6. Land use and climate change scenarios.

The outputs of interest focus on reservoir dynamics, including inflow, storage, outflow, withdrawal, and unmet demand. Using the unmet demand time series, the Reliability, Resilience, and Vulnerability indices were calculated.

2.4 Reliability, Resilience and Vulnerability framework

To evaluate the performance of the reservoir system over the study period (2024–2074), the Reliability, Resilience, and Vulnerability (RRV) framework was applied using daily time steps. The RRV indexes are defined by Hashimoto, 1982:

- Reliability was calculated as the proportion of days in which the reservoir storage met or exceeded the water demand. This indicator reflects the frequency with which the system performs satisfactorily and is a primary measure of operational success under changing conditions.

$$\text{Rel}=1-\frac{\sum_{j=1}^{M} d(j)}{T} \tag{29}$$

  where d (j) is the duration of the jth failure event, M is the number of failure events, and T is the total duration of the observation.

- Resilience was defined as the ratio of recovery events (i.e., transitions from failure to success) to the total number of failure events. This index captures the system's ability to recover from unsatisfactory conditions and reflects its capacity for adaptation over time.

$$\text{Res}=\left[\frac{1}{M}\sum_{j=1}^{M} d(j)\right]^{-1}, \tag{30}$$

  where again $d(j)$ is the duration of the j'th failure event and M is the total number of failure events. It is important to note that, both for no-failure events and for events in which the system recovers within one day, Resilience is equal to 1.

- Vulnerability was assessed using the average deficit volume observed during any failure day, the typical severity of failures, without replacing the maximum as the primary vulnerability indicator.

$$\text{Vul}=\frac{1}{M}\sum_{j=1}^{M} v(j), \tag{31}$$

where $v(j)$ is the deficit volume of the j'th failure event.

This combination of performance metrics balances interpretability, statistical robustness, and relevance to water resources risk assessment. It aligns with recent methodological recommendations that emphasize the importance of avoiding redundant or non-monotonic estimators in RRV analyses, while retaining metrics that capture both extreme events and representative system behavior (Hashimoto et al., 1982; Kjeldsen & Rosbjerg, 2009).

3 Results

3.1 Water demand

Figure 11 shows the demographic projections for each municipality in the Aburrá Valley, as well as the total population of the region. The logistic growth model fitted the observed census data and the official projections from DANE satisfactory, as indicated by the R^2 values, equal or superior to 0.97, presented in Table 7.

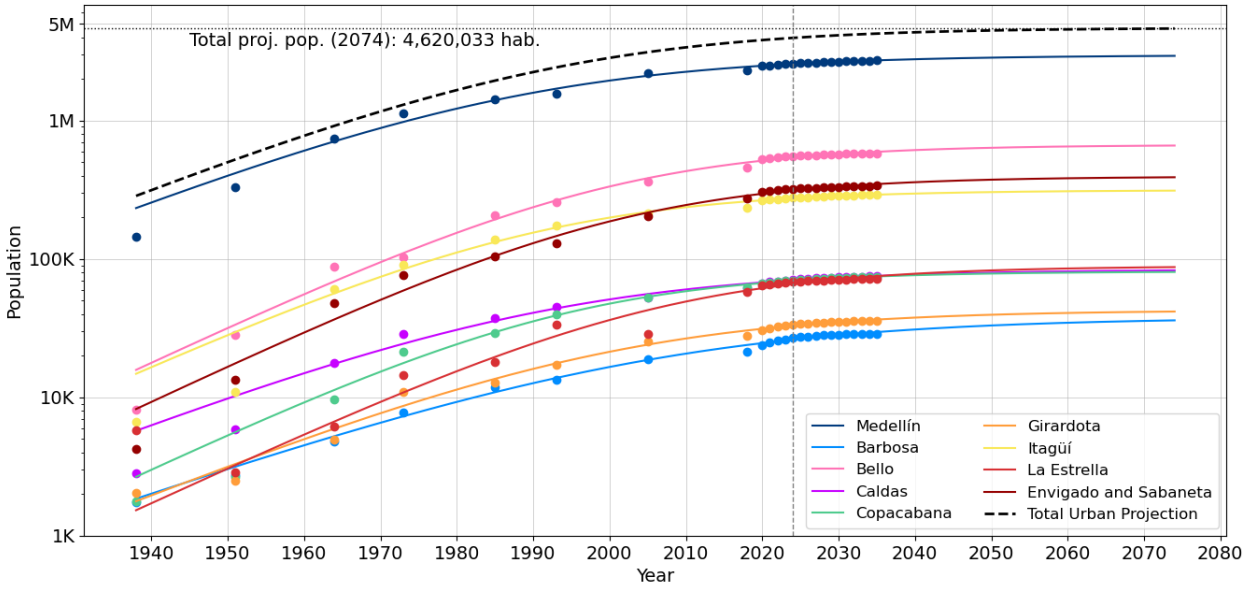

Figure 11. Demographic growth for the Aburrá Valley municipalities projected from 2024 to 2074.

Municipality	R^2	Psat	k	t_m
Medellín	0.99	2,969,971	0.05	1987
Barbosa	0.99	37,788	0.04	2005
Bello	0.99	667,174	0.05	2000
Caldas	0.99	84,116	0.05	1991
Copacabana	0.99	81,194	0.06	1994
Girardota	0.99	42,681	0.05	1999
Itagüí	0.99	314,136	0.05	1990
La Estrella	0.97	88,894	0.05	2006
Envigado and Sabaneta	0.99	394,102	0.06	2001

Table 7. Fitted parameters of Logistic Model for the municipalities of Aburrá Valley.

According to Figure 11, Medellín remains the most populous municipality in the valley, with a projected population of 2,931,774 inhabitants (65.5% of the total) by 2074, followed by followed with ample margin by Bello, with 659,387 inhabitants (14.3%) at the end of the study period. According to the fitted parameters presented in Table 7, these two municipalities will be close to reaching the saturation population by 2074, 2,696,971 and 667,174 inhabitants, respectively. Envigado and Sabaneta surpassed Itagüí around 2005 and exhibited a combined population growth rate of 24.52% throughout the projection period.

Barbosa and La Estrella display the highest growth rates among the municipalities, with 37.78% and 32.77%, respectively. In contrast, the lowest growth rates are observed in Itagüí (13.72%), Medellín (14.40%), and Copacabana (15.78%).

By the end of the projection period in 2074, the total population of the Aburrá Valley is expected to reach 4,620,033 inhabitants, reflecting a cumulative growth of 16.88%. According to municipal projections from DANE (2023), the region's population in 2024 was approximately 3,992,029 inhabitants. These results suggest that the Aburrá Valley is approaching a saturation point in the population growth.

Based on the estimated maximum net water demand per capita and the system's water loss rate, the gross annual water demand per inhabitant was calculated following the RAS 330/2017 standard:

$$D_b = \frac{D_{\text{net}}}{1-p} = \frac{130}{1-0.35} = 200\,\frac{l}{\text{hab day}} = 73\,\frac{m^3}{\text{hab yr}}$$

from which the total domestic demand is

$$\text{Total domestic demand} = 0.9 \times D_b = 65.7\,\frac{m^3}{\text{hab yr}}$$

The total domestic water demand was then multiplied by the annual population projections to estimate the total gross water demand for the Aburrá Valley. Figure 12 presents the projected total annual demand for the Aburrá Valey and its municipalities.

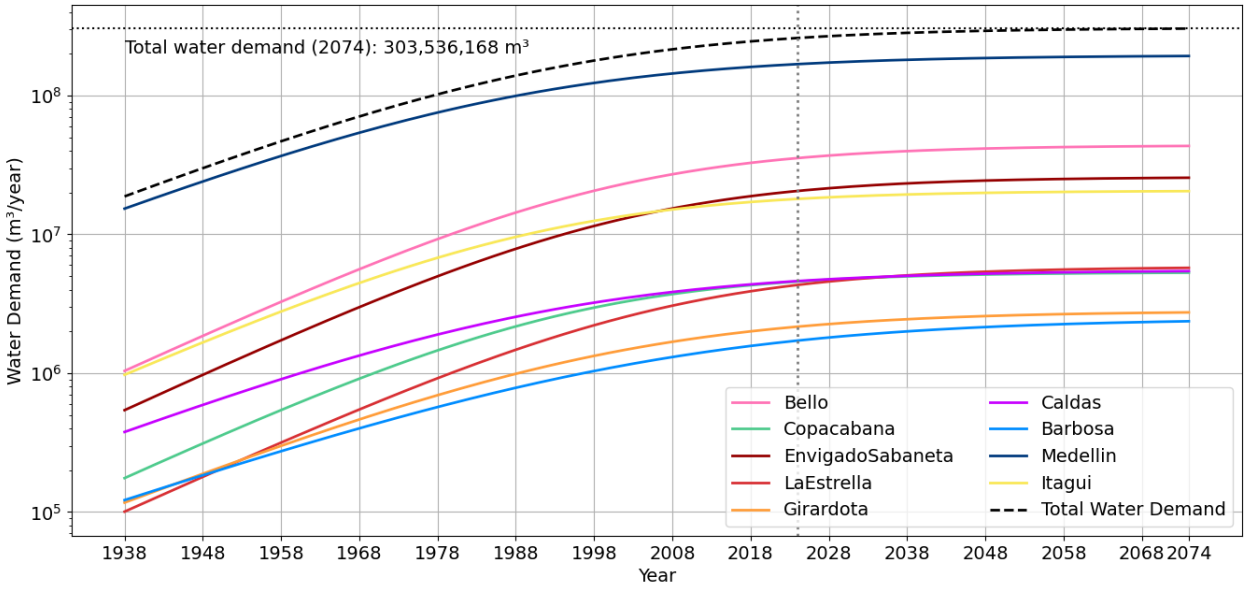

Figure 12. Total domestic water demand for the Aburrá Valley municipalities projected from 2024 to 2074.

Since the domestic water demand is calculated using the population projections, the curves in Figure 11 present the same behaviour observed in Figure 12. By 2074, the annual domestic water demand in the Aburrá Valley is expected to reach 303,536,168 m³. Since the population projection is already approaching the saturation value, domestic water demand is expected to increase slightly over the study period.

To determine the Aburrá Valley real-time water demand, it was developed a reservoir dynamics simulator based on the daily water balance between the different hydrological components and the total water withdrawal (resv_dyn python module, Appendix B). The withdrawal includes the WTP treatment flow and the environmental flow.

For the year 2024, the nominal treatment flow of WTP Manantiales was 4.3 m^3/s, responsible for supplying 40% of the Aburrá Valley demand (EPM, 2024a), for a corresponding region population of 3,952,868 inhabitants. Using Equations (20) and (19), the individual demand can be calculated based on the WTP production rate at the given population level:

$$\begin{aligned} \text{VIND} &= \frac{\text{OPER_REF}}{\text{POP_REF}\times\text{DEMFR}}, \\ \text{VIND} &= \frac{4.3\,\text{m}^3/\text{s}}{3{,}952{,}868\,\text{hab}\times 0.4} = \frac{371{,}520\,\text{m}^3/\text{day}}{1581147.2\,\text{hab}} = 0.23\,\frac{m^3}{\text{hab}\times\text{day}}. \end{aligned}$$

Which can then be used to determine the total population demand at any time by multiplying by the projected population. Considering a environmental flow of 13.27 m^3/s and the projected population in 2074, the base demand of Riogrande II reservoir is

$$\begin{aligned} \text{base_demand} &= \text{VDECO}+\text{DEMFR}\times\text{POP_REF}\times\text{VIND}+\text{EXTRA_OUT}, \\ \text{base_demand}(2074) &= 1{,}146{,}528\,\frac{m^3}{\text{day}}+0.4\times 4{,}620{,}033\,\text{hab}\times 0.23\,\frac{m^3}{\text{day}}+0 \\ &= 1{,}571{,}571.04\,\frac{m^3}{\text{day}}, \end{aligned}$$

so that the total annual volume is

$$\text{total_volume}(2074) = 573{,}623{,}428.1\,\text{m}^3.$$

Analogously, for La Fe reservoir, the WTP treatment plant in 2024 was 5.5 m^3/s, supplying water for 50% of the region, with an environmental flow of 4.35 m^3/s (EPM, 2024a) and an additional outflow of 0.6 m^2/s to supply water for the San Nicolás Valley (Appendix E). The daily individual water demand takes the form

$$\begin{aligned} \text{VIND} &= \frac{\text{OPER_REF}}{\text{POP_REF}\times\text{DEMFR}}, \\ \text{VIND} &= \frac{5.5\,\text{m}^3/\text{s}}{3{,}952{,}868\,\text{hab}\times 0.5} = \frac{475{,}200\,\text{m}^3/\text{day}}{1{,}976{,}434\,\text{hab}} = 0.24\,\frac{m^3}{\text{hab}\times\text{day}}. \end{aligned}$$

Leading to the total base demand of the reservoir for 2074

$$\begin{aligned} \text{base_demand} &= \text{VDECO}+\text{DEMFR}\times\text{POP_REF}\times\text{VIND}+\text{EXTRA_OUT}, \\ \text{base_demand}(2074) &= 375{,}840\,\frac{m^3}{\text{day}}+0.5\times 4{,}620{,}033\,\text{hab}\times 0.24\,\frac{m^3}{\text{day}}+51{,}840\frac{m^3}{\text{day}} \\ &= 982{,}083.96\,\frac{m^3}{\text{day}}, \end{aligned}$$

so that the total annual volume is

$$\text{total_volume}(2074) = 358{,}460{,}645.4\,\text{m}^3.$$

Therefore, the total base demand for 90% of the Aburrá Valley in 2074 is 932,084,073.5 m³, approximately three times that of the total domestic demand for the same year. To the base demand it was added to the energy generation demand, depending on the reservoir's storage volume. The results are presented in Section 3.3.

3.2 Water availability

3.2.1 SWAT+ calibration and validation

The calibrated parameters of monthly streamflow calibration using the Dynamically Dimensioned Search (DDS) algorithm after 500 iterations are presented in Table 8. The resulting calibration metrics are discused along with the results.

Parameter	Change type	Riogrande II	La Fe
alpha	Replace	0.01	0.01
revap_min	Replace	0.00	0.01
flo_min	Replace	24.76	3.32
revap_co	Replace	0.04	0.03
sp_yld	Replace	-	0.28
awc	Relative	-30.00	10.00
k	Relative	21.05	20.00
cn2	Relative	30.00	20.00
ovn	Relative	-23.08	-20.00
cn3_swf	Replace	1.00	0.97
esco	Replace	0.09	0.76
epco	Replace	0.45	-
perco	Replace	0.73	0.37
petco	Replace	-	1.04
lat_len	Relative	-40.00	4.67
surlag	Replace	3.54	1.55

Table 8. Calibrated parameters for the SWAT+ model for both hydrographic basins.

Figures 13 and 14 show the calibration and validation results of the SWAT+ model for the Riogrande II reservoir watershed, using the Puente Belmira and Río Chico gauging stations, respectively.

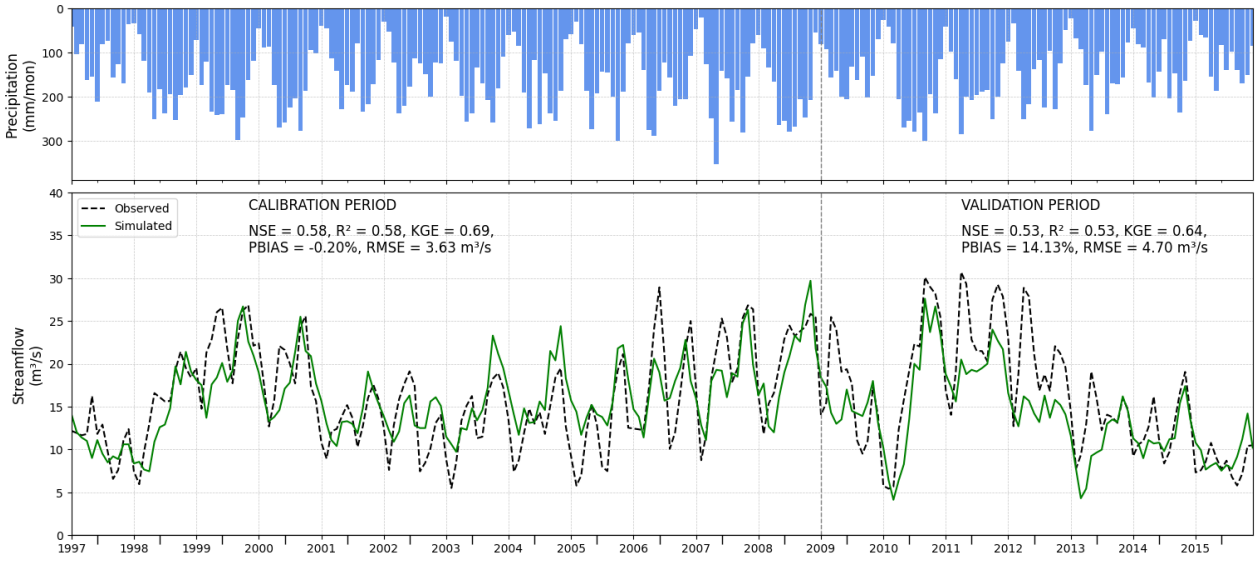

Figure 13. Calibration (1997–2008) and validation periods (2009–2015) of SWAT+ for monthly streamflow of Puente Belmira gauge station, basin Riogrande II reservoir.

According to the Figure 13 performance classification proposed by Moriasi et al. (2007, 2015), model calibration at Puente Belmira station is considered "unsatisfactory" (NSE = 0.58; R^2 = 0.58), "good" performance considering KGE = 0.69, and "very good" based on a PBIAS of -0.20%. The root mean square error (RMSE) during calibration was 3.63 m^3/s. During validation, model performance had slight variations: NSE and R^2 decreased to 0.53, KGE decreased to 0.64, while PBIAS increased to 14.13%. RMSE increased to 4.70 m^3/s.

At the Río Chico station (Figure 14), model performance during calibration is classified as "unsatisfactory" with NSE and R^2 equal to 0.47, "good" as KGE = 0.59 and PBIAS = 9.33%. The RMSE is 1.44 m^3/s. In the validation period, the performance metrics slightly change since NSE and R^2 are equal to 0.51 ("satisfactory"), KGE increased to 0.62 ("good"), PBIAS increased to 17.69% and RMSE was 1.62 m^3/s.

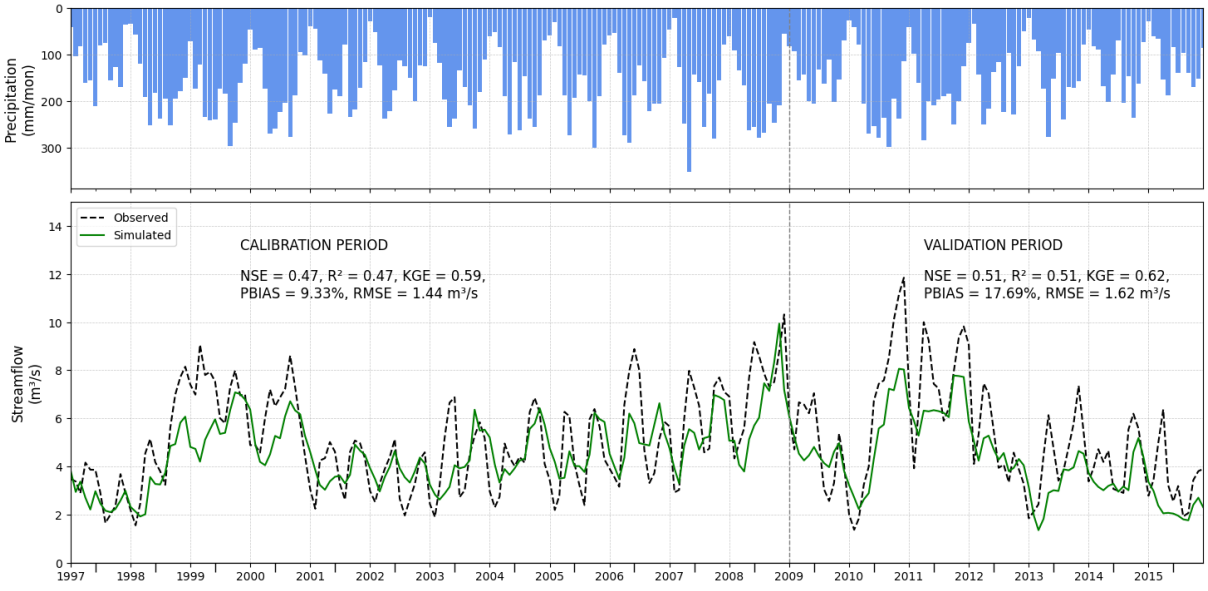

Figure 14. Calibration (1997–2008) and validation (2009–2015) of SWAT+ for monthly streamflow of Rio Chico gauge station, basin Riogrande II reservoir.

Although the NSE score falls in the "unsatisfactory" range, the high KGE score of 0.60, approximately, in both stations, suggests that the model performs reasonably well in capturing the key statistical characteristics of the observed data, while presenting a clear temporal correlation with the observation with similar flow patterns. This indicates a reasonably accurate description of the physical processes in the basin, providing confidence in the model's applicability for scenario analysis or decision-making, particularly when the goal includes capturing general patterns and accumulated flows rather than exact replication of peaks and valleys. Overall, as shown in Figures 13 and 14 and supported by the performance metrics, the model tends to underestimate streamflows, particularly during peak events, and exhibits a small lag in the rising limb of the hydrograph in the Riogrande II watershed.

Figure 15 presents the observed and simulated curves of monthly average streamflow for the Quebrada Las Palmas station in the La Fe reservoir watershed.

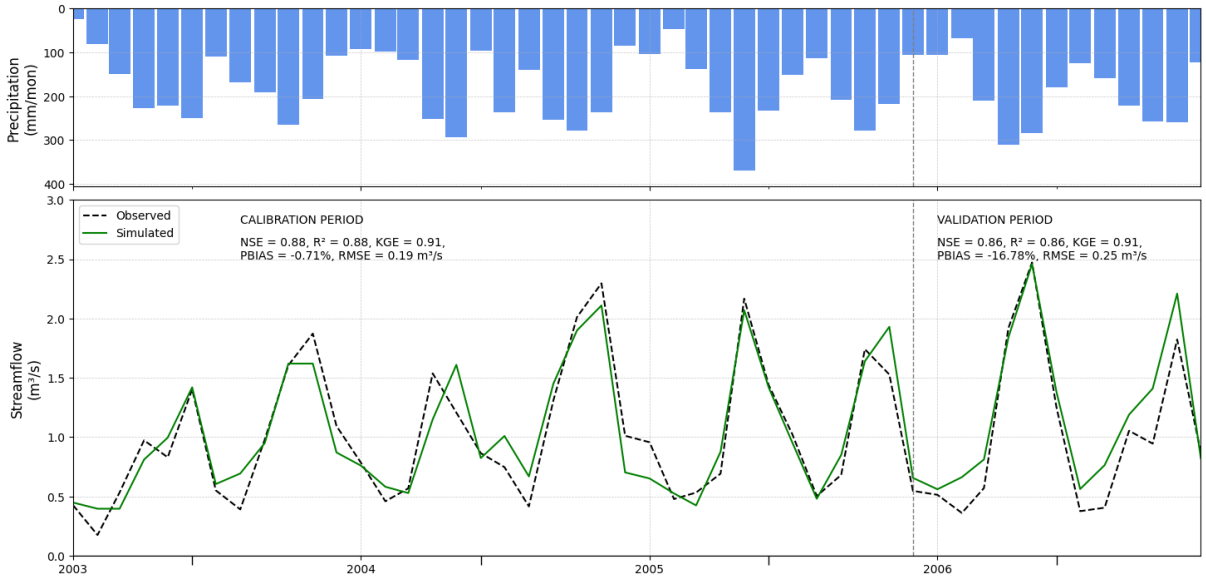

Figure 15. Calibration (2003–2005) and validation (2006) of SWAT+ for monthly streamflow of Quebrada Las Palmas gauge station, basin La Fe reservoir.

According to Figure 15, model performance for quebrada Las Palmas station was classified as "very good" in both calibration and validation, with NSE and R^2 values of 0.88 and 0.86, in calibration and validation period, respectively. The model classification based on KGE was also "very good" in calibration and validation period, with value equal to 0.91 in both periods. PBIAS also indicated "very good" performance during calibration with -0.71%. However, in validation, the model underestimated observed streamflows by 16.78%, which is considered "unsatisfactory".

In general, some of the performance limitations observed, especially in terms of flow bias, may be attributed to uncertainties in the input climate data, which are derived from physical models and reanalysis products that inherently carry biases due to resolution, data assimilation, and modeling assumptions. Furthermore, uncertainties in the observed monthly streamflow data, which were extracted from previous studies and pre-processed, may also affect the accuracy of the model by not fully reproducing the flow magnitude.

It is also important to consider the length of the calibration and validation periods. For Riogrande II watershed, calibration covered a relatively long period (1997–2008) followed by a seven-year validation period (2009–2015), allowing a more comprehensive evaluation of model performance under diverse hydrological conditions. In contrast, the La Fe reservoir watershed calibration (2003–2005) and validation (2006) periods were much shorter due to the limited available data. Although the performance metrics were high for La Fe reservoir watershed, the limited time frame may reduce the model's robustness and its ability to generalize to different climatic or hydrological scenarios. These results should therefore be interpreted with caution, and future work should aim to include longer time series for more reliable calibration and validation.

3.2.2 Land use scenarios

Land use model validation

The transition matrices and weights of evidence used to generate the probability maps are presented in Appendix C. Based on the error matrices Appendix D, we can calculate the overall accuracy, which was 83.08% for Riogrande II and 68.73% for La Fe.

The validation metrics, Figure of Merit (FoM), Producer's Accuracy, and User's Accuracy calculated from the error matrices through spatial overlay analysis are presented in Table 9. The land use change modeling results show varying levels of agreement between the simulated and observed maps for the

two watersheds. For the Riogrande II watershed, the FoM was 28.31%, which is considered moderate and suggests that the model was able to capture a reasonable portion of actual land use changes. Producer's and User's Accuracies were also similar, 43.22% and 43.83%, respectively, indicating balanced performance in terms of both the proportion of observed changes correctly simulated (Producer's Accuracy) and the proportion of predicted changes that were correct (User's Accuracy).

Metric	Riogrande II	La Fe
Figure of Merit (%)	28.31	11.96
Producer's Accuracy (%)	43.22	19.04
User's Accuracy (%)	43.83	22.67

Table 9. Validation metrics of land use change model for Riogrande II watershed and La Fe watershed

In contrast, the model's performance for the La Fe watershed was lower, with a FoM of 11.96%, and Producer's and User's Accuracies of 19.04% and 22.67%, respectively. These results suggest that the model had more difficulty capturing the detailed land use dynamics in La Fe, potentially due to limitations in input data, model assumptions, or differences in the spatial complexity of land change processes in that region. Although there are no universally accepted thresholds for these metrics, similar studies have reported FoM values ranging from 10% to 40% under realistic modeling scenarios (Pontius et al., 2008; Camacho Olmedo et al., 2013), supporting the interpretation of Riogrande's performance as good and La Fe's as acceptable.

It is important to note that these metrics are calculated based on the spatial overlay of simulated and observed change maps. Therefore, they are strongly influenced by the resolution and precision of the spatial data. In this research, the land use maps have a spatial resolution of 30 meters, which poses a challenge for pixel-level agreement, especially when using probabilistic or stochastic models that estimate the likelihood of change rather than its exact location. Small spatial mismatches between predicted and observed changes can reduce the performance of these metrics, even when the model successfully captures broader patterns and quantities of change. As a result, FoM and related accuracy scores can be overly strict when applied at high spatial resolution.

To address this issue, a multiple window similarity analysis was performed. Figure 16 illustrates the similarity between the observed and simulated maps as a function of window size. The x-axis represents the number of pixels that define the side of a square analysis window: for example, a 3×3 window corresponds to an area of 90 meters per side, a 5×5 window to 150 meters, and so on. For stochastic land use models, a similarity above 50% is generally considered acceptable.

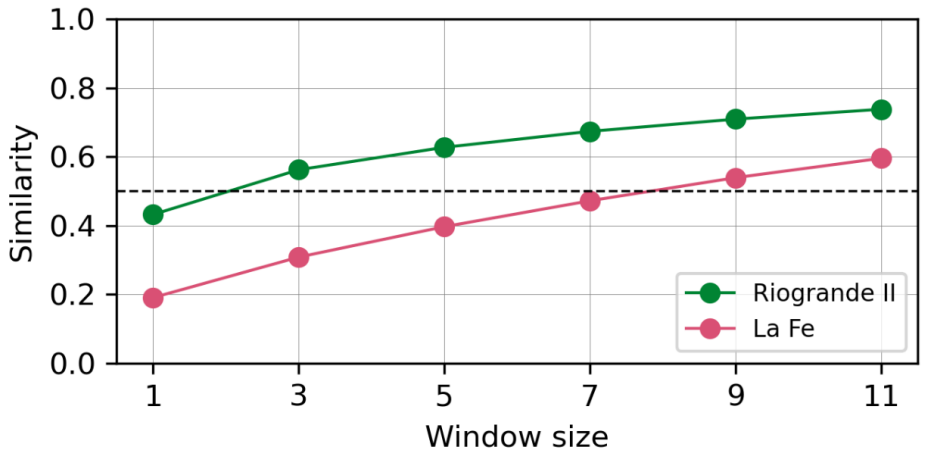

Figure 16. Multiple window similarity analysis for the Riogrande II and La Fe watershed

As shown in the Figure 16, the Riogrande II model reaches the 50% similarity threshold with a window of just 2 pixels per side (i.e., 60 meters), indicating relatively strong spatial agreement even at

finer resolutions. In contrast, the La Fe model reaches this threshold only with a 240-meter window, suggesting lower spatial precision in replicating land use change patterns.

These findings indicate that the Riogrande II model demonstrates higher spatial accuracy than the La Fe model, particularly at finer resolutions. The need for a larger window to reach acceptable similarity in La Fe suggests that the model has limited capacity for capturing the pixel-level spatial distribution of changes, but reproduces satisfactorily the land-use distribution at lower resolutions. While this is not problematic for describing the overall transport phenomena at a watershed level it is worth mentioning that such limitations may be attributed to smaller watershed size, or more fragmented and complex land use dynamics.

Land use projections

Figure 17 presents the land use and cover projection for the period 2024 - 2074, for the Riogrande II reservoir watershed.

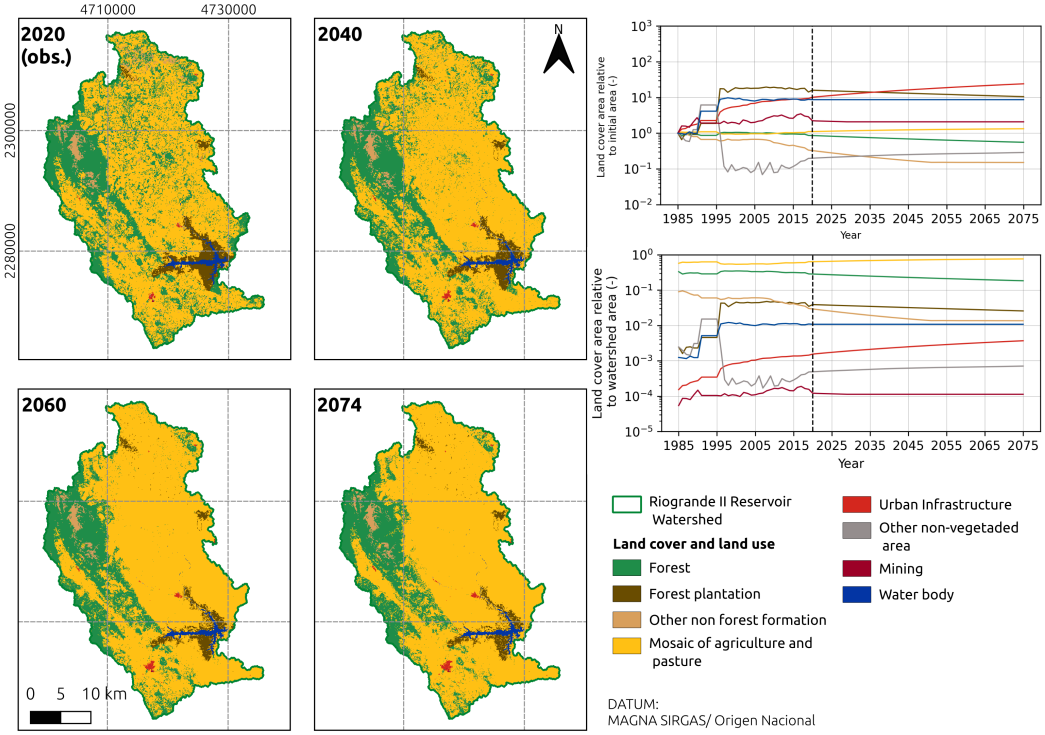

Figure 17. Land use change projections for the Riogrande II watershed for the period of 2024 - 2074. Land use area relative to the initial area (right, top), Land use area relative to the watershed area (right, bottom), and the projected spatial distribution of the land use (left).

In the Riogrande II watershed (Figure 17), the dominant land use is Agriculture and Pasture Mosaic, followed by Forest cover. Over the course of the simulation period, significant changes are projected. Forest cover is expected to decrease from 33% to 18.5%, while the Agriculture and Pasture Mosaic is projected to expand, from 57% to 76% of the watershed area. The Páramo ecosystem (classified as Other Non-Forest Formation) is also anticipated to decline sharply, shrinking from 9% to just 1.35%. Although Urban areas occupy a relatively small portion of the watershed, urbanization is projected to increase 12 times by 2074, reaching 0.36% of the total area.

Figure 18 presents the land use and cover projection for the period 2024 - 2074, for the La Fe reservoir watershed.

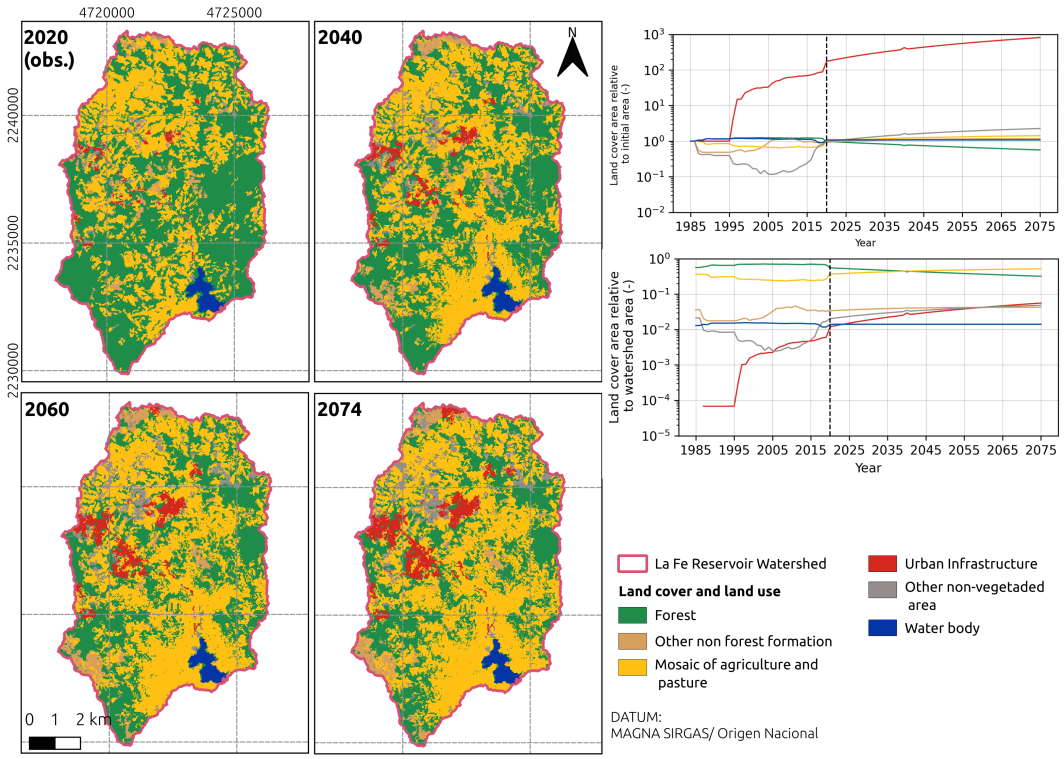

Figure 18. Land use change projections for the La Fe watershed for the period of 2024 - 2074. Land use area relative to the initial area (right, top), Land use area relative to the watershed area (right, bottom), and the projected spatial distribution of the land use (left).

In the La Fe watershed (Figure 18), Forest remains the dominant land cover until around 2040, when it is overtaken by the Agriculture and Pasture Mosaic. Over the study period, Forest is projected to decline significantly, from 56.5% to 32.2%, while the Agriculture and Pasture Mosaic increases from 36.4% to 51.75%. Urbanization shows the most dramatic growth, expanding nearly 800 times, from virtually 0% to approximately 5% of the watershed area by the end of the projection period. Similarly, Other Non-Vegetated Areas are expected to grow substantially, increasing about 20 times, from 2% to 5% of the total area.

The projected land use changes in both the Riogrande II and La Fe watersheds is consistent with the ongoing and increasing human pressure on natural ecosystems. Natural Forest and Páramo ecosystems are the most affected land covers, primarily due to the expansion of the Agriculture and Pasture Mosaic, which shows significant growth in both regions.

3.2.3 Climate change scenarios

Table 10 presents the statistics from the reference climate scenario and the difference between reference and moderate and extreme climate change scenarios.

Precipitation	**(mm)**				
Scenario	**Mean**	**Median**	**Std.Dev.**	**Minimum**	**Maximum**
R	5.14	2.81	6.27	0	72.20
M - R	+0.87	-0.31	+1.87	0	+18.98
E - R	+0.54	-0.45	+1.61	0	+12.15
Min. Temperature	**(ºC)**				
Scenario	**Mean**	**Median**	**Std.Dev.**	**Minimum**	**Maximum**
R	10.04	10.08	0.94	5.16	13.02
M - R	+0.64	+0.62	+0.06	-0.15	+0.83
E - R	+1.00	+0.92	+0.27	-0.47	+1.74
Max. Temperature	**(ºC)**				
Scenario	**Mean**	**Median**	**Std.Dev.**	**Minimum**	**Maximum**
R	19.29	19.28	1.65	12.77	25.12
M - R	+0.62	+0.60	-0.01	+0.59	+0.42
E - R	+0.97	+0.92	+0.22	+0.20	+1.11
Solar Radiation	**(MJ/m²)**				
Scenario	**Mean**	**Median**	**Std.Dev.**	**Minimum**	**Maximum**
R	18.28	18.56	3.80	3.27	28.30
M - R	-0.39	-0.19	+0.23	-2.08	-0.27
E - R	-0.27	-0.14	+0.06	-1.23	-0.50

Table 10. Statistics of the climate scenario Reference (R), and the comparison the Moderate with Reference (M - R) and Extreme with Reference (E - R)

According to Table 10, there is an increase in the probability of extreme precipitation events under both the moderate and extreme climate change scenarios when compared to the reference scenario. The cumulative distribution function (CDF) (Figure 19) shows that daily precipitation events of up to 20 mm/day account for approximately 98% of occurrences in the reference scenario, while they represent 90% and 88% of events in the moderate and extreme scenarios indicating an increase in heavier rain events. Moreover, the probability of daily precipitation exceeding 60 mm/day rises from 0.02% in the reference scenario to 0.04% and 0.09% in the moderate and extreme scenarios, respectively.

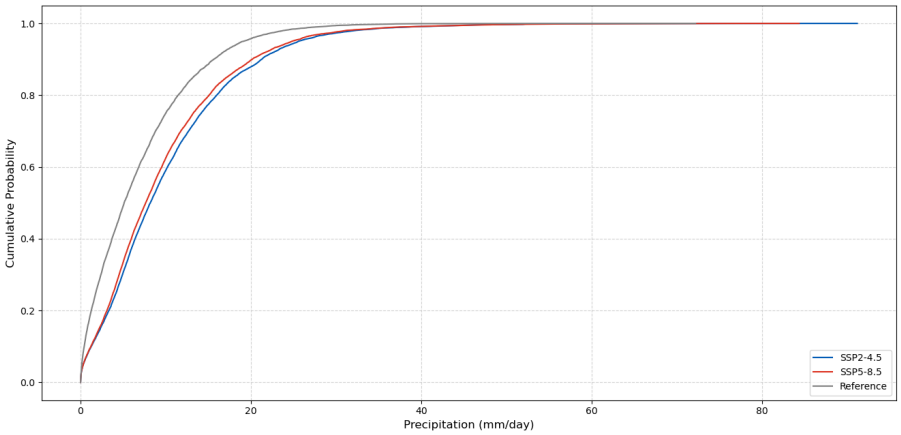

Figure 19. Cumulative distribution function of precipitation for the different climate scenarios.

In parallel, the reduction in the proportion of moderate rainfall events and the increase in dry days under climate change scenarios (Figure 20) indicates a shift towards more intense but less frequent rainfall.

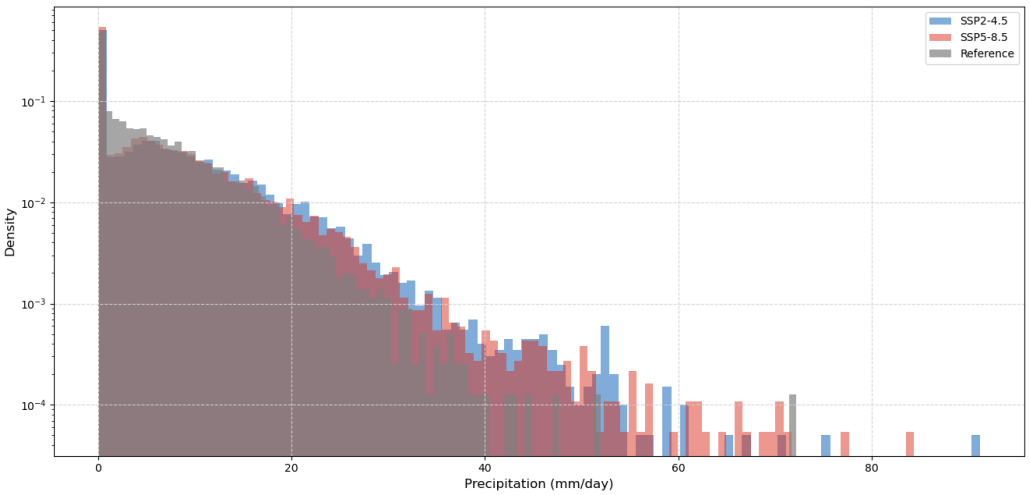

Figure 20. Histogram of precipitation for the different climate scenarios.

On the other hand, daily temperature shows an average increase of 0.63°C and 1.0°C under the moderate and extreme climate change scenarios, respectively, compared to the reference scenario. The extreme scenario also exhibits increased variability, with the standard deviation rising by 0.27°C relative to the reference. These changes are observed in both the minimum and maximum daily temperature values. The increase in mean temperatures is consistent with global climate change projections and can significantly impact hydrological processes, such as increased evapotranspiration and heavier rains.

There are no significant changes in daily solar radiation reaching the ground in the future climate scenarios when compared to the reference scenario.

3.3 RRV framework and reservoir modeling

3.3.1 Riogrande II reservoir

Figures 21, 22, and 23 illustrate the annual evolution of the Reliability, Resilience, and Vulnerability indices for the Riogrande II reservoir throughout the study period. As the Reliability index approaches 0, the probability of the reservoir operating under satisfactory conditions decreases. A Resilience value of 1 may indicate either the absence of failures or that the average recovery time for each failure was just one day. The closer the Resilience value is to zero, the slower the reservoir's average recovery time. Vulnerability reflects the average volume of unmet demand during failure events.

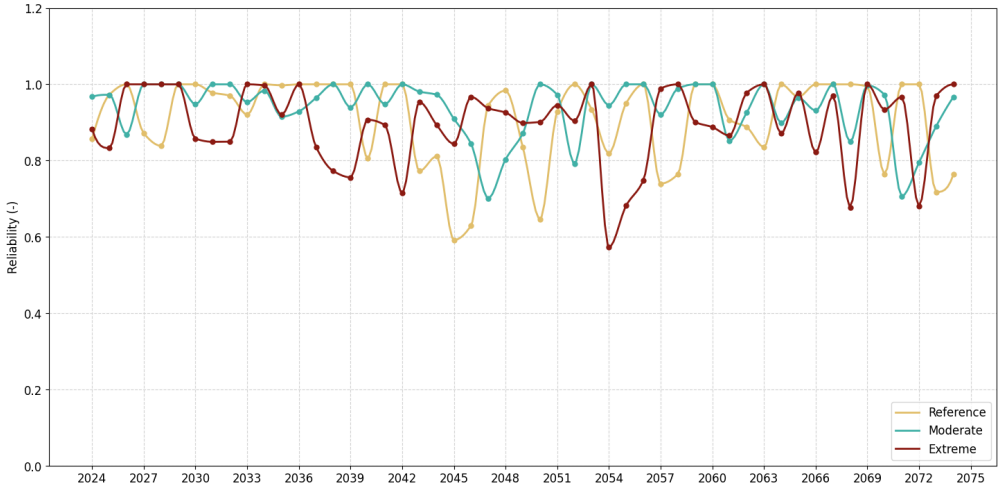

Figure 21. Reliability index for the Riogrande II Reservoir in the different climate scenarios, in the projection period 2024-2074.

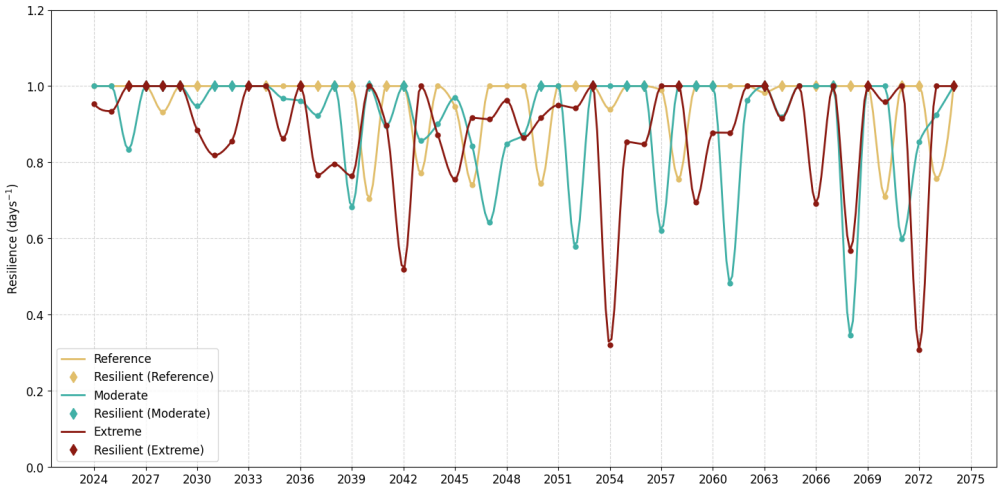

Figure 22. Resilience index for the Riogrande II Reservoir in the different climate scenarios, in the projection period 2024-2074.

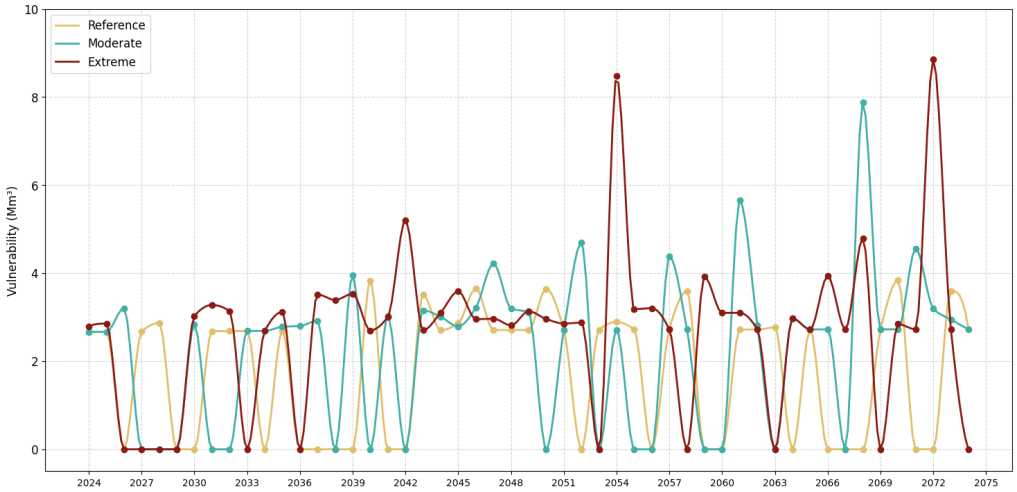

Figure 23. Vulnerability index for the Riogrande II Reservoir in the different climate scenarios, in the projection period 2024-2074.

To assess reservoir performance using the Reliability, Resilience, and Vulnerability (RRV) indices shown in Figures 21, 22, and 23, it is essential to interpret the metrics collectively. For instance, while the Reliability values across different climate scenarios in a given year (e.g., Riogrande II - 2061) may appear similar, the differences between scenarios becomes clear when Resilience and Vulnerability are also considered. In this case, although the Reference, the Moderate and Extreme scenarios show comparable Reliability (0.90, 0.84 and 0.85, respectively for 2061), the Moderate scenario exhibits a slower recovery time (more than two days) and greater water deficits (over 5.5 Mm^3) compared to the others (one or more days of recovery and 3.0 Mm^3, approximately). This highlights that even when RRV components are close in value, the overall system behavior can vary significantly between scenarios.

A more detailed look at the Reference scenario reveals that the Riogrande II reservoir generally performs unsatisfactorily. The system fails to meet the established water demand in 29 of the 51 years. Notably, the worst Reliability values occur in 2045 (0.59), 2046 (0.63) and 2050 (0.65). On the other hand, the longest consecutive period of failure, which means Reliability is less than one, spans 9 years, from 2043 to 2051. Analysing the Resilience, the slowest recoveries occur in 2040 and 2070, with a

Resilience value of 0.71 and 0.72 days^{-1}, respectively, indicating average recovery times of 1.40 days following the failures,. This suggests that while failures may be frequent, the system's recovery time is relatively short. The most frequent value of Vulnerability is 2.70 Mm^3, occurring in 15 of 29 years of failure. The highest vulnerability values are observed in 2040 and 2070, both equating 3.80 Mm^3.

In the Moderate climate scenario, the reservoir demonstrates improved performance in terms of Reliability compared to the Reference scenario. The longest period of continuous failure lasts seven years, from 2043 to 2049. However, out of the 51 projected years, the system fails to meet demand in 34 years. Resilience, however, declines more intensely than in the Reference case. The lowest Resilience values occur in 2061 and 2068, equal to 0.48 and 0.35 days^{-1}, meaning that the system takes in average more than 2.1 and 2.8 days to recover, respectively. Vulnerability also increases significantly in this scenario. Peak values reach 5.5 Mm^3 in 2061 and 7.9 Mm^3 in 2068. This performance under the Moderate climate scenario shows a slight improvement in Reliability compared to the Reference scenario, but the overall system performance remains low, with longer recovery periods and larger volume deficits, which does not ensure adequate long-term reservoir reliability.

The Extreme climate scenario presents the most critical conditions for the Riogrande II reservoir. Reliability drops more frequently and more severely than in the other scenarios. The longest period of continuous failure lasts 16 years (2037–2052), and the index reaches its lowest point in 2054 (0.57). Resilience is also lowest under this scenario. The most prolonged recovery periods are observed in 2054 and 2072, both with a Resilience value of 0.33 days^{-1}, or an average recovery time longer than three days. Vulnerability reaches its highest levels in this scenario, with unmet demand peaking at 8.5 Mm^3 in 2054 and 8.8 Mm^3 in 2072. The figures show that as climate conditions worsen, the reservoir system becomes increasingly vulnerable, with more frequent and severe failures, slower recovery, and a notable decline in overall robustness.

Figures 24, 25 and 26 illustrate the dynamics of the Riogrande II reservoir, showing monthly reservoir total inflow, total outflow and average storage, for the Reference, Moderate and Extreme climate change scenarios, respectively.

There is a noticeable difference between the inflow across the scenarios. The average inflow of the Reference scenario is 83.74 Mm^3, with the peak inflow reaching around 150 Mm^3. In contrast, the average inflow of the Moderate scenario is 103.22 Mm^3 and for the Extreme scenario is 94.18 Mm^3. In both scenarios, the inflow peaks easily exceed 200 Mm^3, with an extreme event reaching 400 Mm^3.

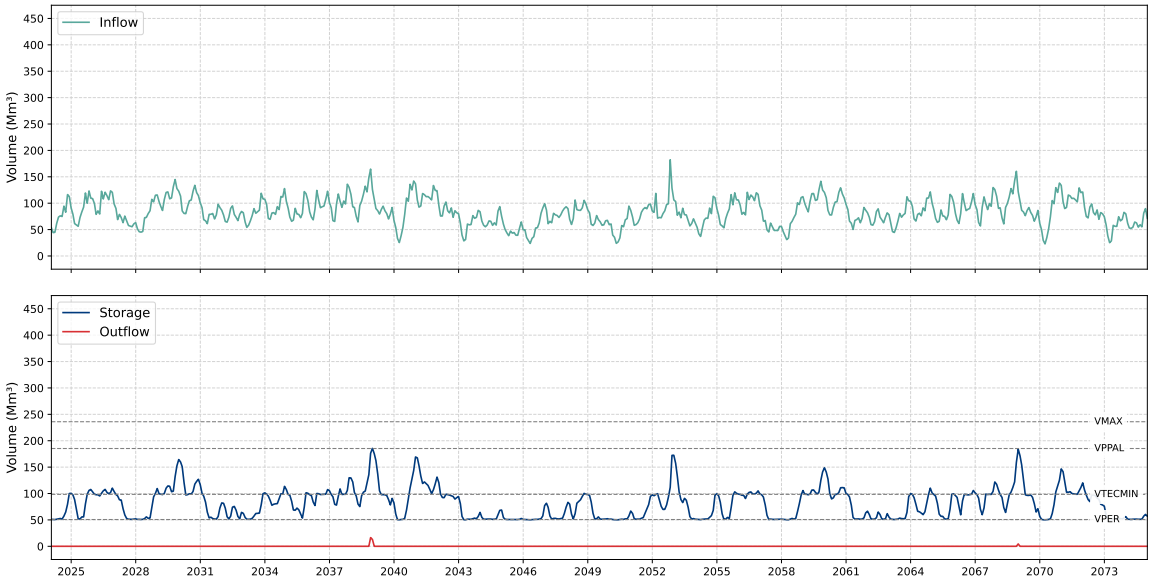

Figure 24. Reservoir dynamics for the climate scenario Reference for the Riogrande II Reservoir, for the period 2024-2074.

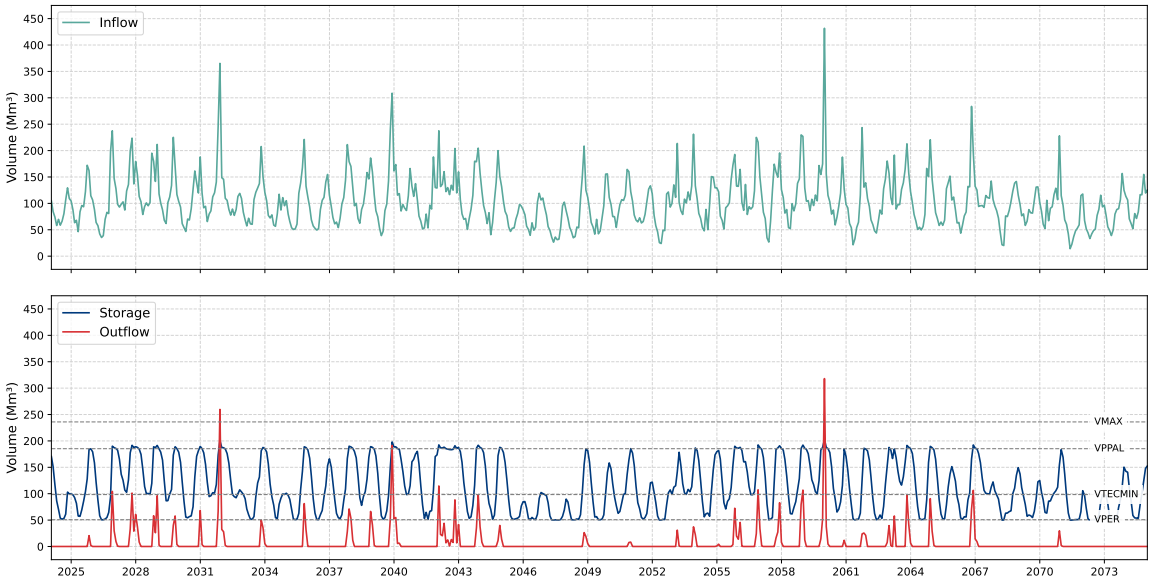

Figure 25. Reservoir dynamics for the Moderate climate change scenario for the Riogrande II Reservoir, for the period 2024-2074.

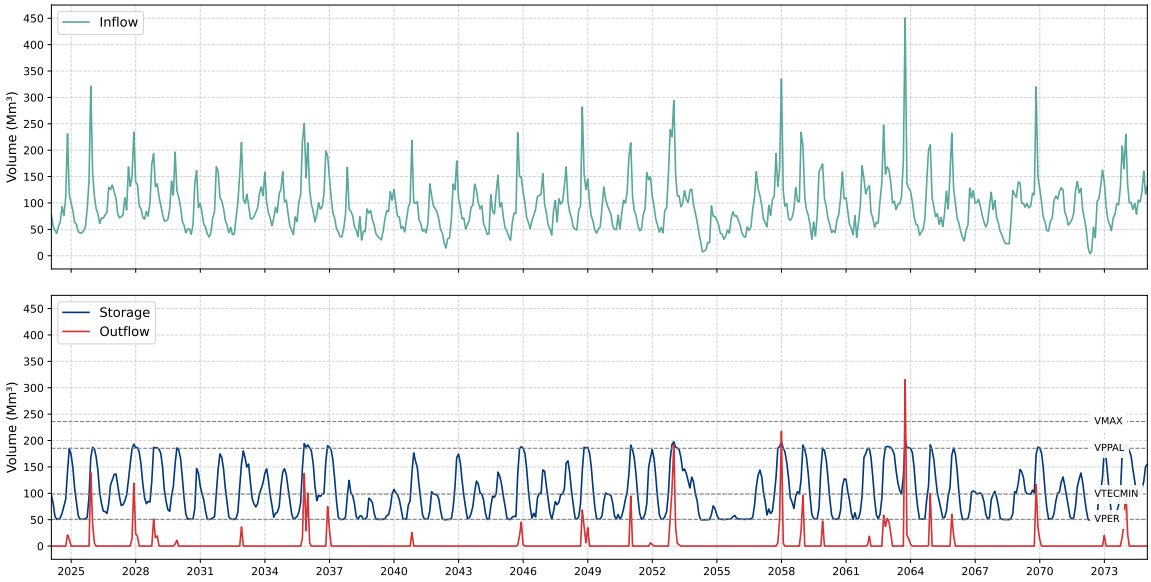

Figure 26. Reservoir dynamics for the Extreme climate change scenario for the Riogrande II Reservoir, for the period 2024-2074.

As we can see in Figures 24, 25 and 26, since the inflow of the Riogrande II reservoir depends only on the runoff naturally drained into it, this variable directly influences the volume of water stored and released. The outflow/inflow ratio is 0.06% for the Reference scenario, 7.26% for the Moderate scenario, and 5.68% for the Extreme scenario. This suggests that although more intense precipitation events can increase the amount of available water it does not mean that it will get stored, and the reservoir security releases lead to greater water losses.

Figures 27, 28 and 29 show the monthly average water storage, total demand, withdrawals, and unmet demand for the Riogrande II reservoir throughout the study period, for the Reference, Moderate and Extreme climate scenarios, respectively.

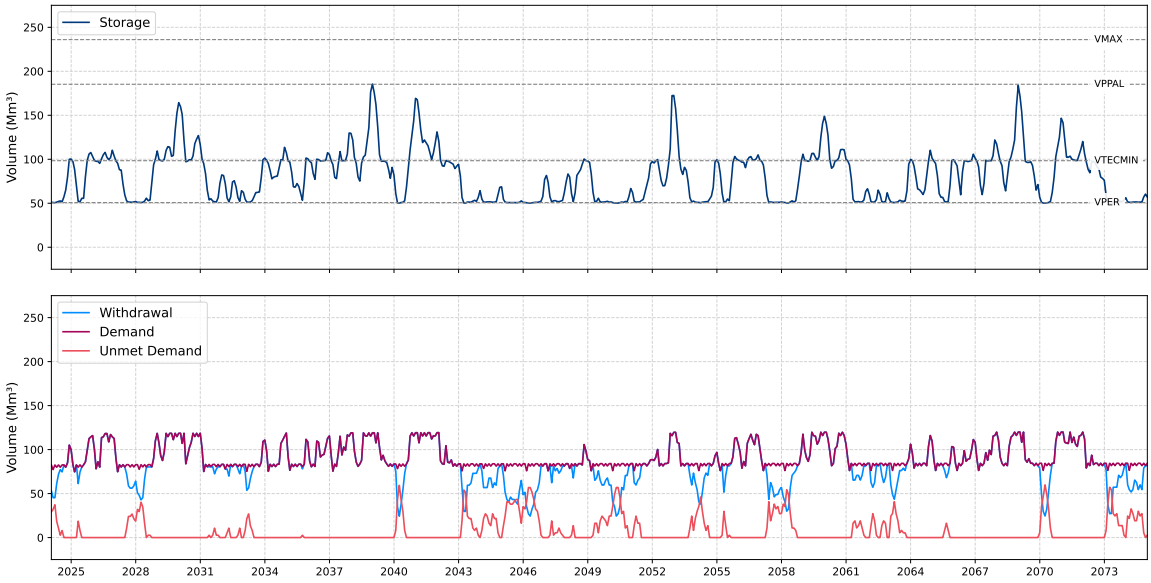

Figure 27. Water demand for the Reference scenario for the Riogrande II Reservoir, for the period 2024-2074.

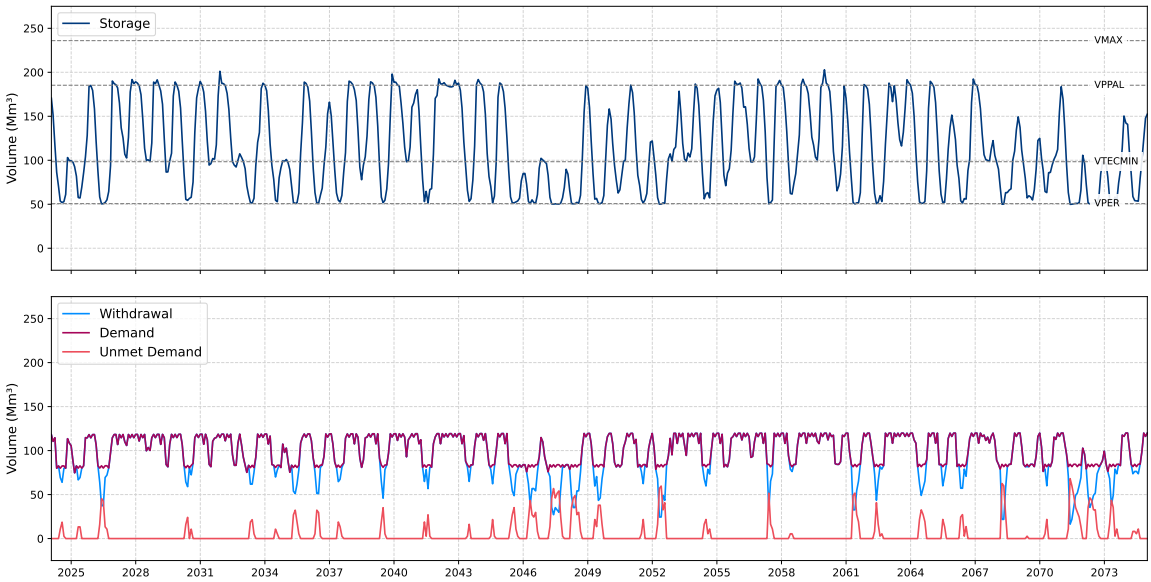

Figure 28. Water demand for the Moderate scenario for the Riogrande II Reservoir, for the period 2024-2074.

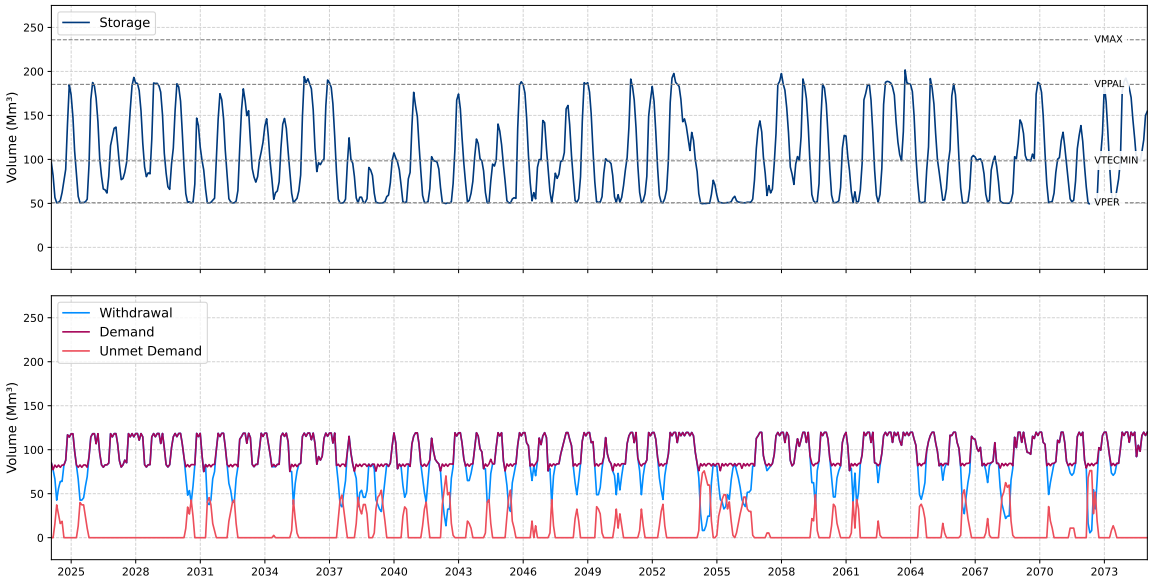

Figure 29. Water demand for the Extreme scenario for the Riogrande II Reservoir, for the period 2024-2074.

In Figures 27, 28 and 29 it can be seen that the unmet demand increases as the climate change gets more severe. The ratio unmet demand/demand for the Reference scenario is 8.13%, 5.05% for the Moderate scenario and 8.72% for the Extreme scenario. This suggests that, despite the higher inflows observed in the Extreme scenario, the unmet demand surpasses that of the Reference case. This indicates that the water that is not wasted during the heavier precipitations is not able to offset the prolonged dry spells under extreme climate, leading to higher water shortages.

3.3.2 La Fe reservoir

Figures 30, 31, and 32 present the Reliability, Resilience, and Vulnerability indices for the La Fe reservoir over the historical period from 1997 to 2023.

It is noticeable that the performance of the La Fe reservoir between 1997 and 2005 is worse compared to the period of 2006 - 2023, after the pumping system was implemented. During the earlier period, the Reliability varies between 0.30 and 0.63, the Resilience from 0.33 to 0.56 days-1, corresponding to a recovery time approximately between 1.78 and three days, and the Vulnerability varies between 1.24 and 2.40 Mm³.

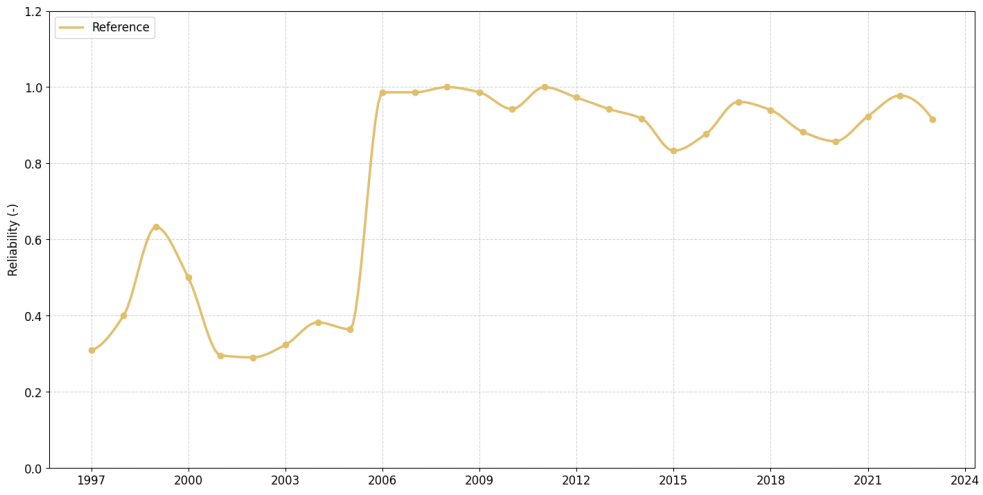

Figure 30. Reliability index for the La Fe Reservoir in the historic period of 1997-2023.

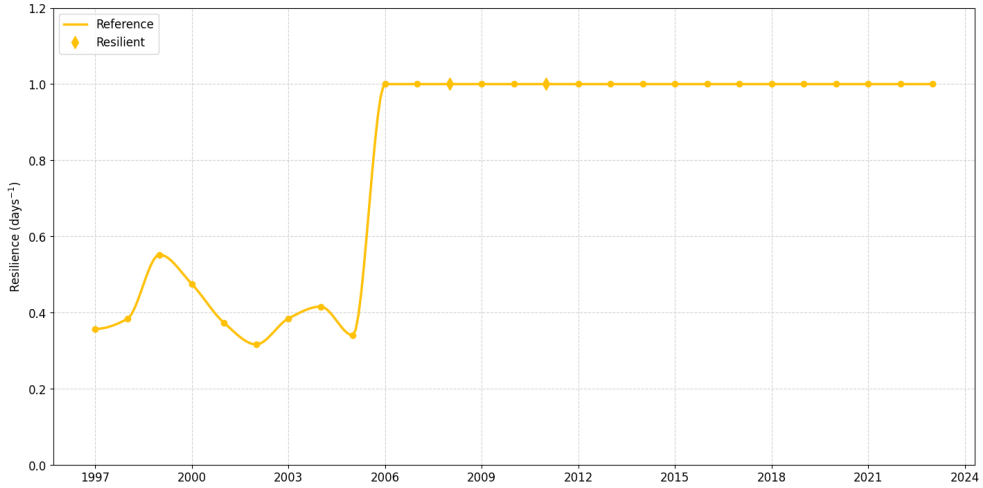

Figure 31. Resilience index for the La Fe Reservoir in the historic period of 1997-2023.

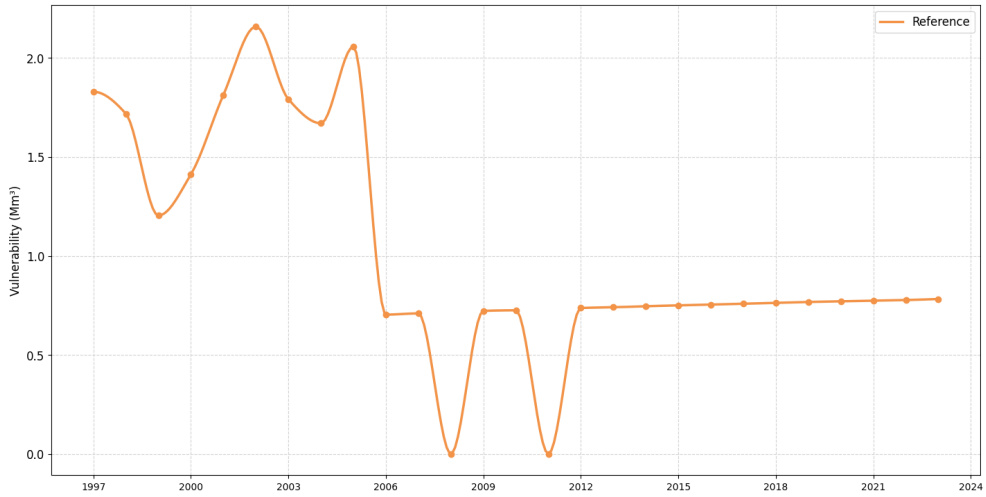

Figure 32. Vulnerability index for the La Fe Reservoir in the historic period of 1997-2023.

After the pumping starts the performance of the La Fe reservoir improves significantly, though it is not perfect. Only the years 2009 and 2011 show a Reliability of 1.0, meaning the reservoir remained in a satisfactory state every day of those years. The worst case occurs in 2015, when Reliability drops to 0.83. Resilience remains at 1.0 throughout this period, indicating a recovery time of one day for all years except 2009 and 2011, during which no failures occurred. This behavior also persists throughout the projected period. Vulnerability shows a linear increase, rising from 0.73 Mm³ in 2006 to 0.77 Mm³ in 2023.

Figures 33 and 34 shows the Reliability and Vulnerability indices for the La Fe reservoir over the projected period from 2024 to 2074, for the Reference, Moderate and Extreme climate scenarios.

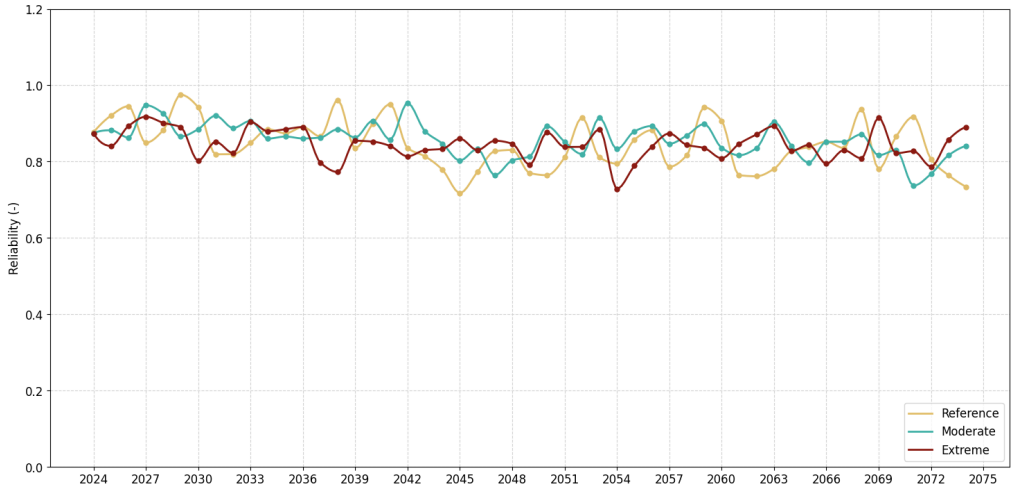

Figure 33. Reliability index for the La Fe Reservoir for the Reference, Moderate and Extreme climate scenarios, in the period of 2024-2074.

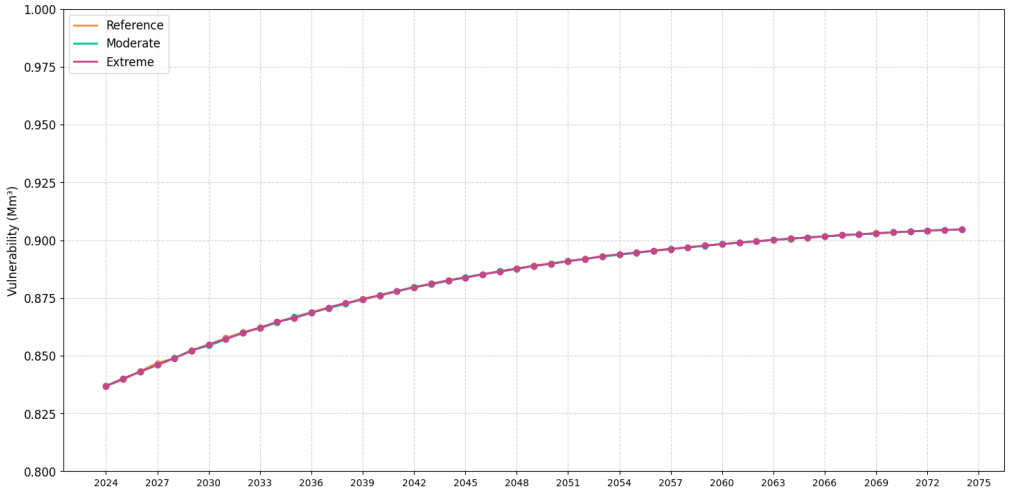

Figure 34. Vulnerability index for the La Fe Reservoir for the Reference, Moderate and Extreme climate scenarios, in the period of 2024-2074.

Both Figures 33 and 34 indicate a general trend of decreasing Reliability and increasing Vulnerability across all three climate scenarios throughout the projected period. However, based solely on the indices, it is difficult to observe significant differences in reservoir performance among the climate scenarios. Reliability does not show a clear variation, and the magnitude of Vulnerability remains approximately the same throughout the projected period.

To better understand the differences between climate scenarios, we can analyze the graphs in Figures 35, 36, and 37, which illustrate the dynamics of the La Fe reservoir. These graphs show monthly inflow, extra inflow, total inflow, outflow, and average storage volume for the Reference, Moderate, and Extreme scenarios, respectively.

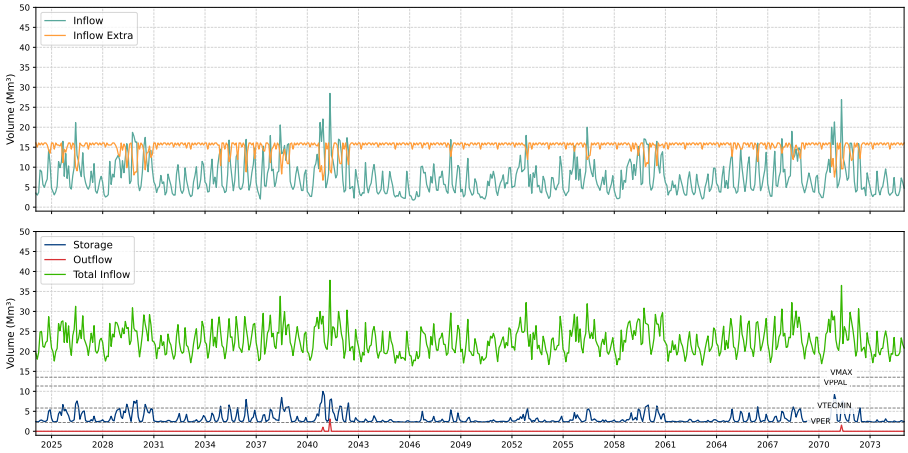

Figure 35. Reservoir dynamics for the Reference climate scenario for the La Fe Reservoir, for the period 2024-2074.



Figure 36. Reservoir dynamics for the Moderate climate change scenario for the La Fe Reservoir, for the period 2024-2074.



Figure 37. Reservoir dynamics for the Extreme climate change scenario for the La Fe Reservoir, for the period 2024-2074.

As observed in Riogrande II reservoir, there is an increase in 'natural' inflow into La Fe reservoir in the climate change scenarios in relation to the Reference scenario, that can be observed in 35, 36, and 37. The average inflow of the Reference scenario is 7.51 Mm³, with the peak inflow reaching around

37 Mm³. In contrast, the Moderate and Extreme scenarios show higher average inflows of 9.34 Mm³ and 9.15 Mm³, respectively. In both scenarios, peak inflow events frequently exceed 20 Mm³, with one event reaching approximately 50 Mm³.

As a consequence, dependency on pumped inflow ("extra inflow") decreases as climate change intensifies. The ratio of extra inflow to total inflow is 67% in the Reference scenario, compared to around 60% in both the Moderate and Extreme scenarios. The opposite trend is observed for outflows: the ratio of outflow to inflow is 0.12% in the Reference scenario, 4.17% in the Moderate scenario, and 5.82% in the Extreme scenario indicating again an increase in water releases due to heavier rains. This suggests that the increase in natural inflow helps reduce the reliance on pumped inflow, but the reservoir is unable to absorb the peak inflow events, resulting in water losses that could otherwise be used to meet demand.

Figures 38, 39, and 40 show the monthly average water storage, total demand, withdrawals, and unmet demand for the La Fe reservoir throughout the research period, for the Reference, Moderate and Extreme climate scenarios, respectively.

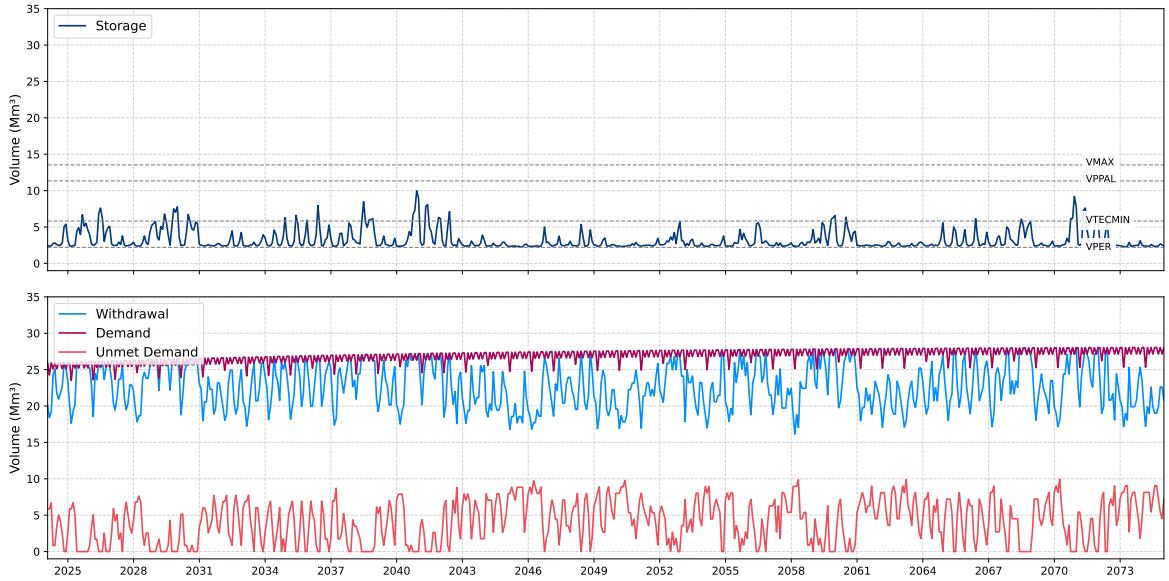

Figure 38. Water demand for the Reference scenario for the La Fe Reservoir, for the period 2024-2074.

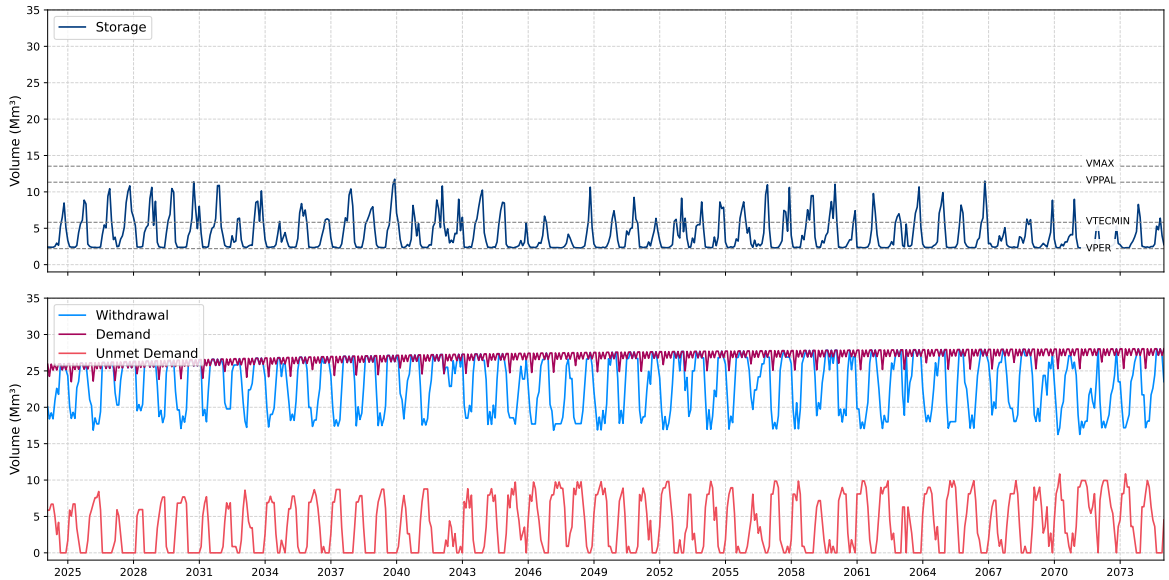

Figure 39. Water demand for the Moderate scenario for the La Fe Reservoir, for the period 2024-2074.

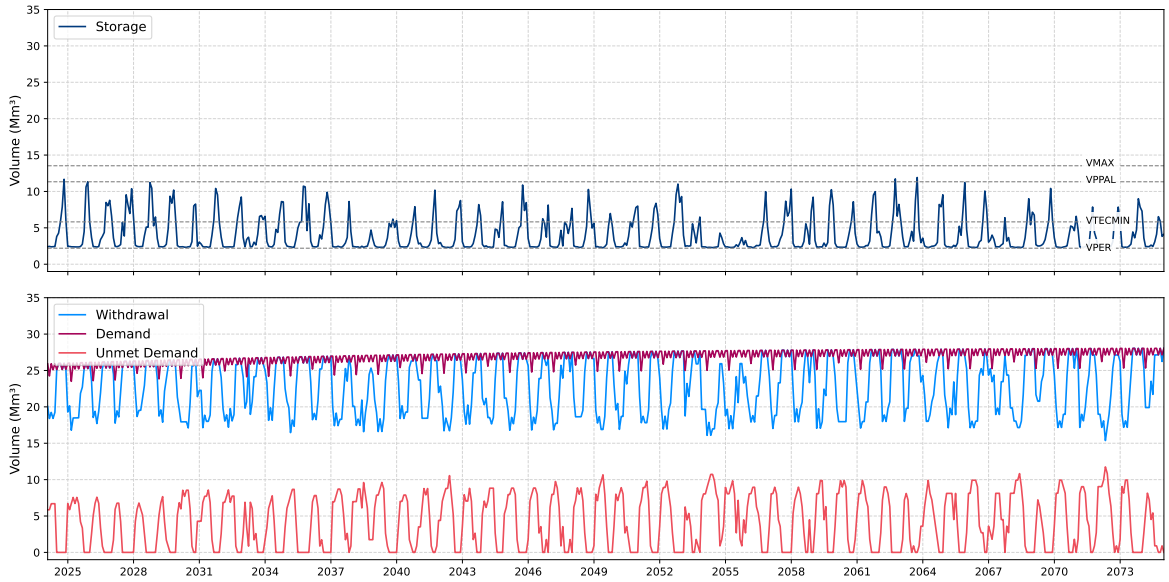

Figure 40. Water demand for the Extreme scenario for the La Fe Reservoir, for the period 2024-2074.

It is possible to note in Figures 38, 39, and 40 that the unmet demand by La Fe reservoir remains almost the same among the climate scenarios, differently that occurs in Riogrande II. The ratio of unmet demand/demand for the Reference scenario is 15.46%, 14.29% for the Moderate scenario and 15.49% for the Extreme scenario.

4 Discussion

The results of this research indicate that both Riogrande II and La Fe reservoirs are expected to face increasing challenges in meeting the growing water demands of the Aburrá Valley in the research period. These challenges are shaped by a combination of climatic and anthropogenic pressures that are transforming the hydrological behavior of their watersheds.

Domestic water demand is projected to increase steadily, intensifying the pressure on both reservoirs. However, the population model used is relatively simple, assuming asymptotic stabilization and not accounting for migratory trends or population decline, which can be accounted for in more sophisticated models. The demand-side growth is compounded by ongoing land use changes within the watersheds. The Riogrande II and La Fe watersheds are projected to experience growth in mosaic of agriculture and pasture and urbanization. These land cover transformations typically reduce infiltration capacity and increase both surface runoff and evapotranspiration, thereby increasing the peak flows and reducing the basin storage capacity worsening the operation conditions for the reservoirs.

Climate change further exacerbates these hydrological pressures. Future climate scenarios project more intense rainfall events, longer dry periods, and rising temperatures (Section Bias Correction). As discussed by Eekhout et al. (2018), extreme precipitation events reduce soil water content, shifting the water availability from the soil to the stream network and reservoirs, which increases dependence on reservoir storage. Moreover, the increase in runoff also contributes to soil erosion, mostly on steep slopes watersheds, that can lead to decrease the long-term storage capacity of reservoirs through sedimentation.

The results from the reservoir simulations in this research support these findings. While extreme precipitation events marginally improve water availability during the rainy events, the inability of reservoirs to retain the large inflow peaks results in substantial water releases. These releases represent a missed opportunity to store water for use during drier months, ultimately threatening water security in the region. In fact, the results of Riogrande II reservoir show that under the Moderate climate scenario, the amount of water released (7.26%) could cover the unmet water demand (5.05%).

Based on the RRV analysis, the Riogrande II reservoir is projected to show a clear trend of declining performance under future climate scenarios. In the Reference scenario, the system already struggles to meet water demand in more than half the years, with frequent failures, modest recovery rates, and moderate vulnerability levels. Under the Moderate climate scenario, reliability slightly improves, but the system suffers from slower recovery and more severe unmet demand volumes, indicating a weakening resilience and growing vulnerability. The Extreme climate scenario shows the most critical performance, with long periods of consecutive failures, the slowest recovery times, and the highest levels of unmet demand. Overall, the reservoir's behavior across all scenarios highlights its increasing susceptibility to climate stress, marked by persistent reliability issues, declining resilience, and increasing vulnerability, pointing to a reduced ability to ensure water supply under future conditions.

The La Fe reservoir demonstrates a particularly high dependence on pumped inflows, which comprise at least 60% of its total inflow. While this research assumes the availability of an unlimited water supply from the Buey-Piedras-Pantanillo rivers system, this assumption may not hold under more severe climate or upstream usage conditions. As a result of the use of pumping inflow, La Fe reservoir exhibits relatively stable performance, with unmet demand/demand ratios consistently ranging between 14.29% and 15.49%, regardless of climate scenario. However, the persistently high unmet demand ratio points to a fundamental limitation in the reservoir's ability to meet supply requirements.

From RRV framework analysis, the performance of La Fe reservoir is mostly Resilient, since for all the years and scenarios the recovery time is of one day (Resilience = 1). However, for all scenarios the Reliability decreases and Vulnerability increases over time, indicating that the number of failures and the magnitude of unmet water increases consistently.

Generally, the impacts of climate variability are more significant than land use change impacts (Dwarakish & Ganasri, 2015), but land use management can be used to mitigate the excess of water resulting from the extreme events of precipitation enhancing the community resilience in the watersheds by implementing rainwater harvesting (Eta et al., 2025) and terrace farming (Sarkar & Tanmoy, 2025), mostly in steep slope regions. These actions increase infiltration, reducing the peak of inflow to the reservoirs and subsequently the frequency and magnitude of security releases. In general, such increase in the catchment efficiency leads to an increase in the channel's baseflow resulting from the enhancement of slower soil transport processes.

In summary, water security in the Aburrá Valley is increasingly threatened by a convergence of factors: reduced infiltration and soil moisture, greater surface runoff, increased reliance on already burdened reservoirs, and heightened erosion risks. The findings underscore the urgency of developing integrated watershed and reservoir management strategies that account not only for climatic variability but also for ongoing land use changes and sedimentation dynamics. Future planning must prioritize demand-side management, protection of soil and water resources, and investments in infrastructure that enhance reservoir resilience and capacity.

5 Conclusions

This research evaluated the water security of the Aburrá Valley by applying the Reliability, Resilience, and Vulnerability framework under multiple scenarios of land use/land cover change and climate change. The analysis revealed that water demand in the region is approaching a saturation value due to the decrease in the population growth rate, with only minor increases expected in the coming decades. For the year of 2074, the annual domestic water demand of The Aburrá Valley is expected to reach 303,536,168 m^3. Considering an increase in economic activities proportional to the population and the environmental flows the base water demand is projected to reach 932,084,073 m^3.

Both reservoir Riogrande II and La Fe watersheds are increasingly affected by anthropogenic activities. In Riogrande II watershed, the Mosaic of Agriculture and Pasture increases from 57% to 76% and the urban infrastructure grow 12 times. A similar behaviour was projected in the La Fe watershed, where the Mosaic of Agriculture and Pasture increases from 36.4% to 51.75% and urban infrastructure grows from 0 to 5% of the watershed total area.

These changes alter the soil's ability to store and transport water, generally resulting in increased surface runoff. Climate change scenarios project more intense rainfall events, prolonged dry periods, and warmer temperatures leading to a higher evapotranspiration. Together, these drivers lead to higher peak flows and reduced baseflow, ultimately lowering soil water retention during dry seasons. As a consequence, water tends to be excessive during the rainy season and does not get stored due to security releases. In some scenarios the volume of water losses could cover the unmet demand during the dry season, or at least significantly reduce the volume deficit. Water security analysis indicated that the two main reservoirs, Riogrande II and La Fe, show different behaviors. Riogrande II is increasingly affected by climate change since its ability to maintain reliable supply is projected to decline, with lower resilience and greater vulnerability under more severe climate scenarios. In the worst case scenario, the lowest Reliability was 0.57 in 2054, the most prolonged recovery time had than three days of recovery and average Vulnerability of 8.8 Mm^3 in 2072.

On the other hand, for the La Fe reservoir higher values of Reliability and Resilience are observed in general. This is expected since the reservoir strongly depends on water pumping from a lower source, reducing the effects of the increasing climate variability. However the Reliability and Vulnerability are consistently declining along the projected period due to the increase in water demand. Although the system maintains a better performance than Riogrande II under adverse hydrological conditions, its dependence on pumping creates a structural vulnerability by relying on external watersheds and energy inputs, which may compromise long-term sustainability and operational autonomy. Additionally, the availability of water in the Buey-Piedras-Pantanillo system was not assessed and assumed to be constant, so that more realistic results require an additional analysis of this pumping source.

The RRV framework analysis suggests that the Aburrá Valley may face growing challenges in sustaining water availability from Riogrande II reservoir, especially during critical dry periods. Meanwhile, La Fe reservoir is dependent on an operational model that carries its own long-term risks. The future water security of the region, therefore, depends not only on climate resilience but also on the robustness and sustainability of its water transfer systems and reservoir and watershed management strategies, such as rainwater harvesting and terrace farming upright the reservoirs.

The research was based on gridded climate datasets and reanalysis products, along with streamflow data derived from previous hydrological studies. Additional parameters were informed by news reports and publicly available information like bathymetry reports, compliance documents from the Superintendency of Public Services and other public reports to reservoir parametrization and operation formulation. While reasonable, the assumptions and hypothetical reservoir operation scenarios introduce uncertainties. These uncertainties can be reduced by the introduction of observed data.

Nonetheless, this approach enabled the development of a complete methodology to assess water security through the performance of multipurpose reservoirs under combined anthropogenic and climatic pressures. The framework proposed can be refined and strengthened considering the interconnected reservoir system modeling.

6 References

Aboelnga, H. T., Ribbe, L., Frechen, F.-B., & Saghir, J. (2019). Urban Water Security: Definition and Assessment Framework. *Resources*, *8*(4), Article 4. https://doi.org/10.3390/resources8040178

Adcroft, A., Anderson, W., Balaji, V., Blanton, C., Bushuk, M., Dufour, C. O., Dunne, J. P., Griffies, S. M., Hallberg, R., Harrison, M. J., Held, I. M., Jansen, M. F., John, J. G., Krasting, J. P., Langenhorst, A. R., Legg, S., Liang, Z., McHugh, C., Radhakrishnan, A., ... Zhang, R. (2019). The GFDL Global Ocean and Sea Ice Model OM4.0: Model Description and Simulation Features. Journal of Advances in Modeling Earth Systems, 11(10), 3167–3211. https://doi.org/10.1029/2019MS001726

Adhikari, K., & Raya, H. (2018). Population Projection of Nepal: A Logistic Approach. Journal of Nepal Mathematical Society, 1, 1–8. https://doi.org/10.3126/jnms.v4i2.41482

Almeida, C. M., Gleriani, J. M., Castejon, E. F., & Soares-Filho, B. S. (2008). Using neural networks and cellular automata for modelling intra-urban land-use dynamics. *International Journal of Geographical Information Science*, 22(9), Article 9. https://doi.org/10.1080/13658810701731168

Amaringo, F., Puerta, Y., & Molina, F. (2022). Probabilistic Risk Assessment of Polycyclic Aromatic Hydrocarbons in a Colombian Reservoir. *Bulletin of Environmental Contamination and Toxicology*, 109(3), Article 3. https://doi.org/10.1007/s00128-022-03567-7

Área Metropolitana del Valle de Aburrá, Universidad Nacional de Colombia sede Medelín, COR-ANTIOQUIA, & CORNARE. (2008). *Plan de Ordenación y Manejo de Cuenca Hidrográfica—Rio Aburrá*. https://www.metropol.gov.co/ambiental/recurso-hidrico/pomca/2007/pomca-c2-subsistema-abiotico-recursoagua.pdf

Área Metropolitana del Valle de Aburrá. (2023, October 9). Historia. https://www.metropol.gov.co:443/area/Paginas/somos/Historia.aspx

Arias, P. A., Ortega, G., Villegas, L. D., & Martínez, J. A. (2021). Colombian climatology in CMIP5/CMIP6 models: Persistent biases and improvements. *Revista Facultad de Ingeniería Universidad de Antioquia*, 100, Article 100. https://doi.org/10.17533/udea.redin.20210525

Aristizábal, E., Garcia, E. F., Marin, R. J., Gómez, F., Guzmán-Martínez, J., Aristizábal, E., Garcia, E. F., Marin, R. J., Gómez, F., & Guzmán-Martínez, J. (2022). Rainfall-intensity effect on landslide hazard assessment due to climate change in north-western Colombian Andes. *Revista Facultad de Ingeniería Universidad de Antioquia*, 103, 51–66. https://doi.org/10.17533/udea.redin.20201215

Arnold, D. N. Moriasi, P. W. Gassman, K. C. Abbaspour, M. J. White, R. Srinivasan, C. Santhi, R. D. Harmel, A. Van Griensven, M. W. Van Liew, N. Kannan, & M. K. Jha. (2012). SWAT: Model Use, Calibration, and Validation. *Transactions of the ASABE*, 55(4), 1491–1508. https://doi.org/10.13031/2013.42256

Arnold, J. G., Bieger, K., White, M. J., Srinivasan, R., Dunbar, J. A., & Allen, P. M. (2018). Use of Decision Tables to Simulate Management in SWAT+. *Water*, 10(6), Article 6. https://doi.org/10.3390/w10060713

ASF DAACScience Data Systems. (2024). *ALOS PALSAR High Resolution Radiometric Terrain Corrected Product [Dataset]* [Dataset]. Earth Science Data Systems, NASA. https://www.earthdata.nasa.gov/data/catalog/asf-alos-psr-rtc-high-1

Bieger, K., Arnold, J. G., Rathjens, H., White, M. J., Bosch, D. D., Allen, P. M., Volk, M., & Srinivasan, R. (2017). Introduction to SWAT+, A Completely Restructured Version of the Soil and Water Assessment Tool. *JAWRA Journal of the American Water Resources Association*, 53(1), 115–130. https://doi.org/10.1111/1752-1688.12482

Biglarbeigi, P., Strong, W. A., Finlay, D., McDermott, R., & Griffiths, P. (2020). A Hybrid Model-Based Adaptive Framework for the Analysis of Climate Change Impact on ReservoirPerformance. *Water Resources Management*, 34(13), 4053–4066. https://doi.org/10.1007/s11269-020-02654-w

Bourgault, P., Huard, D., Smith, T. J., Logan, T., Aoun, A., Lavoie, J., Dupuis, É., Rondeau-Genesse, G., Alegre, R., Barnes, C., Laperrière, A. B., Biner, S., Caron, D., Ehbrecht, C., Fyke, J., Keel, T., Labonté, M.-P., Lierhammer, L., Low, J.-F., ... Whelan, C.(2023). xclim: Xarray-based climate data analytics. *Journal of Open Source Software*, 8(85), 5415. https://doi.org/10.21105/joss.05415

Cannon, A. J., Sobie, S. R., & Murdock, T. Q. (2015). Bias Correction of GCM Precipitation by Quantile Mapping: How Well Do Methods Preserve Changes in Quantiles and Extremes? https://doi.org/10.1175/JCLI-D-14-00754.1

Cannon, A. J., S. R. Sobie, and T. Q. Murdock, 2015: Bias Correction of GCM Precipitation by Quantile Mapping: How Well Do Methods Preserve Changes in Quantiles and Extremes?. *J. Climate*, 28, 6938–6959, https://doi.org/10.1175/JCLI-D-14-00754.1.

Chakraborty, A., Sikder, S., Omrani, H., & Teller, J. (2022). Cellular Automata in Modeling andPredicting Urban Densification: Revisiting the Literature since 1971. *Land*, 11(7), Article 7.https://doi.org/10.3390/land11071113

Chamani, R., Vafakhah, M., & Sadeghi, S. H. (2023). Changes in reliability–resilience–vulnerability-based watershed health under climate change scenarios in the Efin Watershed, Iran. *Natural Hazards*, 116(2), Article 2. https://doi.org/10.1007/s11069-022-05774-1

Chow, V. T., Maidment, D. R., & Mays, L. W. (1988). *Applied hydrology*. McGraw-Hill.

CNO, Consejo Nacional de Operación (2025). Acuerdo 1924 Por el cual se aprueba la actualización de unos parámetros técnicos de los volúmenes del embalse Ríogrande II | Consejo nacional de operación del sector eléctrico CNO. https://www.cno.org.co/content/acuerdo-1924-por-el-cual-se-aprueba-la-actualizacion-de-unos-parametros-tecnicos-de-los

CORANTIOQUIA. (2015). *ACTUALIZACIÓN Y AJUSTE PLAN DE ORDENACIÓN Y MANEJO DE LA CUENCA DE LOS RÍOS GRANDE Y CHICO*.

Cornare. (2023). *SEGUIMIENTO ANUAL 2022, AL PLAN DE ORDENAMIENTO DEL RECURSO HÍDRICO-PORH Y LOS OBJETIVOS DE CALIDAD ESTABLECIDOS MEDIANTE LA RESOLUCIÓN N°112-5304 DEL 26 DE OCTUBRE DE 2016*.

DANE. (2023). DANE - Proyecciones de población. https://www.dane.gov.co/index.php/estadisticas-por-tema/demografia-y-poblacion/proyeccio nes-de-poblacion

Dwarakish, G. S., & Ganasri, B. P. (2015). (PDF) Impact of land use change on hydrological systems: A review of current modeling approaches. *ResearchGate*. https://www.researchgate.net/publication/287374409_Impact_of_land_use_change_on_hydrological_systems_A_review_of_current_modeling_approaches

Eekhout, J. P. C., Hunink, J. E., Terink, W., & de Vente, J. (2018). Why increased extreme precipitation under climate change negatively affects water security. *Hydrology and Earth System Sciences*, *22*(11), 5935–5946. https://doi.org/10.5194/hess-22-5935-2018

EPM. (2015). Análisis de la información batimétrica del embalse Riogrande II.

EPM. (2019). Resultados Batimetría embalses La Fe y Quebradona.

EPM. (2023, October 9). Plantas de potabilización. https://www.epm.com.co/institucional/sobre-epm/nuestras-plantas/plantas-de-agua.html

EPM. (2024a). Presentación—Atención a medios—Modernización planta de potabilización Manantiales. https://www.epm.com.co/content/dam/epm/institucional/sala-de-prensa-epm/noticias-y-novedades/noticias-y-novedades/interrupcion-acueducto-norte-valle-aburra-epm/presentacion-manantiales-05-11-2024.pdf

EPM. (2024b). Aumento del consumo fraudulento de agua en el Valle de Aburrá. Portal EPM. https://www.epm.com.co/content/epm/institucional/sala-de-prensa/noticias-y-novedades/se-incrementa-el-consumo-fraudulento-de-agua-en-el-valle-de-aburraFarinosi, F., Arias, M. E., Lee, E., Longo, M., Pereira, F. F., Livino, A., Moorcroft, P. R., & Briscoe,

Farinosi, F., Arias, M. E., Lee, E., Longo, M., Pereira, F. F., Livino, A., Moorcroft, P. R., & Briscoe, J. (2019). Future Climate and Land Use Change Impacts on River Flows in the Tapajós Basin in the Brazilian Amazon. *Earth's Future*, *7*(8), 993–1017. https://doi.org/10.1029/2019EF001198

Flórez Molina, M. T., Parra Sánchez, L. N., Bolaños Benitez, S. V., Gallo Sánchez, L. J., Poveda Sáenz, A. M., & Agudelo Echavarría, D. M. (2018). Tasas de sedimentación y características de sedimentos de fondo en tres embalses de Antioquia, Colombia. *Ingeniería Del Agua*, 22(4), Article 4. https://doi.org/10.4995/ia.2018.8001Flörke,

Flörke, M., Kynast, E., Bärlund, I., Eisner, S., Wimmer, F., & Alcamo, J. (2013). Domestic and industrial water uses of the past 60 years as a mirror of socio-economic development: A global simulation study. *Global Environmental Change*, *23*(1), 144–156. https://doi.org/10.1016/j.gloenvcha.2012.10.018

Funk, C., Peterson, P., Landsfeld, M., Pedreros, D., Verdin, J., Shukla, S., Husak, G., Rowland, J., Harrison, L., Hoell, A., & Michaelsen, J. (2015). The climate hazards infrared precipitation with stations—A new environmental record for monitoring extremes. *Scientific Data*, *2*(1), 150066. https://doi.org/10.1038/sdata.2015.66

García-Álvarez, D., Camacho Olmedo, M. T., Paegelow, M., & Mas, J. F. (Eds.). (2022). Land Use Cover Datasets and Validation Tools: Validation Practices with QGIS. Springer International Publishing. https://doi.org/10.1007/978-3-030-90998-7

Gassman, P. W., Sadeghi, A. M., & Srinivasan, R. (2014). Applications of the SWAT Model Special Section: Overview and Insights. *Journal of Environmental Quality*, 43(1), 1–8. https://doi.org/10.2134/jeq2013.11.0466

Gesualdo, G. C., Oliveira, P. T., Rodrigues, D. B. B., & Gupta, H. V. (2019). Assessing water security in the São Paulo metropolitan region under projected climate change. *Hydrology and Earth System Sciences*, 23(12), Article 12. https://doi.org/10.5194/hess-23-4955-2019

Giraldo, M. P. S. (2017). Water Distribution and Drainage Systems of Aburrá Valley, Colombia – Empresas Públicas de Medellín E.S.P. *Procedia Engineering*, 186, 4–11. https://doi.org/10.1016/j.proeng.2017.03.201

Gupta, H. V., Kling, H., Yilmaz, K. K., & Martinez, G. F. (2009). Decomposition of the mean squared error and NSE performance criteria: Implications for improving hydrological modelling. *Journal of Hydrology*, 377(1), 80–91. https://doi.org/10.1016/j.jhydrol.2009.08.003

Hagen, A. (2002) Multi-Method Assessment of Map Similarity. In: Ruiz, M., Gould, M. and Ramon, J., Eds., *Proceedings of the 5th AGILE Conference on Geographic Information Science*, European Commission, Palma, 171-182.

Hashimoto. (1982). Reliability, resiliency, and vulnerability criteria for water resource system performance evaluation. https://agupubs.onlinelibrary.wiley.com/doi/abs/10.1029/wr018i001p00014

Held, I. M., Guo, H., Adcroft, A., Dunne, J. P., Horowitz, L. W., Krasting, J., Milly, C., E. Shevliakova, Winton, M., Zhao, M., Bushuk, M., Wittenberg, A. T., B. Wyman, Xiang, B., Zhang, R., Anderson, W., Balaji, V., Donner, L., Dunne, K., ... Zadeh, N. (2019). NOAA-GFDL/CM4: CM4.0 Paper Release (Versions cm4-20190717) [Computer software]. Zenodo. https://doi.org/10.5281/ZENODO.3339397

Held, I. M., Guo, H., Adcroft, A., Dunne, J. P., Horowitz, L. W., Krasting, J., Shevliakova, E., Winton, M., Zhao, M., Bushuk, M., Wittenberg, A. T., Wyman, B., Xiang, B., Zhang, R., Anderson, W., Balaji, V., Donner, L., Dunne, K., Durachta, J., ... Zadeh, N. (2019). Structure and Performance of GFDL's CM4.0 Climate Model. *Journal of Advances in Modeling Earth Systems*, 11(11), 3691–3727. https://doi.org/10.1029/2019MS001829

Hersbach, H., Bell, B., Berrisford, P., Biavati, G., Horányi, A., Muñoz Sabater, J., Nicolas, J., Peubey, C., Radu, R., Rozum, I., Schepers, D., Simmons, A., Soci, C., Dee, D., & Thépaut, J.-N. (2023). *ERA5 hourly data on single levels from 1940 to present*. 10.24381/cds.adbb2d47

IPCC - Intergovernmental Panel on Climate Change. (2024, May 8). Intergovernmental Panel on Climate Change SSP-RCP scenarios. *Ministry for the Environment*. https://environment.govt.nz/what-you-can-do/climate-scenarios-toolkit/climate-scenarios-list/ipccs-ssp-rcp-scenarios/

IPCC - Intergovernmental Panel on Climate Change (IPCC) (Ed.). (2023). Summary for Policymakers. In Climate Change 2021 – *The Physical Science Basis: Working Group I Contribution to the Sixth Assessment Report of the Intergovernmental Panel on Climate Change* (pp. 3–32). Cambridge University Press. https://doi.org/10.1017/9781009157896.001

Kjeldsen, T. R., & and Rosbjerg, D. (2004). Choice of reliability, resilience and vulnerability estimators for risk assessments of water resources systems / Choix d'estimateurs de fiabilité, de résilience et de vulnérabilité pour les analyses de risque de systèmes de ressources en eau. *Hydrological Sciences Journal*, 49(5), 767. https://doi.org/10.1623/hysj.49.5.755.55136Kling, H., Fuchs, M., & Paulin, M. (2012).

Kling, H., Fuchs, M., & Paulin, M. (2012). Runoff conditions in the upper Danube basin under an ensemble of climate change scenarios. *Journal of Hydrology*, 424–425, 264–277. https://doi.org/10.1016/j.jhydrol.2012.01.011

Krause, P., Boyle, D. P., & Bäse, F. (2005). Comparison of different efficiency criteria for hydrological model assessment. *Advances in Geosciences*, 5, 89–97. https://doi.org/10.5194/adgeo-5-89-2005

Kumar, N., Singh, V. G., Singh, S. K., Behera, D. K., & Gašparović, M. (2023). Modeling of land use change under the recent climate projections of CMIP6: A case study of Indian river basin. *Environmental Science and Pollution Research*. https://doi.org/10.1007/s11356-023-26960-z

Lehner, F., Nadeem, I., & Formayer, H. (2021). Evaluating quantile-based bias adjustment methods for climate change scenarios. *Hydrology and Earth System Sciences Discussions*, 1–26. https://doi.org/10.5194/hess-2021-498

Leite-Filho et al. (2020). Modeling Environmental Dynamics with Dinamica EGO. https://dinamicaego.com/dokuwiki/doku.php?id=guidebook_start

Liu, L., Lopez, E., Dueñas-Osorio, L., Stadler, L., Xie, Y., Alvarez, P. J. J., & Li, Q. (2020). The importance of system configuration for distributed direct potable water reuse. *Nature Sustainability*, 3(7), 548–555. https://doi.org/10.1038/s41893-020-0518-5

Liu, Y., Corcoran, J., & Feng, Y. (2020). Cellular Automata. In A. Kobayashi (Ed.), *International Encyclopedia of Human Geography (Second Edition)* (pp. 101–104). Elsevier. https://doi.org/10.1016/B978-0-08-102295-5.10519-0

Lomax, N., Smith, A. P., Archer, L., Ford, A., & Virgo, J. (2022). An Open-Source Model for Projecting Small Area Demographic and Land-Use Change. *Geographical Analysis*, 54(3), Article 3. https://doi.org/10.1111/gean.12320

López-Ballesteros, A., Nielsen, A., Castellanos-Osorio, G., Trolle, D., & Senent-Aparicio, J. (2023). DSOLMap, a novel high-resolution global digital soil property map for the SWAT + model: Development and hydrological evaluation. *CATENA*, 231, 107339. https://doi.org/10.1016/j.catena.2023.107339

MapBiomas Colombia. (2024). *Colección 1 de la Serie anual de Mapas de Cobertura y Uso del Suelo de Colombia*. https://colombia.mapbiomas.org/descargas/

MapBiomas Colombia. (n.d.a). ATBD (Documento Base Teórico de Algoritmos). Retrieved May 12, 2025, from https://colombia.mapbiomas.org/atbd/

MapBiomas Colombia. (n.d.b). Exactitud. Retrieved May 12, 2025, from https://colombia.mapbiomas.org/exactitud/

Miller, S. J. (n.d.). The Method of Least Squares.

Minvivienda. (2017). Resolución 0330—2017. https://minvivienda.gov.co/normativa/resolucion-0330-2017-0

Mishra, B. K., Kumar, P., Saraswat, C., Chakraborty, S., & Gautam, A. (2021). Water Security in a Changing Environment: Concept, Challenges and Solutions. Water, 13(4), Article 4. https://doi.org/10.3390/w13040490

Moghadam, N. T., & Malekmohammadi, B. (2025). Assessment of drought change trends and watershed health using a reliability-resilience-vulnerability framework in mountainous watersheds. Current Research in Environmental Sustainability, 9, 100285. https://doi.org/10.1016/j.crsust.2025.100285

Moriasi et al. (2015). Hydrologic and Water Quality Models: Performance Measures and Evaluation Criteria. Transactions of the ASABE, 58(6), 1763–1785. https://doi.org/10.13031/trans.58.10715

Moriasi, J. G. Arnold, M. W. Van Liew, R. L. Bingner, R. D. Harmel, & T. L. Veith. (2007). Model Evaluation Guidelines for Systematic Quantification of Accuracy in Watershed Simulations. Transactions of the ASABE, 50(3), 885–900. https://doi.org/10.13031/2013.23153

Municipio de Sabaneta. (n.d.). Pasado, presente y futuro. Retrieved May 11, 2025, from https://sabaneta.gov.co/acerca-del-municipio/pasado-presente-y-futuro/

Nash, J. E., & Sutcliffe, J. V. (1970). River flow forecasting through conceptual models part I — A discussion of principles. Journal of Hydrology, 10(3), 282–290. https://doi.org/10.1016/0022-1694(70)90255-6

Neitsch, S. L., Arnold, J. G., Kiniry, J. R., & Williams, J. R. (2009). Soil and Water Assessment Tool Theoretical Documentation Version 2009.

Nguyen, A., Cochrane ,Thomas A., & and Pahlow, M. (2022). Optimising water allocation and land management to mitigate the effects of land use and climate change on reservoir performance. Hydrological Sciences Journal, 67(14), 2129–2146. https://doi.org/10.1080/02626667.2022.2132162

O'Neill, B. C., Kriegler, E., Ebi, K. L., Kemp-Benedict, E., Riahi, K., Rothman, D. S., van Ruijven, B. J., van Vuuren, D. P., Birkmann, J., Kok, K., Levy, M., & Solecki, W. (2017). The roads ahead: Narratives for shared socioeconomic pathways describing world futures in the 21st century. Global Environmental Change, 42, 169–180. https://doi.org/10.1016/j.gloenvcha.2015.01.004

Ortega, G., Arias, P. A., Villegas, J. C., Marquet, P. A., & Nobre, P. (2021). Present-day and future climate over central and South America according to CMIP5/CMIP6 models. International Journal of Climatology, 41(15), Article 15. https://doi.org/10.1002/joc.7221

Osorio Giraldo, D. F. (2019). Vulnerabilidad de la disponibilidad actual y futura del recurso hídrico en el valle de Aburrá y sus cuencas abastecedoras [Trabajo de grado - Maestría, Universidad Nacional de Colombia]. https://repositorio.unal.edu.co/handle/unal/77492

Ossa, J., Ana Karina Campillo, Cristian Omar, & Teresita Betancur. (2021). Representación espacial de zonas de recarga del agua subterránea a partir de mapas isotópicos de precipitación. Caso de estudio: Valle de Aburrá, Colombia. BOLETÍN GEOLÓGICO Y MINERO, 132(1–2), Article 1–2. https://doi.org/10.21701/bolgeomin.132.1-2.007

Pabón-Caicedo, J. D., Arias, P. A., Carril, A. F., Espinoza, J. C., Borrel, L. F., Goubanova, K., Lavado-Casimiro, W., Masiokas, M., Solman, S., & Villalba, R. (2020). Observed and Projected Hydroclimate Changes in the Andes. Frontiers in Earth Science, 8. https://doi.org/10.3389/feart.2020.00061

Performance Indexes Analysis of the Reservoir-Hydropower Plant System Affected by Climate Change | Water Resources Management. (n.d.). Retrieved May 18, 2025, from https://link.springer.com/article/10.1007/s11269-022-03295-x

Priestley, C. H. B., & Taylor, R. J. (1972). On the Assessment of Surface Heat Flux and Evaporation Using Large-Scale Parameters. https://journals.ametsoc.org/view/journals/mwre/100/2/1520-0493_1972_100_0081_otaosh_2_3_co_2.xml

Rahaman, M. H., Masroor, M., Rehman, S., Singh, R., Ahmed, R., Sahana, M., & Sajjad, H. (2022). State of Art of Review on Climate Variability and Water Resources: Bridging Knowledge Gaps and the Way Forward. Water Resources, 49(4), Article 4. https://doi.org/10.1134/S0097807822040169

Ramírez, D. G., Narváez Valderrama, J. F., Palacio Tobón, C. A., García, J. J., Echeverri, J. D., Sobotka, J., & Vrana, B. (2023). Occurrence, sources, and spatial variation of POPs in a mountainous tropical drinking water supply basin by passive sampling. Environmental Pollution, 318, 120904. https://doi.org/10.1016/j.envpol.2022.120904

Ren, K., Huang, S., Huang, Q., Wang, H., Leng, G., Fang, W., & Li, P. (2020). Assessing the reliability, resilience and vulnerability of water supply system under multiple uncertain sources. Journal of Cleaner Production, 252, 119806. https://doi.org/10.1016/j.jclepro.2019.119806

Rodrigues, H., & Soares-Filho, B. (2018). A Short Presentation of Dinamica EGO. In M. T. Camacho Olmedo, M. Paegelow, J.-F. Mas, & F. Escobar (Eds.), *Geomatic Approaches for Modeling Land Change Scenarios* (pp. 493–498). Springer International Publishing. https://doi.org/10.1007/978-3-319-60801-3_35

Sánchez-Gómez, A., Arnold, J. G., Bieger, K., Čerkasova, N., Sammons, N. B., Martínez-Pérez, S., & Molina-Navarro, E. (2025). Modelling Water Management using SWAT+: Application of Reservoirs Release Tables and the New Water Allocation Module in a Highly Managed River Basin. Water Resources Management, 39(5), 2357–2399. https://doi.org/10.1007/s11269-024-04071-9

Sepúlveda-Sánchez, M., Arismendy-González, L. M., Arboleda-Baena, C. M., Múskus López, C. E., Pohlon, E., Flórez Molina, M. T., & Palacio Baena, J. A. (2021). FIRST EVIDENCE OF POTENTIAL TOXIC CYANOBACTERIA IN THE WATER-SEDIMENT INTERFACE OF A TROPICAL DRINKING WATER RESERVOIR. Revista Internacional de Contaminación Ambiental. https://doi.org/10.20937/RICA.53696

Shrestha, B., Cochrane, T. A., Caruso, B. S., Arias, M. E., & Piman, T. (2016). Uncertainty in flow and sediment projections due to future climate scenarios for the 3S Rivers in the Mekong Basin. Journal of Hydrology, 540, 1088–1104. https://doi.org/10.1016/j.jhydrol.2016.07.019

Soares-Filho, B., Rodrigues, H., & Follador, M. (2013). A hybrid analytical-heuristic method for calibrating land-use change models. *Environmental Modelling & Software*, 43, 80–87. https://doi.org/10.1016/j.envsoft.2013.01.010

Soares-Filho, B. S., Coutinho Cerqueira, G., & Lopes Pennachin, C. (2002). dinamica—Astochastic cellular automata model designed to simulate the landscape dynamics in an Amazonian colonization frontier. *Ecological Modelling*, 154(3), Article 3. https://doi.org/10.1016/S0304-3800(02)00059-5

Superintendencia Servicios Públicos Domiciliarios. (2021). Evaluación de prestadores. Retrieved May 11, 2025, from https://www.superservicios.gov.co/Empresas-vigiladas/Acueducto-alcantarillado-y-aseo/Acueducto-y-alcantarillado/Evaluacion-de-prestadores

Tolson, B. A., & Shoemaker, C. A. (2007). Dynamically dimensioned search algorithm for computationally efficient watershed model calibration. *Water Resources Research*, *43*(1). https://doi.org/10.1029/2005WR004723

Tong, X., & Feng, Y. (2020). A review of assessment methods for cellular automata models of land-use change and urban growth. International Journal of Geographical Information Science, 34(5), Article 5. https://doi.org/10.1080/13658816.2019.1684499

UN-Water. (2019). Water security and the sustainable development goals—UNESCO Digital Library. https://unesdoc.unesco.org/ark:/48223/pf0000367904

Uribe, N., Srinivasan, R., Corzo, G., Arango, D., & Solomatine, D. (2020). Spatio-temporal critical source area patterns of runoff pollution from agricultural practices in the Colombian Andes. *Ecological Engineering*, 149, 105810. https://doi.org/10.1016/j.ecoleng.2020.105810

Valencia, S., Marín, D. E., Gómez, D., Hoyos, N., Salazar, J. F., & Villegas, J. C. (2023). Spatio-temporal assessment of Gridded precipitation products across topographic and climatic gradients in Colombia. *Atmospheric Research*, 285, 106643. https://doi.org/10.1016/j.atmosres.2023.106643

Valencia, S., Villegas, J. C., Hoyos, N., Duque-Villegas, M., & Salazar, J. F. (2024). Streamflow response to land use/land cover change in the tropical Andes using multiple SWAT model variants. *Journal of Hydrology: Regional Studies*, 54, 101888. https://doi.org/10.1016/j.ejrh.2024.101888

Vargas-Pineda, O. I., Trujillo-González, J. M., & Torres-Mora, M. A. (2020). Supply–Demand of Water Resource of a Basin With High Anthropic Pressure: Case Study Quenane-Quenanito Basin in Colombia. Air, Soil and Water Research, 13, 1178622120917725. https://doi.org/10.1177/1178622120917725

Vörösmarty, C. J., Green, P., Salisbury, J., & Lammers, R. B. (2000). Global Water Resources: Vulnerability from Climate Change and Population Growth. *Science*, 289(5477), 284–288. https://doi.org/10.1126/science.289.5477.284

Willmott, C. J. (1981). On the Validation of Models. *Physical Geography*, 2(2), 184–194. https://doi.org/10.1080/02723646.1981.10642213

Yang, W., Mu, L., & Hou, K. (2022). Progress on Geographic Cellular Automata Model. *2022 Global Conference on Robotics, Artificial Intelligence and Information Technology (GCRAIT)*, 333–336. https://doi.org/10.1109/GCRAIT55928.2022.00077

Zhang, P., Zhang, L., Chang, Y., Xu, M., Hao, Y., Liang, S., Liu, G., Yang, Z., & Wang, C. (2019). Food-energy-water (FEW) nexus for urban sustainability: A comprehensive review. *Resources, Conservation and Recycling*, 142, 215–224. https://doi.org/10.1016/j.resconrec.2018.11.018

Zhu, K., Cheng, Y., Zang, W., Zhou, Q., El Archi, Y., Mousazadeh, H., Kabil, M., Csobán, K., & Dávid, L. D. (2023). Multiscenario Simulation of Land-Use Change in Hubei Province, China Based on the Markov-FLUS Model. *Land*, 12(4), Article 4. https://doi.org/10.3390/land12040744

Appendix A - Lookup tables Land use for SWAT+

The land use parametrization for the Riogrande II reservoir watershed is present in Table 11.

LANDUSE_ID	SWAT_CODE
3	FRST
9	PINE
13	FESC
21	PAST
24	URHD
25	BSVG
30	BSVG
33	WETW

Table 11. Land use parametrization for Riogrande II watershed

The land use parametrization for the La Fe reservoir watershed is present in Table 12.

LANDUSE_ID	SWAT_CODE
3	FRST
13	FESC
21	PAST
24	URHD
25	BSVG
33	WETW

Table 12. Land use parametrization for Riogrande II watershed

Appendix B

resv_ dyn.py algorithm

The following routine calculates the reservoir dynamics for provided vectors of climatic data: observation times (`time`), daily inflow volume (`inflow`), daily precipitation over the reservoir (`pcp_rate`), daily evaporation over the reservoir (`evap_rate`), the corresponding population values (`population`) and the initial reservoir volume (`vol_init`). The relevant function is `evolve_period` and the remaining are auxiliary functions. In the following version the parameters for the La Fe reservoir are used, but an the usage for the Riogrande II reservoir is analogous.

```
import pandas as pd

# LA_FE
vol_nom = 11.33e6                   # principal volume
vol_min = 0.1942 * vol_nom          # dead volume
vol_mid = 0.5137 * vol_nom          # technical minimum
vol_max = 13.53e6                   # emergency volume

city_demand_frac = 0.5
ref_population = 3849641 # population relate to ref_use_rate_day (2021)
ref_use_rate_day = 4.6 * 60 * 60 * 24 # m³/s -> m³/day

extra_outflow_start_year = 2024
extra_outflow_end_year = 2080
extra_outflow = 0.6 * 60 * 60 * 24 # Rionegro starts in 2024
extra_population = extra_outflow * ref_population / ref_use_rate_day

extra_inflow_start_year = 2011
extra_inflow_end_year = 2080
extra_inflow_slow = 3.0 * 60 * 60 * 24
extra_inflow_fast = 6.0 * 60 * 60 * 24

# demands take into account water distribution system: do not add more sinks that there
are
person_demand_day = ref_use_rate_day /(ref_population * city_demand_frac)
eco_demand_day = 4.35 * 60 * 60 * 24
reg_erg_demand_day = 0 * 60 * 60 * 24 # already included in person demand
min_erg_demand_day = 0 * 60 * 60 * 24 # already included in person demand

outflow_nom_days = 2
outflow_max_days = 1

def calc_demand(vol, population):
    base_demand = eco_demand_day +
                  city_demand_frac * person_demand_day * population
    if vol >= vol_mid:
        return base_demand + reg_erg_demand_day
    if vol < vol_mid:
        return base_demand + min_erg_demand_day

def calc_outflow(vol):
    if vol > 0.95*vol_max:
        return (vol - vol_nom)/outflow_max_days
    elif vol > vol_nom:
        return (vol - vol_nom)/outflow_nom_days
    else:
        return 0
```

```
def calc_outflow_dumb(vol):
    if vol > 0.95*vol_max:
        return (vol - vol_nom)
    elif vol > vol_nom:
        return (vol - vol_nom)
    else:
        return 0

def calc_extra_inflow(date, vol):
    if vol < vol_mid and date.year > extra_inflow_start_year and
       date.year < extra_inflow_end_year:
        return extra_inflow_fast
    elif vol < vol_nom and date.year > extra_inflow_start_year and
         date.year < extra_inflow_end_year:
        return extra_inflow_slow
    else:
        return 0

def evolve_one_day(date, vol, inflow, pcp_rate, evap_rate, population):
    evap = evap_rate * vol
    pcp = pcp_rate * vol
    demand = calc_demand(vol, population)
    withdraw = 0
    unmet_demand = 0
    if (vol > vol_min):
        unmet_demand = 0
        withdraw = demand
    else:
        unmet_demand = demand
        withdraw = 0

    outflow = calc_outflow(vol)

    # add extra inflow
    extra_inflow = calc_extra_inflow(date, vol)
    inflow = inflow + extra_inflow

    # the volume for the next day
    vol = vol + inflow + pcp - outflow - evap - withdraw
    return {'vol': vol, 'demand': demand, 'outflow': outflow,
            'withdraw': withdraw, 'unmet_demand': unmet_demand,
            'extra_inflow': extra_inflow }


def evolve_period(time, vol_init, inflow, pcp_rate, evap_rate,
                  population):
    vol = []
    pcp = []
    evap = []
    demand = []
    outflow = []
    withdraw = []
    unmet_demand = []
    extra_inflow = []
    for i in range (len(time)):
        vol.append(vol_init)
        pcp.append(vol_init * pcp_rate[i])
        evap.append(vol_init * evap_rate[i])
        corr_population = population[i]
```

```
        if time[i].year >= extra_outflow_start_year and time[i].year <
           extra_outflow_end_year:
            corr_population += extra_population
        evo = evolve_one_day(time[i], vol_init, inflow[i], pcp_rate[i],
              evap_rate[i], corr_population)
        demand.append(evo['demand'])
        outflow.append(evo['outflow'])
        withdraw.append(evo['withdraw'])
        unmet_demand.append(evo['unmet_demand'])
        extra_inflow.append(evo['extra_inflow'])
        vol_init = evo['vol']

    df = pd.DataFrame({
        'time': time,
        'Inflow_m3': inflow,
        'Outflow_m3': outflow,
        'StorageFlow_m3': vol,
        'Demand_m3': demand,
        'Withdrawal_m3': withdraw,
        'Unmet_demand_m3': unmet_demand,
        'pcp_m3': pcp,
        'evap_m3': evap,
        'extra_inflow_m3': extra_inflow
        })
    return df
```

Appendix C - Transition matrices and Weights of Evidence

The Transition Matrix for the Riogrande II and La Fe watershed is presented in Table 13.

Transition		**Rate ($\times 10^{-5}$)**	
To	**From**	**Riogrande II**	**La Fe**
Forest	Pinus	1.14	-
Forest	Other form	44.06	-
Forest	Mosaic Agricult.	1294.22	1077.38
Forest	Urban	-	25.88
Forest	Other non-veg.	1.26	67.02
Pinus	Forest	0.80	-
Pinus	Other form	37.71	-
Pinus	Mosaic Agricult.	946.59	-
Pinus	Urban	-	-
Pinus	Other non-veg.	-	-
Other form	Forest	231.81	214.70
Other form	Pinus	69.19	-
Other form	Mosaic Agricult.	3787.71	1837.16
Other form	Urban	14.23	214.70
Other form	Other non-veg.	-	360.79
Mosaic Agricult.	Forest	116.97	289.61
Mosaic Agricult.	Pinus	8.51	-
Mosaic Agricult.	Other form	28.86	105.36
Mosaic Agricult.	Urban	4.06	69.07
Mosaic Agricult.	Other non-veg.	2.21	134.44
Other non-veg.	Forest	25.75	79.49
Other non-veg.	Pinus	103.00	-
Other non-veg.	Other form	476.40	5.68
Other non-veg.	Mosaic Agricult.	630.90	562.11
Other non-veg.	Urban	1248.93	817.61
Other non-veg.	Minery	51.50	-
Minery	Forest	337.23	-
Minery	Other form	74.94	-
Minery	Mosaic Agricult.	449.64	-
Minery	Urban	374.70	-
Minery	Other non-veg.	299.76	-

Table 13. Transition matrix multistep for the three study region

The Weights of Evidence for the Riogrande II watershed are presented below.

From	To	Digital Elevation Model																
3	9	low limit	0	2360	2370	2380	2390	2550	2560	2580	2590	2700	2710	2720	2730	2750	2760	2840
		weight	0.782	0.000	1.404	0.000	-1.451	0.000	-1.173	0.000	-1.721	-0.740	0.000	-0.671	0.074	1.629	1.225	0.000
		low limit	2850	2860	2870	2900	2920	2930										
		weight	0.914	2.566	1.584	0.646	0.000	0.000										
3	13	low limit	0	2360	2370	2450	2460	2470	2480	2490	2510	2520	2530	2580	2590	2610	2650	2660
		weight	-2.179	-1.301	-0.878	-0.271	0.209	0.446	0.035	0.271	0.499	0.752	0.527	-0.317	-0.557	-0.318	0.137	-0.205
		low limit	2670	2680	2700	2710	2880	2890	2900	2910	2930	2950	2960	2990	3100			
		weight	0.034	0.386	0.643	0.433	-2.764	-0.296	-1.349	-0.915	-1.315	-2.280	-1.621	-2.265	-2.206			
3	21	low limit	0	2310	2320	2330	2350	2360	2380	2390	2430	2490	2610	2620	2700	2710	2790	2800
		weight	-1.779	-1.095	-0.610	-0.306	0.086	0.272	0.574	0.809	1.058	0.781	0.333	0.172	-0.036	-0.198	-0.779	-1.010
		low limit	2810	2820	2830	3010												
		weight	-1.283	-1.618	-2.47	-6.223												
3	24	low limit	0	2500	2510	2520	2530	2550	2560	2600	2610	2620	2770	2780	2790	2800	2810	1
		weight	0.522	3.253	0.796	1.412	1.010	0.000	-0.158	0.705	0.000	-0.527	0.502	0.000	0.680	0.000	0.000	1.522
3	25	low limit	0	2500	2510	2680	2700	2710	2720	2730								
		weight	-1.441	1.4179	1.0439	0.1027	-0.8404	0.795	0	0								
9	3	low limit	0	2420	2430	2440	2470	2480	2510	2520	2590	2600	2720	2730	2740	2750	2770	2780
		weight	-1.835	1.639	0.000	1.242	0.000	2.143	0.000	1.299	0.000	0.822	0.000	3.754	0.000	3.642	0.000	0.000
9	13	low limit	0	2300	2570	2580	2620	2630	2660	2670	2700							
		weight	-1.516	-1.046	2.929	1.7646	0	-0.302	1.7927	2.6912	2.444							
9	21	low limit	0	2220	2230	2300	2310	2350	2510	2520	2530	2540	2550	2560	2570	2640		
		weight	1.014	1.812	0.512	-0.367	-0.265	-0.089	0.286	-0.778	-0.436	-0.178	0.592	1.088	0.720	0.727		
9	25	low limit	0	2290	2320	2330	2340											
		weight	2.8705	1.5613	-0.027	0	0											
13	3	low limit	0	2410	2420	2430	2440	2460	2470	2550	2560	2570	2580	2680	2690	2860	2870	2900
		weight	-2.111	0.902	-0.502	1.190	1.855	3.136	1.556	0.397	0.094	1.741	0.925	0.113	0.171	1.814	1.130	-0.180
		low limit	2910	2920	2940	2950	2960	2970	2990	3000	3020	3030	3040	3060	3070	3080	3090	3100
		weight	-0.786	-0.438	0.191	-0.258	-0.994	-0.788	-0.257	-0.047	0.418	-0.135	0.045	-1.211	-0.323	-0.590	-0.295	0.223
		low limit	3110	3120	3140	3150	3160	3180	3260	3280	3310	3320						
		weight	-0.228	-0.407	-1.618	-0.925	-0.498	-0.768	-1.147	-1.484	0.000	-3.949						
13	9	low limit	0	2250	2260	2270	2280	2290	2300	2310	2320	2330	2340	2350	2410	2420	2480	2490
		weight	3.141	0	0.7615	0	1.7423	2.6964	1.3211	0	0	2.3709	0	1.4546	2.3991	1.5396	0	0
		low limit	2500	2510	2530	2550	2560	2570	2580	2680	2690	2700	2910	2920				
		weight	0.000	0.000	-1.119	-0.240	0.416	2.796	1.524	0.081	0.692	0.482	0.000	0.000				
13	21	low limit	0	2250	2390	2400	2440	2450	2460	2480	2630	2670	2680	2700	2710	2720	2730	2780
		weight	-1.96	-1.265	0	1.5142	1.3437	2.2559	2.6162	2.174	1.4965	0.249	-0.024	-0.0981	0.0412	0.4135	0.5068	0.6737
		low limit	2830	2840	2880	2890	2900	2940	3240	3250	3310	3320						
		weight	2.335	1.002	0.259	-1.433	-3.344	-6.213	0.000	0.000	0.000	0.000						
13	24	low limit	0	2310	2320	2680	2690	2700	2780									
		weight	1.5643	5.5352	2.0235	0	0	0	0									
13	25	low limit	0	2310	2320	2420	2690	2700	2720	2730								
		weight	1.111	0.000	3.321	1.740	0.000	-1.559	0.000	0.000								
21	3	low limit	0	2310	2320	2330	2460	2570	2580	2910	2920							
		weight	-1.311	-0.63	-0.898	-0.666	-0.42	0.0907	0.2776	2.0954	2.732							
21	9	low limit	0	2300	2320	2360	2370	2410	2420	2430	2460	2470	2480	2560	2570	2580	2610	2620
		weight	3.533	2.016	1.444	0.183	-0.029	-0.469	0.158	-0.138	-1.701	-2.682	-1.832	0.089	-2.326	-0.975	0.148	0.709
		low limit	2630	2650	2660	2670	2680	2690	2700	2720	2740	2750	2760	2770	2780	2790	2800	2810
		weight	0.0221	-1.13	-2.284	0.4004	1.1127	1.6172	1.1836	0.7683	0.2167	-0.7746	0	-1.8936	0	-2.155	0	-0.792
		low limit	2850	2860	2880	2890												
		weight	-1.131	-1.658	0.000	0.000												
21	13	low limit	0	2310	2320	2330	2350	2360	2370	2380	2390	2440	2450	2460	2470	2480	2490	2530
		weight	0.886	0.5948	0.251	0.0129	-0.7218	-0.974	-2.3006	-1.238	-0.7724	-0.3281	-0.529	-0.8432	-0.553	-0.927	-0.645	-0.361
		low limit	2540	2560	2580	2590	2680	2690	2720	2730	2740	2960	2970					
		weight	-0.555	-0.248	-0.662	-0.338	-0.131	0.120	0.332	0.615	0.849	3.393	4.347					
21	24	low limit	0	2300	2310	2330	2340	2350	2380	2480	2490	2510	2520	2530	2540	2550	2580	2590
		weight	1.9715	4.4576	2.3525	-0.301	0	0	-1.8957	1.937	1.3931	0.5462	0.213	-0.1372	-2.178	-1.127	1.2577	0.1911
		low limit	2600	2610	2770	2780	2790	2800	2810									
		weight	0.000	-2.008	0.351	0.142	0.378	0.000	0.000									
21	25	low limit	0	2300	2370	2380	2390	2400	2410	2460	2470	2480	2490	2500	2510	2520	2530	2540
		weight	3.6787	2.0536	0	-0.865	-0.2701	0	-2.0547	-0.863	-0.0797	1.4085	-0.633	0.6651	1.4026	0.7306	0.4068	-0.471
		low limit	2550	2560	2570	2600	2610	2620	2720	2730	2780	2790	2800	2810				
		weight	-0.801	0.000	-1.271	-0.668	0.000	-1.906	0.000	-1.336	1.731	0.293	0.000	0.000				
25	3	low limit	0	2710	2790	2810	3260											
		weight	-0.534	0	3.4177	0	0											
25	9	low limit	0	2340	2350	2490	2500											
		weight	0.134	0.000	0.933	0.000	0.000											
25	13	low limit	0	2300	2310	2320	2490	2500	2600	2610	2670	2710	2790	2800				
		weight	-0.403	0.5	0	-0.599	0.5	1.5986	0	0	0	1.1931	0	0				
25	21	low limit	0	2490	2500	2590	2700	2710	2720	2800	2810	3260						
		weight	-2.156	0.912	0.000	-1.573	0.000	0.000	1.200	0.000	-0.069	0.000						
25	24	low limit	0	2310	2320	2490	2500	2510	2670	2790								
		weight	-2.073	0	2.3294	1.408	0	0.6813	0	0								
25	30	low limit	0	2490	2500	2590												
		weight	0.062	2.031	0.000	0.000												
30	3	low limit	0	2480	2490	2500												
		weight	3.344	0.2995	0	0												
30	13	low limit	0	2500														
		weight	0.139	0.000														
30	21	low limit	0	2490	2500	2510												
		weight	0.2085	-0.365	0.253	0												

From	To		Municipal boundaries															
3	9	low limit	10	11	12	13	14	15	16	17	18	19	20	21	22	23	24	25
		weight	0.000	0.000	0.000	0.000	0.000	-1.640	0.000	0.000	0.000	0.000	0.000	0.000	0.000	0.667	0.000	3.590
3	13	low limit	10	11	12	13	14	15	16	17	18	19	20	21	22	23	24	25
		weight	0	0	0	0	0	-0.1465	0.4053	0	0	-0.24	-1.128	0	1.0436	0.8377	0	1.2132
3	21	low limit	10	11	12	13	14	15	16	17	18	19	20	21	22	23	24	25
		weight	-0.483	0.238	0.249	0.000	-0.020	0.154	0.772	-2.994	0.000	-0.048	-1.376	0.000	-1.341	0.796	2.807	0.198
3	24	low limit	10	11	12	13	14	15	16	17	18	19	20	21	22	23	24	25
		weight	0	0	0	0	0	1.7045	0	0	0	0	0	0	0	-0.899	0	2.7874
3	25	low limit	10	11	12	13	14	15	16	17	18	19	20	21	22	23	24	25
		weight	0.000	0.000	0.000	0.000	0.000	1.537	0.000	0.000	0.000	0.704	0.000	0.000	0.000	-1.099	0.000	0.000
9	3	low limit	10	11	12	13	14	15	16	17	18	19	20	21	22	23	24	25
		weight	0	0	0	0	0	-0.3739	0	0	0	0.2051	0	0	0	0.3871	0	0
9	13	low limit	10	11	12	13	14	15	16	17	18	19	20	21	22	23	24	25
		weight	0.000	0.000	0.000	0.000	0.000	-1.782	-1.973	0.000	0.000	-0.585	0.000	0.000	0.000	1.091	0.000	0.000
9	21	low limit	10	11	12	13	14	15	16	17	18	19	20	21	22	23	24	25
		weight	0	0	0	0	0	-0.2462	0.0453	0	0	0.0671	0	0	0	0.1941	0	0
9	24	low limit	10	11	12	13	14	15	16	17	18	19	20	21	22	23	24	25
		weight	0.000	0.000	0.000	0.000	0.000	0.000	0.000	0.000	0.000	0.000	0.000	0.000	0.000	0.000	0.000	0.000
9	25	low limit	10	11	12	13	14	15	16	17	18	19	20	21	22	23	24	25
		weight	0	0	0	0	0	0	0.0049	0	0	1.1059	0	0	0	0	0	0
13	3	low limit	10	11	12	13	14	15	16	17	18	19	20	21	22	23	24	25
		weight	0.363	0.000	0.000	0.000	0.000	1.143	0.213	0.000	0.000	0.384	-0.486	0.000	0.000	0.339	0.000	-0.243
13	9	low limit	10	11	12	13	14	15	16	17	18	19	20	21	22	23	24	25
		weight	0	0	0	0	0	0.9663	0.5994	0	0	0	0	0	0	0.985	0	-0.565
13	21	low limit	10	11	12	13	14	15	16	17	18	19	20	21	22	23	24	25
		weight	0.828	0.000	-1.044	0.000	-0.233	1.882	0.267	-0.351	0.000	-0.361	-1.966	0.000	-0.676	0.779	0.000	-0.439
13	24	low limit	10	11	12	13	14	15	16	17	18	19	20	21	22	23	24	25
		weight	0	0	0	0	0	3.1404	0	0	0	1.539	0	0	0	0.0364	0	0
13	25	low limit	10	11	12	13	14	15	16	17	18	19	20	21	22	23	24	25
		weight	0.000	0.000	0.000	0.000	0.000	3.991	3.011	0.000	0.000	-1.294	0.000	0.000	0.000	-1.641	0.000	0.000
21	3	low limit	10	11	12	13	14	15	16	17	18	19	20	21	22	23	24	25
		weight	0	1.2385	0	0	-0.789	-0.2816	-0.531	2.4982	0	-0.178	0.622	0	-0.232	-0.337	-0.623	-0.058
21	9	low limit	10	11	12	13	14	15	16	17	18	19	20	21	22	23	24	25
		weight	0.000	0.000	0.000	0.000	0.000	0.006	-3.896	0.000	0.000	-0.821	0.000	0.000	0.000	0.798	0.000	0.047
21	13	low limit	10	11	12	13	14	15	16	17	18	19	20	21	22	23	24	25
		weight	0	0	0	0	0.9664	-0.5885	0.5064	3.9659	0	-0.522	0.4607	0	0.1127	-0.108	0.321	1.7203
21	24	low limit	10	11	12	13	14	15	16	17	18	19	20	21	22	23	24	25
		weight	0.000	0.000	0.000	0.000	0.000	1.148	0.000	0.000	0.000	-0.257	-1.272	0.000	0.000	-0.839	-0.202	1.991
21	25	low limit	10	11	12	13	14	15	16	17	18	19	20	21	22	23	24	25
		weight	0	0	0	0	0	0.9566	0	0	0	0.4012	-1.551	0	0	-1.316	3.4977	0
25	3	low limit	10	11	12	13	14	15	16	17	18	19	20	21	22	23	24	25
		weight	0.000	0.000	0.000	0.000	0.000	0.000	0.000	0.000	0.000	0.000	0.933	0.000	0.000	3.418	0.000	0.000
25	9	low limit	10	11	12	13	14	15	16	17	18	19	20	21	22	23	24	25
		weight	0	0	0	0	0	2.5014	0	0	0	0	0	0	0	0	0	0
25	13	low limit	10	11	12	13	14	15	16	17	18	19	20	21	22	23	24	25
		weight	0.000	0.000	0.000	0.000	0.000	-0.011	-0.098	0.000	0.000	0.000	0.000	0.000	0.000	2.985	0.000	0.000
25	21	low limit	10	11	12	13	14	15	16	17	18	19	20	21	22	23	24	25
		weight	0	0	0	0	0	0.4014	0	0	0	0	-0.186	0	0	3.7156	0	0
25	24	low limit	10	11	12	13	14	15	16	17	18	19	20	21	22	23	24	25
		weight	0.000	0.000	0.000	0.000	0.000	2.131	0.000	0.000	0.000	0.000	0.000	0.000	0.000	2.532	0.000	0.000
25	30	low limit	10	11	12	13	14	15	16	17	18	19	20	21	22	23	24	25
		weight	0	0	0	0	0	2.5014	0	0	0	0	0	0	0	0	0	0
30	3	low limit	10	11	12	13	14	15	16	17	18	19	20	21	22	23	24	25
		weight	0.000	0.000	0.000	0.000	0.000	0.000	0.000	0.000	0.000	0.000	0.000	0.000	0.000	0.000	0.000	0.000
30	13	low limit	10	11	12	13	14	15	16	17	18	19	20	21	22	23	24	25
		weight	0	0	0	0	0	0	0	0	0	0	0	0	0	0	0	0
30	21	low limit	10	11	12	13	14	15	16	17	18	19	20	21	22	23	24	25
		weight	0.000	0.000	0.000	0.000	0.000	0.000	0.000	0.000	0.000	0.000	0.000	0.000	0.000	0.000	0.000	0.000
30	24	low limit	10	11	12	13	14	15	16	17	18	19	20	21	22	23	24	25
		weight	0	0	0	0	0	0	0	0	0	0	0	0	0	0	0	0
30	25	low limit	10	11	12	13	14	15	16	17	18	19	20	21	22	23	24	25
		weight	0.000	0.000	0.000	0.000	0.000	0.000	0.000	0.000	0.000	0.000	0.000	0.000	0.000	0.000	0.000	0.000

From	To	Slope							
3	9	low limit	1	2	3	4	5	6	7
		weight	1.415	0.638	-1.600	0.535	-0.246	0.000	0.000
3	13	low limit	1	2	3	4	5	6	7
		weight	-0.081	0.0067	0.1999	0.2674	-0.0425	-1.811	-1.126
3	21	low limit	1	2	3	4	5	6	7
		weight	0.416	0.387	0.426	0.355	-0.220	-1.793	-2.196
3	25	low limit	1	2	3	4	5	6	7
		weight	1.1731	-0.991	-0.2325	-0.075	-0.2573	0.26	2.431
9	3	low limit	1	2	3	4	5	6	7
		weight	0.000	0.000	0.000	-0.523	0.561	0.000	0.000
9	13	low limit	1	2	3	4	5	6	7
		weight	0.8073	0.2898	0.2242	0.0292	-0.0962	-1.402	0
9	21	low limit	1	2	3	4	5	6	7
		weight	0.136	0.123	0.119	0.006	-0.044	-0.038	0.714
9	24	low limit	1	2	3	4	5	6	7
		weight	0	0	0	0	0	0	0
9	25	low limit	1	2	3	4	5	6	7
		weight	0.000	0.000	0.991	0.378	-1.023	0.000	0.000
13	3	low limit	1	2	3	4	5	6	7
		weight	-0.186	-0.318	-0.1505	-0.012	0.1416	1.0955	0
13	9	low limit	1	2	3	4	5	6	7
		weight	-0.078	-0.274	0.099	0.061	-0.081	0.000	0.000
13	21	low limit	1	2	3	4	5	6	7
		weight	-0.223	-0.305	-0.1549	0.0037	0.1384	0.5082	2.7406
13	24	low limit	1	2	3	4	5	6	7
		weight	-0.150	0.353	0.561	0.112	-1.375	0.000	0.000
13	25	low limit	1	2	3	4	5	6	7
		weight	0.2778	0.558	0.1785	0.034	-0.5051	0	0
21	3	low limit	1	2	3	4	5	6	7
		weight	-0.388	-0.317	-0.275	-0.131	0.239	1.261	1.796
21	9	low limit	1	2	3	4	5	6	7
		weight	0.3925	0.4102	0.3565	-0.054	-0.2789	-1.61	0
21	13	low limit	1	2	3	4	5	6	7
		weight	-0.349	-0.425	-0.235	-0.073	0.250	0.589	-0.110
21	24	low limit	1	2	3	4	5	6	7
		weight	1.283	1.1297	0.8148	-0.267	-2.0553	0	0
21	25	low limit	1	2	3	4	5	6	7
		weight	1.497	1.250	0.570	-0.325	-1.340	-0.229	0.000
25	3	low limit	1	2	3	4	5	6	7
		weight	1.404	0	0.5167	0	0	0	0
25	9	low limit	1	2	3	4	5	6	7
		weight	0.000	0.000	-0.870	0.865	2.369	0.000	0.000
25	13	low limit	1	2	3	4	5	6	7
		weight	0	-0.903	-0.2039	0.6553	1.8184	0	0
25	21	low limit	1	2	3	4	5	6	7
		weight	-0.696	-0.847	0.026	0.711	0.557	0.000	0.000
25	24	low limit	1	2	3	4	5	6	7
		weight	-0.323	-0.143	0.1112	0.1938	-0.0513	0	0
25	30	low limit	1	2	3	4	5	6	7
		weight	0.000	0.405	0.517	0.000	0.000	0.000	0.000
30	3	low limit	1	2	3	4	5	6	7
		weight	0	0	0	1.2238	0	0	0
30	13	low limit	1	2	3	4	5	6	7
		weight	0.000	1.307	0.000	0.000	0.000	0.000	0.000
30	21	low limit	1	2	3	4	5	6	7
		weight	0	-0.079	-0.6072	0.5306	0.8591	0	0
30	24	low limit	1	2	3	4	5	6	7
		weight	0.000	0.103	-0.425	0.531	0.000	0.000	0.000
30	25	low limit	1	2	3	4	5	6	7
		weight	0.2838	0	-0.8949	0.7538	1.2646	0	0

From	To		Soils										
3	9	low limit	2	4	5	9	10	13	15	17	18	19	20
		weight	0.000	0.000	0.000	0.000	0.026	0.000	0.000	0.000	0.000	1.046	0.000
3	13	low limit	2	4	5	9	10	13	15	17	18	19	20
		weight	-0.927	0.000	-0.576	-2.005	0.709	0.000	-0.818	-1.266	0.000	0.719	3.447
3	21	low limit	2	4	5	9	10	13	15	17	18	19	20
		weight	-0.982	0.000	0.390	-5.921	0.388	0.219	-0.731	-3.060	1.753	0.681	0.760
3	24	low limit	2	4	5	9	10	13	15	17	18	19	20
		weight	0.000	0.000	0.000	0.000	0.000	0.000	0.135	0.000	0.000	-0.029	8.741
3	25	low limit	2	4	5	9	10	13	15	17	18	19	20
		weight	0.062	0.000	0.000	0.000	0.619	0.000	0.685	0.000	0.000	-1.682	6.595
9	3	low limit	2	4	5	9	10	13	15	17	18	19	20
		weight	0.000	0.000	-0.908	0.000	0.000	0.000	0.823	0.000	0.000	0.350	0.000
9	13	low limit	2	4	5	9	10	13	15	17	18	19	20
		weight	0.000	-3.011	-1.667	0.000	-1.787	0.000	0.000	0.000	0.000	0.569	0.000
9	21	low limit	2	4	5	9	10	13	15	17	18	19	20
		weight	0.567	-0.131	-0.201	0.000	-0.342	0.000	-0.351	0.000	0.000	0.129	0.000
9	24	low limit	2	4	5	9	10	13	15	17	18	19	20
		weight	0.000	0.000	0.000	0.000	0.000	0.000	0.000	0.000	0.000	0.000	0.000
9	25	low limit	2	4	5	9	10	13	15	17	18	19	20
		weight	0.000	2.656	0.000	0.000	0.000	0.000	0.000	0.000	0.000	-0.828	0.000
13	3	low limit	2	4	5	9	10	13	15	17	18	19	20
		weight	-0.283	0.000	0.807	-0.835	0.245	1.932	0.069	-1.204	0.000	0.398	0.000
13	9	low limit	2	4	5	9	10	13	15	17	18	19	20
		weight	0.000	2.553	2.017	0.000	-1.613	0.000	0.000	0.000	0.000	0.931	0.000
13	21	low limit	2	4	5	9	10	13	15	17	18	19	20
		weight	-1.475	0.000	1.403	-9.463	0.353	2.694	-0.496	-1.485	0.000	0.759	-1.855
13	24	low limit	2	4	5	9	10	13	15	17	18	19	20
		weight	0.000	0.000	0.000	0.000	1.066	0.000	0.057	0.000	0.000	-0.426	5.601
13	25	low limit	2	4	5	9	10	13	15	17	18	19	20
		weight	0.000	0.000	0.000	0.000	0.000	0.000	0.767	0.000	0.000	-0.053	5.147
21	3	low limit	2	4	5	9	10	13	15	17	18	19	20
		weight	0.629	0.000	-0.527	2.659	-0.463	-0.257	0.379	1.866	1.192	-0.239	-0.768
21	9	low limit	2	4	5	9	10	13	15	17	18	19	20
		weight	-3.551	0.000	0.808	0.000	-0.895	0.000	-1.573	0.000	0.000	0.311	0.000
21	13	low limit	2	4	5	9	10	13	15	17	18	19	20
		weight	0.763	0.000	0.203	3.084	-0.969	-1.651	0.281	1.643	0.000	-0.261	1.239
21	24	low limit	2	4	5	9	10	13	15	17	18	19	20
		weight	-3.503	0.000	0.000	0.000	1.008	0.000	0.368	0.000	0.000	-1.193	5.458
21	25	low limit	2	4	5	9	10	13	15	17	18	19	20
		weight	-1.509	0.000	0.000	0.000	1.370	0.000	0.101	0.000	0.000	-0.692	4.726
25	3	low limit	2	4	5	9	10	13	15	17	18	19	20
		weight	0.000	0.000	0.000	0.000	0.000	0.000	0.000	0.000	0.000	0.585	0.000
25	9	low limit	2	4	5	9	10	13	15	17	18	19	20
		weight	0.000	0.000	0.000	0.000	0.000	0.000	0.000	0.000	0.000	0.000	0.000
25	13	low limit	2	4	5	9	10	13	15	17	18	19	20
		weight	0.000	-0.599	0.000	0.000	-0.704	0.000	0.000	0.000	0.000	0.886	0.000
25	21	low limit	2	4	5	9	10	13	15	17	18	19	20
		weight	0.000	0.000	0.000	0.000	-0.474	0.000	0.000	0.000	0.000	0.882	1.318
25	24	low limit	2	4	5	9	10	13	15	17	18	19	20
		weight	0.000	0.000	0.000	0.000	0.412	0.000	0.000	0.000	0.000	-0.407	3.225
25	30	low limit	2	4	5	9	10	13	15	17	18	19	20
		weight	0.000	0.000	0.000	0.000	0.000	0.000	0.000	0.000	0.000	0.000	4.111
30	3	low limit	2	4	5	9	10	13	15	17	18	19	20
		weight	0.000	0.000	0.000	0.000	0.636	0.000	0.000	0.000	0.000	0.000	0.695
30	13	low limit	2	4	5	9	10	13	15	17	18	19	20
		weight	0.000	0.000	0.000	0.000	0.000	0.000	0.000	0.000	0.000	0.000	0.946
30	21	low limit	2	4	5	9	10	13	15	17	18	19	20
		weight	0.000	0.000	0.000	0.000	1.265	0.000	0.012	0.000	0.000	0.000	-1.539
30	24	low limit	2	4	5	9	10	13	15	17	18	19	20
		weight	0.000	0.000	0.000	0.000	0.000	0.000	-0.499	0.000	0.000	0.000	0.589
30	25	low limit	2	4	5	9	10	13	15	17	18	19	20
		weight	0.000	0.000	0.000	0.000	0.754	0.000	-1.374	0.000	0.000	0.000	0.476

The Weights of Evidence for the La Fe watershed are presented below.

From	To	Digital Elevation Model																
3	13	low limit	0	2260	2270	2280	2340	2350	2360	2480	2490	2510	2530	2540	2610	2630	2650	2660
		weight	-2.425	-0.819	-1.092	-0.726	-0.272	-0.785	-0.461	0.623	0.883	0.520	-0.182	0.006	0.289	-0.181	-1.125	-1.670
		low limit	2680	2690	2710	2720	2730	2740	2750	2810	2820	2830	2860	2870	2880	2890		
		weight	0.000	-2.186	-0.934	-0.403	0.440	1.806	1.247	0.022	0.639	0.888	0.647	0.379	0.000	0.000		
3	21	low limit	0	2170	2180	2190	2200	2270	2280									
		weight	1.370	0.419	0.121	0.707	0.446	0.082	-0.039									
3	24	low limit	0	2190	2200	2240	2250	2260	2350	2360	2370	2380	2400	2410	2420	2450	2460	2470
		weight	-0.844	0.000	-1.334	0.027	0.000	-1.929	-1.382	0.191	-0.799	-0.495	-1.694	0.000	-2.276	-0.011	-2.050	-0.315
		low limit	2480	2490	2500	2540	2550	2570	2580	2590	2640	2650	2660	2670	2680	2690	2700	2740
		weight	1.011	0.533	0.775	0.399	0.093	0.547	0.000	-0.218	0.000	-0.219	-0.608	1.063	0.755	1.579	1.055	0.000
		low limit	2750	2760	2770													
		weight	-0.071	0.000	0.000													
3	25	low limit	0	2180	2200	2210	2220	2240	2250	2260	2270	2280	2300	2310	2320	2330	2340	2350
		weight	1.132	0.835	-0.832	-0.173	-0.946	-1.617	-0.500	-0.289	-1.766	-1.109	0.000	-2.175	-0.255	-1.082	-2.280	0.499
		low limit	2360	2370	2380	2390	2400	2410	2440	2450	2470	2480	2490	2510	2540	2560	2570	2580
		weight	-0.578	-2.444	-0.931	-1.857	0.000	-1.927	-1.445	-0.941	-0.493	0.420	0.638	0.946	1.251	0.858	0.219	-0.834
		low limit	2590	2610	2630	2640	2660	2670	2700	2710	2740	2750	2770	2780				
		weight	-0.536	-0.310	-1.459	-2.383	0.000	-2.229	0.000	-1.458	-0.072	-0.341	0.000	0.000				
13	3	low limit	0	2190	2200	2210	2230	2240	2250	2260	2270	2300	2320	2330	2360	2390	2400	2410
		weight	2.104	-0.094	0.000	0.000	0.000	0.089	0.312	0.000	0.000	-0.381	0.000	0.600	0.000	-0.499	0.000	0.445
		low limit	2420	2450	2460	2470	2480	2490	2500	2510	2520	2530	2550	2560	2570	2580	2590	2600
		weight	-0.669	0.000	-0.381	-0.941	0.474	0.851	1.159	0.040	-0.303	0.652	0.064	-0.339	0.312	-0.148	0.000	-0.036
		low limit	2610	2620	2630	2640	2650	2670	2710									
		weight	0.782	-0.094	-1.346	0.000	-0.700	0.000	0.000									
13	21	low limit	0	2190	2200	2210	2220	2230	2240	2250	2260	2300	2310	2320	2330	2340	2350	2360
		weight	0.650	-0.294	-0.161	0.000	-0.449	0.650	0.245	0.650	0.266	-0.449	0.468	-0.225	0.000	0.245	0.000	0.372
		low limit	2400	2410	2420	2450	2460	2470	2480	2500	2510	2520	2540	2550	2560	2570	2580	2590
		weight	-0.854	-0.092	-0.225	1.210	0.468	0.208	0.422	0.895	0.268	-0.115	0.245	-0.904	-0.811	-0.536	-1.196	-0.069
		low limit	2600	2610	2620	2640	2650	2660	2670	2680	2790							
		weight	-0.337	0.293	-0.138	-1.324	-0.449	-0.736	0.000	0.608	-2.528							
13	24	low limit	0	2350	2370	2390	2420	2430	2440	2450	2460	2470	2480	2490	2500	2510	2520	2530
		weight	-1.798	0.000	0.000	-1.393	1.005	0.445	-0.148	1.005	-0.381	0.158	1.809	1.005	1.410	0.263	0.000	-2.194
		low limit	2540	2550	2560	2570	2580	2590	2600	2620	2630	2640	2650	2660	2670	2690	2790	
		weight	0.089	0.287	0.000	-0.094	0.140	0.520	0.012	0.000	-1.346	-0.787	-0.248	0.000	0.000	1.005	0.000	
13	25	low limit	0	2190	2200	2210	2230	2240	2250	2270	2290	2300	2410	2420	2430	2480	2490	2500
		weight	2.278	0.000	0.000	0.000	0.000	0.000	0.000	-1.018	0.000	-1.593	-0.767	0.000	-0.980	1.054	0.620	0.081
		low limit	2510	2540	2550	2560	2570	2580	2590	2600	2610	2620	2630	2650	2660	2670	2690	2710
		weight	0.267	0.525	0.238	0.529	0.081	-0.379	-0.693	-0.268	0.486	-1.306	-0.931	0.332	0.891	0.000	1.872	0.000
		low limit	2790															
		weight	0.000															
21	3	low limit	0	2190	2200	2210	2220	2230	2270	2280	2300	2310	2320	2330	2410	2420	2430	2440
		weight	-1.057	-1.646	-0.748	-1.100	-0.200	-0.398	-0.108	0.138	0.444	0.732	1.232	0.846	-0.696	-0.057	-0.329	1.019
		low limit	2450	2490	2500	2510	2520	2530	2560	2580	2590	2610	2620	2630	2640	2650	2660	2680
		weight	0.733	0.262	0.821	0.239	0.442	0.194	-0.126	-0.446	-0.184	0.033	-0.453	0.109	-0.191	-0.525	-0.039	-1.253
		low limit	2690	2700	2710	2720	2730	2740	2750	2760	2770							
		weight	-0.136	-0.782	-1.238	0.211	-1.157	0.000	-1.943	0.000	0.000							
21	13	low limit	0	2220	2230	2270	2280	2290	2310	2320	2330	2340	2350	2360	2370	2420	2430	2440
		weight	-2.181	0.000	-1.621	-0.195	-1.166	-0.628	-0.337	0.251	-0.215	0.000	-0.908	0.000	-2.338	0.954	1.529	0.778
		low limit	2450	2490	2500	2510	2520	2530	2540	2570	2580	2620	2630	2640	2650	2660	2680	2690
		weight	0.303	-0.413	0.892	0.084	0.377	0.681	0.408	-0.500	-0.714	-2.809	-1.131	-0.235	-1.459	-2.286	0.000	-1.808
		low limit	2710	2720	2730	2740	2750	2770	2790	2800								
		weight	0.000	0.711	1.751	3.103	1.974	3.129	0.000	0.000								
21	24	low limit	0	2250	2260	2280	2290	2310	2320	2460	2470	2490	2510	2520	2530	2560	2570	2580
		weight	-2.262	-1.516	-0.459	0.000	-0.899	0.000	-2.279	0.670	0.019	0.679	-0.647	0.731	0.435	-1.952	0.191	-0.399
		low limit	2590	2610	2620	2630	2640	2650	2700	2710	2720							
		weight	0.144	1.597	0.871	-0.486	0.000	-0.858	0.364	0.000	0.000							
21	25	low limit	0	2190	2200	2210	2230	2240	2250	2260	2270	2280	2290	2300	2310	2470	2490	2510
		weight	-0.877	-1.284	-0.609	-1.207	0.000	-0.812	0.016	-0.245	-1.538	0.000	-1.569	0.000	-2.210	-0.108	0.173	0.506
		low limit	2520	2530	2590	2600	2610	2630	2640	2650	2670	2680	2690	2700	2710	2740	2750	2760
		weight	0.758	0.502	0.031	-0.701	-1.013	-2.068	-0.161	-0.504	-1.672	0.000	-1.314	0.000	-0.487	0.795	-0.482	0.000
		low limit	2770															
		weight	0.000															
25	3	low limit	0	2290	2300	2450	2470	2490	2500	2520	2530	2540	2550	2560	2570	2580	2590	
		weight	-1.231	0.000	0.591	0.000	-0.749	0.000	0.350	0.000	1.785	1.091	2.295	0.000	-1.000	0.000	0.000	
25	13	low limit	0	2570	2580													
		weight	0.310	0.000	0.000													
25	21	low limit	0	2190	2200	2210	2220	2230	2240	2280	2380	2390	2460	2470	2480	2490	2510	2520
		weight	-2.059	0.000	-1.963	0.339	0.000	0.339	0.000	-1.858	0.000	0.339	0.000	-0.577	-1.047	-1.858	-0.759	-0.354
		low limit	2530	2540	2550	2560	2570	2580	2590									
		weight	0.000	-0.865	0.339	1.726	0.540	1.474	2.642									
25	24	low limit	0	2180	2190	2210	2220	2240	2280	2290	2300	2340	2350	2370	2380	2390	2400	2410
		weight	1.063	-1.134	0.000	0.000	-1.422	0.370	-0.441	-0.728	-0.035	0.000	-0.035	1.351	-0.952	0.000	-0.728	0.000
		low limit	2430	2490	2500	2510	2550	2560	2580	2590								
		weight	0.295	0.552	1.217	0.465	1.063	-0.883	-1.539	0.000								

From	To	Municipal Boundaries				
3	9	low limit	2	5	7	9
		weight	0.000	0.000	0.000	0.000
3	13	low limit	2	5	7	9
		weight	0.087	-0.230	0.000	0.000
3	21	low limit	2	5	7	9
		weight	-0.058	0.123	0.187	-0.152
3	24	low limit	2	5	7	9
		weight	-0.540	0.679	0.000	1.092
3	25	low limit	2	5	7	9
		weight	-0.790	0.826	0.000	0.000
9	3	low limit	2	5	7	9
		weight	0.000	0.000	0.000	0.000
9	13	low limit	2	5	7	9
		weight	0.000	0.000	0.000	0.000
9	21	low limit	2	5	7	9
		weight	0.000	0.000	0.000	0.000
9	24	low limit	2	5	7	9
		weight	0.000	0.000	0.000	0.000
9	25	low limit	2	5	7	9
		weight	0.000	0.000	0.000	0.000
13	3	low limit	2	5	7	9
		weight	-0.188	0.172	0.000	0.000
13	9	low limit	2	5	7	9
		weight	0.000	0.000	0.000	0.000
13	21	low limit	2	5	7	9
		weight	0.041	-0.047	0.000	0.000
13	24	low limit	2	5	7	9
		weight	-0.262	0.225	0.000	0.000
13	25	low limit	2	5	7	9
		weight	-0.438	0.328	0.000	0.000
21	3	low limit	2	5	7	9
		weight	0.053	-0.027	0.255	1.003
21	9	low limit	2	5	7	9
		weight	0.000	0.000	0.000	0.000
21	13	low limit	2	5	7	9
		weight	-0.320	0.109	0.000	0.000
21	24	low limit	2	5	7	9
		weight	-1.498	0.277	0.000	0.000
21	25	low limit	2	5	7	9
		weight	-1.451	0.274	0.000	0.000
25	3	low limit	2	5	7	9
		weight	-0.477	0.182	0.000	0.000
25	9	low limit	2	5	7	9
		weight	0.000	0.000	0.000	0.000
25	13	low limit	2	5	7	9
		weight	1.063	0.000	0.000	0.000
25	21	low limit	2	5	7	9
		weight	-1.047	0.294	0.000	0.000
25	24	low limit	2	5	7	9
		weight	0.313	-0.215	0.000	0.000

From	To		Slope						
3	13	low limit	1	2	3	4	5	6	7
		weight	0.275	0.213	0.253	0.083	-0.050	-0.811	-2.049
3	21	low limit	1	2	3	4	5	6	7
		weight	0.119	0.176	0.136	0.141	-0.094	-0.590	-1.144
3	24	low limit	1	2	3	4	5	6	7
		weight	0.677	1.130	0.706	0.191	-0.593	-3.116	0.000
3	25	low limit	1	2	3	4	5	6	7
		weight	1.162	0.915	0.616	0.253	-0.652	-1.669	-1.116
13	3	low limit	1	2	3	4	5	6	7
		weight	0.000	0.596	0.223	0.061	-0.119	0.000	0.000
13	21	low limit	1	2	3	4	5	6	7
		weight	-0.292	-0.264	-0.091	0.110	-0.055	-0.041	0.000
13	24	low limit	1	2	3	4	5	6	7
		weight	-0.097	1.066	0.356	-0.180	-0.462	0.634	0.000
13	25	low limit	1	2	3	4	5	6	7
		weight	0.083	0.825	0.329	0.218	-0.770	-0.690	0.000
21	3	low limit	1	2	3	4	5	6	7
		weight	0.014	-0.271	-0.137	-0.064	0.265	1.225	1.173
21	13	low limit	1	2	3	4	5	6	7
		weight	-0.296	0.219	-0.152	-0.036	0.116	0.341	0.000
21	24	low limit	1	2	3	4	5	6	7
		weight	-0.074	-0.214	0.146	0.016	-0.113	0.293	0.000
21	25	low limit	1	2	3	4	5	6	7
		weight	0.282	0.312	0.184	-0.022	-0.503	0.000	0.000
25	3	low limit	1	2	3	4	5	6	7
		weight	0.000	-0.379	0.504	0.310	0.000	0.000	0.000
25	13	low limit	1	2	3	4	5	6	7
		weight	0.000	0.000	1.533	0.000	0.000	0.000	0.000
25	21	low limit	1	2	3	4	5	6	7
		weight	0.745	0.498	0.435	-0.548	-1.142	0.000	0.000
25	24	low limit	1	2	3	4	5	6	7
		weight	-0.035	-0.569	-0.258	0.127	0.429	0.252	0.000

From	To		Soils					
3	13	low limit	2	4	10	11	15	20
		weight	-1.333	0.000	-0.377	0.103	0.007	0.000
3	21	low limit	2	4	10	11	15	20
		weight	0.896	-0.087	0.232	-1.291	0.056	-0.750
3	24	low limit	2	4	10	11	15	20
		weight	0.890	0.000	2.152	-2.174	0.017	0.000
3	25	low limit	2	4	10	11	15	20
		weight	1.548	-0.034	2.263	-4.224	-0.015	0.929
13	3	low limit	2	4	10	11	15	20
		weight	0.000	0.000	0.000	0.000	0.004	0.000
13	21	low limit	2	4	10	11	15	20
		weight	1.631	0.000	2.036	0.000	-0.027	0.000
13	24	low limit	2	4	10	11	15	20
		weight	2.391	0.000	3.084	0.000	-0.071	0.000
13	25	low limit	2	4	10	11	15	20
		weight	1.179	0.000	3.376	0.000	-0.066	0.000
21	3	low limit	2	4	10	11	15	20
		weight	-0.375	0.000	0.581	-0.116	-0.011	1.568
21	13	low limit	2	4	10	11	15	20
		weight	0.000	0.000	0.000	0.000	0.041	0.000
21	24	low limit	2	4	10	11	15	20
		weight	-0.146	0.000	0.450	1.828	-0.034	1.392
21	25	low limit	2	4	10	11	15	20
		weight	0.169	0.000	0.360	1.057	-0.017	0.000
25	3	low limit	2	4	10	11	15	20
		weight	-0.796	0.000	-1.072	0.000	-0.761	4.375
25	13	low limit	2	4	10	11	15	20
		weight	0.000	0.000	0.000	0.000	0.492	0.000
25	21	low limit	2	4	10	11	15	20
		weight	-1.142	0.000	-1.082	0.000	0.351	0.339
25	24	low limit	2	4	10	11	15	20
		weight	-0.035	0.000	0.094	0.000	-0.012	-0.035

Appendix D - Error matrices

The error matrices used to calculate the validation metrics of land use models for the Riogrande II watershed and La Fe watershed are present in Table 14 and 15.

		Reference								
	Classes	**3**	**9**	**13**	**21**	**24**	**25**	**30**	**33**	**Total**
Simulated	**3**	255776	84	4174	74344	30	90	0	17	334515
	9	86	36706	480	7935	0	15	0	637	45859
	13	3524	200	19507	11397	41	34	0	4	34707
	21	74561	8220	10151	651094	391	263	33	66	744779
	24	0	1	44	288	1299	53	23	0	1708
	25	92	7	31	264	38	62	1	0	495
	30	9	0	2	12	10	8	85	0	126
	33	278	520	5	397	0	48	0	11959	13207
	Total	334326	45738	34394	745731	1809	573	142	12683	1175396

Table 14. Error matrix of Riogrande II Reservoir in pixel units

		Reference						
	Classes	**3**	**13**	**21**	**24**	**25**	**33**	**Total**
Simulated	**3**	36833	1567	9200	212	552	1	48365
	13	1513	508	774	51	108	0	2954
	21	9157	820	21135	351	779	3	32245
	24	267	18	353	293	78	0	1009
	25	496	60	774	139	250	0	1719
	33	111	0	16	0	9	1234	1370
	Total	48377	2973	32252	1046	1776	1238	87662

Table 15. Error matrix of La Fe Reservoir in pixel units

Appendix E - San Nicolás Valley water treatment project

Medellín, 2 de mayo de 2024

Ingeniera **20240130104510**
NATHALIA JASTROMBEK VIEIRA
Estudiante maestría en Ingeniería Ambiental en la Universidad de Antioquia
Correo electrónico: nathalia.jastrombek@udea.edu.co
Celular: +57 311 620 8459
Medellín

Asunto: Solicitud de información para tesis de grado.

En atención a su solicitud del 18 de abril de 2024 vía correo electrónico y con radicado 20240120070054 de las Empresas Públicas de Medellín ESP, en donde solicita información técnica y detallada para realizar su tesis de grado, le informamos que los análisis que usted plantea son realizados directamente por EPM para definir su plan de inversiones de largo plazo y la flexibilidad con que se requerirá atender el territorio del valle de San Nicolás y Valle de Aburrá.

En particular, la respuesta puntual a sus preguntas es la siguiente:

¿Existen planes futuros para cambiar la configuración de abastecimiento de agua del Valle de Aburrá? Si existen, su ejecución depende del comportamiento del sistema y otros factores determinantes para la toma de decisiones. Son modelados de forma anual, con proyecciones de demanda anuales y los análisis de entorno respectivos.

¿Cuál es el caudal de diseño para el proyecto que conecta el Embalse La Fe al municipio? El sistema del municipio de Rionegro hoy utiliza un caudal de 290 l/s, que se captan en el río Negro. Adicionalmente, existe una interconexión entre el embalse La Fe y el Valle de San Nicolás para un caudal de diseño de 600 l/s.

La invitamos a contactar la Gerencia de Servicios Públicos del Departamento de Antioquia y con ellos conseguir la información de algunos de los sistemas de los municipios donde no opera Empresas Públicas de Medellín, para que aplique la metodología propuesta para su tesis de grado de maestría y que sean aplicables a la realidad de una región. Este

Por ti, estamos ahí

Empresas Públicas de Medellín E.S.P.
Carrera 58 N° 42-125
Conmutador: 604 3808080
Medellín - Colombia
www.epm.com.co

ejercicio será de alto beneficio en las subregiones del Bajo Cauca, Magdalena Medio, Nordeste, Norte y Suroeste.

Atentamente,

CATALINA ALZATE JARAMILLO
Jefe Unidad Planeación Infraestructura Aguas.